Lecture Notes in Physics

Volume 867

For further volumes:
www.springer.com/series/5304

The Lecture Notes in Physics

The series Lecture Notes in Physics (LNP), founded in 1969, reports new developments in physics research and teaching—quickly and informally, but with a high quality and the explicit aim to summarize and communicate current knowledge in an accessible way. Books published in this series are conceived as bridging material between advanced graduate textbooks and the forefront of research and to serve three purposes:

- to be a compact and modern up-to-date source of reference on a well-defined topic
- to serve as an accessible introduction to the field to postgraduate students and nonspecialist researchers from related areas
- to be a source of advanced teaching material for specialized seminars, courses and schools

Both monographs and multi-author volumes will be considered for publication. Edited volumes should, however, consist of a very limited number of contributions only. Proceedings will not be considered for LNP.

Volumes published in LNP are disseminated both in print and in electronic formats, the electronic archive being available at springerlink.com. The series content is indexed, abstracted and referenced by many abstracting and information services, bibliographic networks, subscription agencies, library networks, and consortia.

Proposals should be sent to a member of the Editorial Board, or directly to the managing editor at Springer:

Christian Caron
Springer Heidelberg
Physics Editorial Department I
Tiergartenstrasse 17
69121 Heidelberg/Germany
christian.caron@springer.com

Karsten Balzer • Michael Bonitz

Nonequilibrium Green's Functions Approach to Inhomogeneous Systems

Springer

Karsten Balzer
Max Planck Research Department
for Structural Dynamics
University of Hamburg, CFEL
Hamburg
Germany

Michael Bonitz
Institut für Theoretische Physik und
Astrophysik
University of Kiel
Kiel
Germany

ISSN 0075-8450
Lecture Notes in Physics
ISBN 978-3-642-35081-8
DOI 10.1007/978-3-642-35082-5
Springer Heidelberg New York Dordrecht London

ISSN 1616-6361 (electronic)

ISBN 978-3-642-35082-5 (eBook)

Library of Congress Control Number: 2012955345

Dedicated to Bożena and Christine

Preface

While *nonequilibrium Green's Functions* (NEGFs) are a mature theory with a history of some 50 years, it is only recently that they have turned into a practical tool for quantitative analysis in many-body physics [1–4]. Despite the attractive features of NEGFs—generality and selfconsistency, conservation laws, diagram technique and applicability to ultrafast processes—the relatively large computational effort in treating the dynamics of functions that depend on two times has prevented a broad use of this technique.

Yet, the dramatic progress in available computational resources has made NEGF calculations practical, as was demonstrated by many applications to spatially homogeneous systems in nuclear matter, plasmas and condensed matter systems over the last 15 years. Recently, attempts have been made to extend the use of NEGFs to *spatially inhomogeneous systems* which requires a substantially increased numerical effort. However, new strategies such as the finite element-discrete variable representation, the generalized Kadanoff-Baym ansatz (GKBA), and clever program parallelization make such applications well feasible. This monograph discusses these techniques in detail and should pave the way for a broad application of NEGFs to inhomogeneous systems that are of great importance in atomic, condensed matter and high energy physics.

Acknowledgments We thank Sebastian Bauch for close collaboration over the last years and Sebastian Hermanns for providing numerical results based on the GKBA, cf. Sect. 5.2.1. This monograph has greatly benefited from discussions with students and postdocs at the chair of MB in Kiel, in particular, Alexei Filinov and David Hochstuhl, as well as many colleagues from the Nonequilibrium Green's functions community, first of all Pawel Danielewicz, Robert van Leeuwen, Vaclav Špička, Arnau Rios Huguet and Matthias Garny.

The authors are grateful to the Deutsche Forschungsgemeinschaft and the Bundesministerium für Bildung und Forschung for financial support of this work. Furthermore, the North-German Supercomputing Alliance (HLRN) is acknowledged for providing computing time.

Kiel, Germany

Karsten Balzer
Michael Bonitz

Contents

Acronyms

AEL	Approximate excitation level
BSE	Bethe-Salpeter equation
DE	Double excitation
DFT	Density functional theory
DVR	Discrete variable representation
FE-DVR	Finite element-discrete variable representation
FO	Frozen-orbital (Koopmans') approximation
GGL	Generalized Gauss-Lobatto (quadrature)
GKBA	Generalized Kadanoff Baym ansatz
GW	*GW* approximation
HF	Hartree-Fock (approximation)
KBE	(Keldysh-)Kadanoff-Baym equation(s)
IC	Initial correlation(s)
KMS	Kubo-Martin-Schwinger (conditions)
LDA	Local-density approximation
MBA	Many-body approximation
MBPT	Many-body perturbation theory
MPI	Message passing interface
MS	Martin-Schwinger (hierarchy)
NEGF	Nonequilibrium Green's function
NO	Natural orbital (basis)
PDE	Partial differential equation
QFT	Quantum field theory
RAM	Random access memory
SCF	Self-consistent field (method)
SE	Single excitation
TDDFT	Time-dependent density functional theory
TDSE	Time-dependent Schrödinger equation
TM	T-matrix (approximation)

1pNEGF	One-particle nonequilibrium Green's function
1pRDM	One-particle reduced density matrix
1pSE	One-particle self-energy
2B	Second Born (approximation)
2pNEGF	Two-particle nonequilibrium Green's function

Part I
Introduction

Chapter 1
Quantum Many-Particle Systems out of Equilibrium

In various fields of physics, the out-of-equilibrium dynamics of interacting quantum many-body systems are of fundamental interest, both, theoretically and experimentally. This includes applications in condensed matter physics—from quantum transport and molecular electronics to few-electron dynamics in quantum confined systems; atomic and molecular physics—electron dynamics following photoexcitation and photoionization, plasma physics—laser-matter interaction; and high energy physics—nuclear collisions, baryogenesis and much more.

The interest in ultrafast excitation and relaxation is triggered by the practical needs of nanoelectronics, on the one hand, and by the availability of ultrashort coherent light sources, on the other. Intense lasers and free electron lasers now provide femtosecond and subfemtosecond pulses from the infrared to the X-ray range posing fundamental questions about the behavior of matter at ultrashort time scales. Among the questions of interest are

- single and double ionization cross sections of atoms and molecules on the femtosecond scale,
- many-electron effects during photoionization (shake up and Auger processes),
- non-linear effects at high intensity, time-dependent energy renormalization,
- decay of initial correlations and dynamics of the formation of correlations,
- dynamics of the formation of quasiparticles,
- ultrafast electron dynamics in semiconductor devices, dynamics of screening,
- ultrafast spin dynamics,
- ultrafast double excitations in atoms and condensed matter, carrier multiplication[1],
- dynamics of few-electron systems, quantum normal modes as novel diagnostics,
- dynamics of fermionic and bosonic systems in traps or optical lattices,
- ultrafast dynamics of quantum coherence effects such as entanglement, superfluidity and superconductivity.

[1] E.g., Ref. [5].

K. Balzer, M. Bonitz, *Nonequilibrium Green's Functions Approach to Inhomogeneous Systems*, Lecture Notes in Physics 867,
DOI 10.1007/978-3-642-35082-5_1,

This list can be extended arbitrarily. A theoretical description of the phenomena listed above requires a self-consistent description of spin statistics, interaction and correlation effects, field-matter interaction, bound and scattering states, embedding into an environment etc. All this should be described in a nonequilibrium fashion without any *a-priori* assumption on time scale separation, weakness of the external perturbations or weakness of spatial inhomogeneity. While this sounds a bit like a "theory of everything", in fact, as we will show in this monograph, nonequilibrium Green's functions (NEGFs) provide the framework to self-consistently capture all these effects. Naturally, one has to pay a price: First, the computational effort is higher than for most alternative approaches, and, second, there are situations that are particularly difficult for Green's functions in nonequilibrium, most importantly, strongly correlated systems. After these general introductory remarks, we now turn to a more detailed discussion of interaction and correlation effects and to a comparison of NEGFs with alternative theoretical and computational approaches in quantum many-body physics.

The fundamental starting point for the analysis of the quantum few- or many-particle dynamics is (if relativistic effects can be neglected) the time-dependent Schrödinger equation (TDSE),

$$\mathrm{i}\hbar\frac{\partial}{\partial t}\big|\Psi(t)\big\rangle = \hat{H}(t)\big|\Psi(t)\big\rangle, \tag{1.1}$$

where the time-dependent wave function of the system is denoted by $|\Psi(t)\rangle$ and $\hat{H}(t)$ is the Hamilton operator, $\hat{H}(t) = \hat{T} + \hat{V}(t) + \hat{W}$, containing the kinetic ($\hat{T}$) and potential energy ($\hat{V}$) of each individual particle as well as the interaction energy $\hat{W}$ between all pairs. Further, $\hat{V}$ is understood to include confinement potentials, time-dependent external fields and so on. In practice, the wave function $|\Psi(t)\rangle$ depends on many degrees of freedom, such as particle positions, spin, angular momentum, etc., and must be completely (anti-)symmetric with respect to particle exchange for bosons (fermions).

Unfortunately, also with the help of the most powerful computers, the direct numerical solution of Eq. (1.1) is possible only for small systems. This is due to (i) the coupling of the individual particle motion through all kinds of interactions[2] and (ii) due to the dimension of the attributed Hilbert space which scales exponentially with the particle number. In full dimensionality, "small" means usually systems involving a few particles. Moreover, Eq. (1.1) describes only the dynamics of a pure quantum state. In cases where a coupling to the environment is essential this description has to be replaced by a mixed ensemble.

To overcome the computational bottleneck of the TDSE, we in this article, resort to a reduced system description on the basis of nonequilibrium Green's function techniques. The central quantity is the one-particle nonequilibrium Green's function

[2]Typically, this concerns charge and spin interactions. Note that, in the absence of charge interactions, the many-body TDSE decouples into a set of one-particle equations. Aside from proper (anti-)symmetrization, the determination of the wave function is then usually simple.

(1pNEGF) which appears as a two-time generalization of the one-particle reduced density matrix,

$$G_{ij}^{(1)}(t,t') = -\frac{\mathrm{i}}{\hbar}\langle \hat{T}_{\mathscr{C}}\hat{c}_i(t)\hat{c}_j^{\dagger}(t')\rangle. \tag{1.2}$$

Here, $\hat{T}_{\mathscr{C}}\{\hat{c}_i(t)\,\hat{c}_j^{\dagger}(t')\}$ is a time-ordered[3] product of one-particle annihilation and creation operators in the Heisenberg picture (cf. Chap. 2), and i and j label all degrees of freedom other than temporal ones, e.g., particle position and spin. Moreover, the brackets denote an appropriate ensemble averaging and, hence, account for the multi-particle nature of the problem under investigation. In the limit of equal times, the common one-particle reduced density matrix (1pRDM) is recovered from Eq. (1.2) by,

$$\rho_{1,ij}(t) = -\mathrm{i}\hbar G_{ij}^{(1)}(t,t^{+}), \tag{1.3}$$

where $\rho_{1,ij}(t) = \langle \hat{c}_j^{\dagger}(t)\hat{c}_i(t)\rangle$, and t^{+} indicates that the second time argument of the 1pNEGF is infinitesimal larger than the first one (leading to the appropriate order of the $\hat{c}$-operators).

In order to give a general idea of how the use of NEGFs compares with other methods that are suited to describe the time evolution of a generic quantum many-body system, we give a brief overview on some existing computational approaches in the next Section.

1.1 Overview on Computational Approaches

Alongside the method of NEGFs, there exist a variety of other approaches which are capable to describe the behavior of quantum many-body systems far from equilibrium. In distinct ways, all of them can be introduced as being complementary to the solution of the time-dependent Schrödinger equation, Eq. (1.1). Among the most common approaches are,

(i) Time-dependent density functional theory (TDDFT), e.g., Ref. [6]: TDDFT takes great advantage of the fact that the fundamental equivalence of the many-body wave function and the electronic density does not only hold in equilibrium [7] but is also applicable for time-dependent systems [8]. The basic equations to be solved are the Kohn-Sham equations for an associated, fictitiously non-interacting system.

(ii) Time-dependent reduced density matrix approaches, e.g., Refs. [9, 10]: Here, in general, a small set of integro-differential equations of the quantum BBGKY (Bogolyubov-Born-Green-Kirkwood-Yvon) hierarchy is solved for the time-dependent reduced density matrix [11]. In practice, this scheme requires a

[3]Time ordering is here understood as ordering along the Schwinger-Keldysh contour, for details, see Sect. 2.1.1.

memory integration and a suitable approximation for a specific s-particle density matrix. It is widely used to develop quantum kinetic equations (master equations).

(iii) Time-dependent density-matrix renormalization group (TDDMRG) approaches, e.g., Refs. [12, 13]: In general, all methods based on DMRG can be formulated as being variational in the space of matrix product states [14] and allow for an efficient treatment of effective degrees of freedom.

(iv) Continuous-time (diagrammatic) quantum Monte Carlo (CTQMC), e.g., [15] and references therein: In this method, all possible configurations that contribute to the one-particle nonequilibrium Green's function of the system are sampled by a Monte Carlo algorithm in a time-dependent fashion on the full Schwinger-Keldysh time contour, cf. Sect. 2.1.1.

(v) Multiconfiguration time-dependent Hartree-Fock (MCTDHF), e.g., Refs. [16, 17]: Here, aside from time-dependent coefficients, also the one-particle orbitals in a configuration interaction (CI) expansion of the correlated many-body wave function become time-dependent (minimizing the action functional). At the same time, one restricts oneself to include only a few Slater determinants in the expansion. Their number acts as a convergence parameter.

All approaches mentioned in (i) to (v) have their own limitations and their individual range of applicability. Though TDDFT, for example, allows for an accurate calculation of excitation energies [18], response properties [19] and photoabsorption spectra of even very complex molecules [20], it requires reasonable assumptions for the generally unknown exchange-correlation potential. Further, TDDMRG can make use of its inherent advantages mainly in the treatment of one-dimensional systems and is not easily extendable to 2D [21]. On the other hand, while CTQMC generally suffers from a dynamical sign problem which limits the real-time propagation to rather short times, the convergence of MCTDHF may be slow with the number of Slater determinants used in the expansion of the many-particle wave function.

Formally, the reduced density matrix approach (ii) is closely related (e.g., Ref. [22]) to the NEGF framework the application of which to spatially inhomogeneous quantum systems is the objective of the present article. The BBGKY hierarchy therein plays the same role as the Martin-Schwinger (MS) hierarchy in the context of the Keldysh-Kadanoff-Baym equations (KBEs)—the equations of motion for the NEGF, see Sect. 2.2.1. However, the introduction of systematic many-body approximations (MBAs) is often difficult in a density matrix approach. For further simplification, one often resorts to the Markov limit, e.g., [10], which destroys total energy conservation and does not allow to describe ultrafast dynamics [11]. On the contrary, the use of nonequilibrium Green's functions allows one to derive conserving MBAs directly by Feynman diagram technique and thus makes the inclusion of correlation and memory effects simple and self-consistent. This aspect reveals one of the main strengths of the NEGF approach.

Another advantage that encourages the use of Green's functions is the fact that there is no (dynamical) sign problem as it occurs in fermionic quantum Monte Carlo, i.e., bosons *and* fermions can be treated on the same footing using the concept of

second quantization[4]. Furthermore, it allows one to describe quantum many-body systems at, both, zero and finite temperatures, and even in general nonequilibrium situations. This is not possible in (standard versions[5] of) TDDFT and MCTDHF which make direct use of a pure-state wave function.

In principle, the computation of the time evolution of the 1pNEGF from the Kadanoff-Baym equations is only limited by the available computer power. Thereby, the main difficulty is the generic two-time structure of the KBEs which consumes many resources. Nevertheless, there also exist simplifications such as the generalized Kadanoff Baym ansatz (GKBA) [23] (cf. Sect. 2.4.2) that allow one to treat the KBEs in the single-time limit. This drastically reduces the computational effort and enables calculations for larger systems and the investigation of the system behavior on longer time scales.

From a more conceptual point of view, the equations of motion for the NEGF are also an optimal starting point to systematically derive other (potentially simpler) kinetic and transport equations, see, e.g., Refs. [24–26] for an overview. Along this line, we emphasize that even Boltzmann- or Landau-type equations for the Wigner distribution function [27] can be obtained directly by applying the GKBA and performing a subsequent separation of time scales, see Ref. [28].

With the above paragraphs, we do not wish to give the impression that a NEGF approach is—in all aspects—superior to other methods. However, we want to emphasize that it provides a very general many-body framework which can be applied to basically all finite and extended quantum many-body systems whether in equilibrium, in nonequilibrium, at zero or at finite temperatures.

1.2 Many-Body Interactions in Inhomogeneous Quantum Systems

In this article, we concentrate on quantum many-body systems which are inhomogeneous in coordinate space. This means that—besides the kinetic energy $\hat{T}$ and the particle-particle interaction $\hat{W}$—the Hamiltonian in Eq. (1.1) contains an additional contribution $\hat{V}$ describing the change of the single-particle potential energy as function of all particle positions: $\hat{V}(\mathbf{r}_1, \ldots, \mathbf{r}_N) = \sum_{i=1}^{N} v^{(1)}(\mathbf{r}_i)$, where the system is assumed to contain only a single species (one-component system). Typically, the potential $\hat{V}$ acts as a confinement such that the system—if there is no periodicity involved—is finite, and the NEGF vanishes outside of a certain range. However, this does not necessarily imply that there exist no regions where the particles can move quasi-freely. For example, in atoms or molecules, the motion of a single electron far away from any nuclei is practically unbounded and can be well described by a

[4] See Sect. 2.1 and Appendix A.

[5] For completeness we mention finite temperature extensions of equilibrium DFT developed by Mermin [29] and others, e.g., [30] and of equilibrium CI and MCHF, e.g., [31].

freely propagating wave packet. To incorporate such circumstances in a NEGF approach one needs to be able to describe, simultaneously, discrete (bound) states and continuum states. In general, this is a challenging task and requires an appropriate representation of the NEGF, cf. Chap. 3.

A central question for the construction of a many-body theory is to properly quantify the strength of interaction and correlation effects. This problem is well familiar from spatially homogeneous systems such as the electron gas or the jellium model. For example, the ground state of the electron gas is governed by the ratio of two relevant energies—the mean interaction energy and mean kinetic energy or, equivalently, the Brueckner parameter r_s (coupling parameter) which is the ratio of two relevant length scales—the mean interparticle distance $\langle r \rangle$ and the effective Bohr radius a_0, e.g., Ref. [32],

$$r_s = \frac{\langle r \rangle}{a_0} \sim \frac{\langle \hat{W} \rangle}{\langle \hat{T} \rangle}. \tag{1.4}$$

While for $r_s \ll 1$ the system resembles a nearly ideal quantum gas (Fermi gas), for $r_s \gg 1$ the particle density becomes localized in space and the behavior resembles that of a strongly correlated nearly classical system such as a Wigner crystal. For intermediate values of r_s a number of non-trivial phases exist.

For a confined system with a general pair interaction $\hat{W}$ the situation is more complex since there exists an additional energy scale related to the mean confinement energy $\langle \hat{V} \rangle$. Again, the state of the system can be characterized by the ratio of two energy scales[6] or, alternatively, two length scales, one (l_0) characterizing the effective range of the confinement. For example, for a harmonic confinement potential with frequency ω, the proper scale is the extension of the ground-state wave function, $l_0 = (\hbar/m\omega)^{1/2}$. On the other hand, in a square well potential such as in a quantum well of thickness L, a proper choice is $l_0 = L$ (see Sect. 6.2). A suitable coupling parameter is then,

$$\lambda = \frac{\langle \hat{W} \rangle}{\langle \hat{V} \rangle} = \left(\frac{l_0}{a_0} \right)^k, \tag{1.5}$$

where k is a positive parameter depending on the interaction potential. For $\lambda \ll 1$, corresponding to a large confinement frequency, as in the homogeneous case above, the interaction is weak and there is a strong wave function overlap corresponding to a nearly ideal quantum gas behavior. In contrast, for large λ (small ω), particles are localized and strongly interacting, behaving similarly to a classical system.

Note that a problem in a confinement potential is typically related to a finite particle number N. If N is small (on the order of 100 or below) symmetry and shell effects may become relevant and the system properties explicitly depend on N. If all parameters (including ω) are fixed and N is increased, the system approaches

[6] In fact, due to the Virial theorem, mean kinetic energy and mean potential energy are related to one another.

an ideal quantum gas, in case of Coulomb interaction and a harmonic confinement. This somewhat counter-intuitive result was obtained by Abraham et al. [33] and indicates interesting properties of finite trapped systems.

For finite temperatures, the concept of the coupling parameter holds as well but one has to compare the interaction energy to the mean kinetic energy (thermal average), e.g., [34]. But with the additional thermal energy scale ($k_B T$) it is clear that the system behavior is governed by two dimensionless parameters instead of a single parameter. A possible choice would be the inverse temperature in units of the oscillator energy, $\beta = \hbar\omega / k_B T$, and the coupling parameter λ. If $\beta \gg 1$ the system is close to the (quantum) ground state whereas for $\beta < 1$ thermal effects are essential, and eventually the system approaches semi-classical behavior.

In nonequilibrium where the system is excited, e.g., by electrical or optical fields, in general, the concept of coupling strengths and coupling parameters is much more complex. But in the important case of weak excitation, when linear response theory is applicable, the interaction strength is adequately captured by ground-state (or equilibrium) results.

For the purposes of the present monograph, we are primarily interested in the regime of small to moderate coupling, where λ is smaller than or of the order of one and $\beta > 1$. In the limit $\lambda \ll 1$, we thereby expect that the application of MBAs that are of low order in the interaction $\hat{W}$ lead to accurate results. This is the regime where NEGFs can be efficiently applied to compute the nonequilibrium response to an external perturbation (weak or strong) since low-order approximations such as Hartree Fock plus second Born approximation can be evaluated at reasonable computational cost. This does not exclude larger couplings, where sometimes simple correlation corrections to the mean-field description can yield acceptable results (compare with Chaps. 5 and 6).

1.3 Correlations

In a very general picture, the term "correlation" is used to describe all binary interactions being present in a classical or quantum system that contains more than just a single particle. In a many-electron system, for example, one often means the entirety of all Coulomb repulsions between the electrons. However, in many-body theory (classical or quantum), the term "correlation" is used more specifically. Here, it indicates those parts of the instantaneous interactions that cannot be described by a structureless mean field created by all particles. In a mathematical sense, correlations are due to those interaction contributions that cannot be described by an effective independent-particle model with a quadratic (second-quantized) Hamiltonian. In perturbation theory, this refers to all interaction effects that cannot be explained by common Hartree-Fock (HF) self-consistent field methods [35] and thus require advanced methodologies. A "correlated treatment" of a many-body problem therefore requires a specific method that is capable to go beyond the HF level. Along these lines, a suitable method for ground-state calculations is, e.g., Møller-Plesset perturbation theory, e.g., [36].

In many cases, correlation effects[7] are important for the system properties. In atomic and molecular physics, they are, e.g., crucial for the electronic structure, the total energy and the formation of chemical bonds. In multi-electron atoms, the most prominent consequence of correlations is the presence of resonance states that can decay by autoionization (Auger decay) [37]. In molecular systems, a similar result is the appearance of conical intersections, see, e.g., Ref. [38]. Regarding nonequilibrium situations, electron correlations, for instance, influence the intense-field ionization of atoms and molecules. This becomes most obvious in the context of non-sequential double ionization, e.g., [17, 39, 40], and shake-up excitation processes [41]. On the other hand, in condensed matter systems, correlations are inter alia responsible for the presence of multi-faceted (e.g., metal-insulator-type) phase diagrams, high-temperature superconductivity and magnetism [42]. For an overview on correlations effects in semiconductors, see, e.g., Ref. [43]. Finally, we note that correlations are related also to the topic of entanglement [44] and are therefore also of great importance in the field of quantum computation [45].

What really drives the theoretical investigation of many-body correlation effects is the fact that an increasing number of experimental techniques become available that allow one to probe correlation effects in a time-dependent fashion [46, 47]. These techniques include COLTRIMS[8] and reaction microscopes [48] which, in coincidence, can measure the vector momenta of electronic and nuclear fragments after field-induced ionization and/or dissociation processes. On top of this, electron correlation effects themselves are today of technological importance as they are exploited to generate ultra-short and coherent radiation [49]. Another powerful technique that can probe correlation effects in a time-resolved manner is a streak camera which has achieved sub-femtosecond resolution [50] and extensions to the VUV[9] frequency range relevant for free electron lasers [51]. Typical correlation effects probed with streak cameras are related to Auger decay and so-called post collision interaction where two electrons in the continuum exchange energy [52, 53].

In the recent decades, there has been much progress in computational *ab initio* methods to account for correlation effects in equilibrium and nonequilibrium quantum many-body systems. While, in the TDSE, correlation effects are represented by time-local interaction contributions, in the Kadanoff-Baym equations, they enter in form of memory or retardation effects and a non-Markovian time evolution of the nonequilibrium Green's functions. This means that the complete future evolution of the system depends, in general, on the NEGF at all previous times, cf. Sect. 2.2.1. Taking the Markov limit in the KBEs leads to substantially simpler expressions for the collision integrals, including the familiar Landau, Boltzmann or Balescu-Lenard integrals. However, at the same time, this limit drastically alters the properties of the theory. The original conservation law of total energy is radically altered, and only kinetic (single-particle) energy is preserved, e.g., [11]. Also, the short-time behavior

[7] In the refined sense.

[8] Abbreviation for "cold target recoil ion momentum spectroscopy", e.g., [54].

[9] Vacuum ultra-violet radiation ($\ll$200 nm).

of the system is no longer accessible. Finally, a Markovian theory even fails to deliver the correct asymptotic states and the thermodynamic functions of a correlated many-body system but converges, instead, to the functions of an ideal (classical or quantum) gas. All this underlines again the importance of a full NEGF approach that overcomes these deficiencies.

Part II
Theory

Chapter 2
Nonequilibrium Green's Functions

Real-time nonequilibrium Green's functions (NEGFs) naturally appear in the extension of the Matsubara formalism of (equilibrium) quantum many-body theory [55, 56] to situations far from equilibrium. In this respect, the term "one-particle NEGF", cf. Sect. 2.1.2, is synonymous for the phrase "propagator" as well as for "correlation function". The great success of NEGFs is, in general, due to the fact that fundamentals of equilibrium theory, e.g., Feynman rules and diagram techniques, can be applied without major conceptual modifications also to nonequilibrium situations.

Nonequilibrium Green's functions are the main ingredients to quantum statistical mechanics and quantum kinetic equations [11], the development of which was pioneered by Martin [57] and Schwinger [58] and was expedited by Kadanoff and Baym [28] in the USA and, in parallel, by Keldysh [59] in the USSR. The main achievements were rendered in the late 1950s and in the 1960s and were stimulated by quantum field theory. Since then, NEGFs have become standard tools to derive quantum transport models on various levels of sophistication, e.g., Refs. [24–26, 60, 61], and have been applied to give quantum corrections to the Boltzmann equation [62–64]. On the other hand, NEGFs have nowadays[1], reached the potential to numerically treat time-dependent quantum systems more or less *ab-initio*[2]. To this end, one solves the basic equations of motion for the one-particle NEGF—the (Keldysh-)Kadanoff-Baym equations (KBEs)—and obtains statistical and dynamical information about the system even in the presence of strong external driving forces. For an overview, see Part IV of this monograph.

[1] Due to the continuously increasing power of computers.

[2] By this we mean that the equations of motion are formally exact with the accuracy determined by the choice (approximation) of a single function—the self-energy.

K. Balzer, M. Bonitz, *Nonequilibrium Green's Functions Approach to Inhomogeneous Systems*, Lecture Notes in Physics 867,
DOI 10.1007/978-3-642-35082-5_2, © Springer-Verlag Berlin Heidelberg 2013

2.1 Introduction

Our ultimate goal is the description of time-dependent processes in a fully interacting quantum many-body system of identical particles.

Using second quantization methods and fermionic creation ($\hat{f}_i^\dagger$) and annihilation ($\hat{f}_i$) operators acting on a many-particle state $|\{n\}\rangle$ in Fock space[3], see Appendix A, we consider a generic time-dependent many-body Hamiltonian,

$$\begin{aligned} \hat{H}(t) &= \sum_{ij} \langle i|h^{(1)}(t)|j\rangle \hat{f}_i^\dagger \hat{f}_j + \frac{1}{2}\sum_{ij,kl}\langle ij|w^{(2)}|kl\rangle \hat{f}_i^\dagger \hat{f}_j^\dagger \hat{f}_l \hat{f}_k, \\ h^{(1)}(t) &= t^{(1)} + v^{(1)}(t), \end{aligned} \tag{2.1}$$

where $t^{(1)}$ ($v^{(1)}$) is the kinetic (potential) energy of a single particle, $w^{(2)}$ denotes the two-body interaction potential, and $\langle i|h^{(1)}(t)|j\rangle$ and $\langle ij|w^{(2)}|kl\rangle$ are the corresponding matrix elements, cf. Eq. (A.18). The great advantage of the second quantization formulation is that the anticommutation relations[4],

$$\left[\hat{f}_i, \hat{f}_j^\dagger\right]_+ = \delta_{ij}, \qquad \left[\hat{f}_i, \hat{f}_j\right]_+ = \left[\hat{f}_i^\dagger, \hat{f}_j^\dagger\right]_+ = 0, \tag{2.2}$$

take care of the correct symmetry of the many-body state. Moreover, the creation and annihilation operators often facilitate a simple form of single-particle operators. While the number operator is just $\hat{n}_i = \hat{f}_i^\dagger \hat{f}_i$, the one-particle reduced density matrix (1pRDM) operator reads,

$$\hat{\rho}_{1,ij} = \hat{f}_i^\dagger \hat{f}_j. \tag{2.3}$$

This matrix of operators yields after ensemble averaging the familiar one-particle density matrix $\rho_{1,ij} = \langle \hat{\rho}_{1,ij}\rangle$. Below, we will express it in terms of the single-particle Green's function, cf. Eq. (2.15).

In quantum mechanics, there exist different ways ("pictures") to account for time dependencies in a system. Despite their mathematical equivalence, the one or the other may allow for a more advantageous formulation of the problem considered. NEGFs make essential use of the Heisenberg picture (H). In contrast to the Schrödinger picture (S), where the system's state vector $\Psi_{\mathrm{S}}^{(N)}$ evolves in time and operators of observables are stationary, the Heisenberg picture allows for the operators to develop with time—at simultaneously time-independent states. The transformation between S and H is mediated by the unitary time evolution operator[5] which obeys the Schrödinger equation,

$$\mathrm{i}\hbar\frac{\partial}{\partial t'}\hat{U}(t',t) = \hat{H}(t')\hat{U}(t',t), \tag{2.4}$$

[3] $\hat{f}_i^\dagger$ ($\hat{f}_i$) adds (removes) a particle to (from) a spin orbital $|i\rangle$, e.g., Ref. [36].

[4] The anticommutator is defined as $[\hat{a},\hat{b}]_+ = \hat{a}\hat{b} + \hat{b}\hat{a}$. In the case of bosons, the same expressions hold with the commutator $[\cdot,\cdot]_+ \to [\cdot,\cdot]_-$.

[5] In matrix representation, the unitarity is expressed by $\hat{U}^\dagger\hat{U} = 1$.

with the initial condition $\hat{U}(t,t)=1$. The solution is,

$$\begin{aligned}\hat{U}(t',t)&=\hat{T}\exp\left(-\frac{\mathrm{i}}{\hbar}\int_t^{t'}\mathrm{d}\bar{t}\,\hat{H}(t)\right),\\ \hat{U}(t,t')\hat{U}(t',t)&=1,\end{aligned}\tag{2.5}$$

where $\hat{H}(t)$ is the full Hamiltonian, and $\hat{T}$ is the standard time-ordering operator[6]. For any operator $\hat{A}_{\mathrm{H}}$ in the Heisenberg picture, it is,

$$\hat{A}_{\mathrm{H}}(t)=\hat{U}(t_0,t)\hat{A}_{\mathrm{S}}\hat{U}(t,t_0),\tag{2.6}$$

$$\mathrm{i}\hbar\frac{\partial}{\partial t}\hat{A}_{\mathrm{H}}(t)=\left[\hat{A}_{\mathrm{H}}(t),\hat{H}_{\mathrm{H}}(t)\right]_-\quad\text{(Heisenberg equation)}.\tag{2.7}$$

The corresponding state vector $\Psi_{\mathrm{H}}^{(N)}(t_0)=\hat{U}(t_0,t)\Psi_{\mathrm{S}}^{(N)}(t)$ remains constant (t_0 gives only a reference time), and any operator that commutes with the Hamiltonian is a constant of motion, as is obvious from Eq. (2.7).

Using the Heisenberg picture, the creation and annihilation operators in Eqs. (2.1) to (2.3) become explicitly time-dependent, i.e., we replace $\hat{f}_i\to\hat{f}_{i,\mathrm{H}}(t)$. The anti-commutation relations of Eq. (2.2) then remain valid in the equal-time limit.

Furthermore, many situations require to properly define the initial state at the reference time t_0. In equilibrium, this may be an eigenstate of the system (for a pure quantum state) or a mixture of eigenstates defined through the statistical operator $\hat{\rho}$, cf. Appendix A. For an interacting many-body system, there are basically two different ways to account for stationary (generally correlated) initial states:

(i) through an adiabatic switch-on of the interaction [59, 65–67], where the system passes through a sequence of intermediate eigenstates, or
(ii) by starting from a (correlated) many-body state formulated in the picture of the grand canonical ensemble (GCE), e.g., [67, 68].

Of course, other approaches exist which *a priori* define (non-)correlated nonequilibrium initial states, see, e.g., Refs. [69–71] and references therein.

In this article, we mainly follow approach (ii), because the mathematical methods behind nonequilibrium Green's functions are most comprehensively developed along this line. However, strategy (i) is not irrelevant, and we will later emphasize its significance when using the generalized Kadanoff-Baym ansatz (GKBA), see Sect. 2.4.2.

2.1.1 Keldysh Contour

From now on, we suppose that the quantum many-body system of Eq. (2.1) [system (a)] exchanges particles and energy with a reservoir at a temperature

[6] In the interaction (or Dirac) picture (I), we deal with a representation intermediate between S and H, where usually the state vector $\Psi_{\mathrm{I}}^{(N)}$ carries the time dependence of some time-independent part $\hat{H}_0$ of the full Hamiltonian $\hat{H}(t)$.

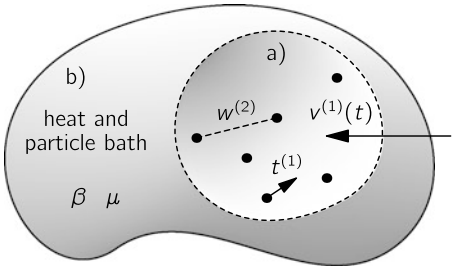

Fig. 2.1 Grand canonical ensemble (GCE) with inverse temperature $\beta = 1/(k_B T)$ and chemical potential μ. Whereas system (b) denotes the heat and particle reservoir, system (a) is the basic (open) system under investigation. In general, particles (*black dots*) and energy can be transferred between (a) and (b). Further, $w^{(2)}$ denotes the two-body interaction between identical particles (here, fermions) with kinetic energy $t^{(1)}$, and $v^{(1)}$ refers to the presence of a time-dependent local potential in (a), cf. Hamiltonian (2.1)

$T = (k_B \beta)^{-1}$ [system (b)]. Physically, this matter of fact is described by the grand canonical ensemble (GCE), see Fig. 2.1, whereby the exact state of the overall system is generally not known, and one has to resort to a mixed state (ensemble) description.

In the GCE, we can evaluate time-dependent averages of an observable $\hat{A}$ according to[7] (the system is in equilibrium for $t \leq t_0$),

$$\langle \hat{A} \rangle(t) = \frac{1}{Z_0} \mathrm{Tr} \left\{ \mathrm{e}^{-\beta(\hat{H}(t) - \mu \hat{N})} \hat{A}_S \right\}, \tag{2.8}$$

where $Z_0 = \mathrm{Tr}\{\mathrm{e}^{-\beta(\hat{H}(t_0) - \mu \hat{N})}\}$ is the partition function, μ denotes the one-particle chemical potential and $\hat{N}$ is the particle number operator. The trace is defined as in Appendix A.4, summing over a complete set of states in the Fock space.

Working out that, for the time-evolution operator of Eq. (2.5), it is $\hat{U}(t_0 - \mathrm{i}\beta, t_0) = \mathrm{e}^{-\beta(\hat{H}(t_0) - \mu \hat{N})}$, i.e., the initial statistical operator acts like an evolution operator in imaginary time, we can rewrite Eq. (2.8) using the cyclic invariance of the trace as[8],

$$\begin{aligned} \langle \hat{A} \rangle(t) &= \frac{1}{Z_0} \mathrm{Tr} \left\{ \hat{U}(t_0 - \mathrm{i}\beta, t_0) \hat{U}(t_0, t) \hat{A}_S \hat{U}(t, t_0) \right\} \\ &= \frac{1}{Z_0} \mathrm{Tr} \left\{ \hat{U}(t_0 - \mathrm{i}\beta, t_0) \hat{A}_H \right\}. \end{aligned} \tag{2.9}$$

From right to left, the first line indicates a successive time evolution of the system along a contour: First, it evolves along the real time axis from time t_0 to time t (where the operator acts) and back from t to t_0. Second, an additional evolution

[7] The subscript S in $\hat{A}_S$ indicates the Schrödinger picture.

[8] We emphasize that, with $\hat{U}(t_0 - \mathrm{i}\beta, t_0) = \hat{\rho}(t_0)$, it is the time-independent density operator that enters in the trace of Eq. (2.9).

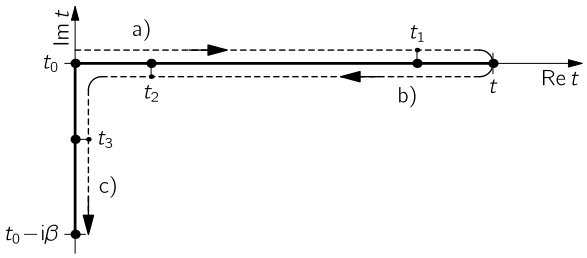

Fig. 2.2 Complex round-trip Keldysh contour $\mathscr{C}$ including three different branches denoted (a), (b) and (c). On $\mathscr{C}$, time t_2 is later than t_1, and time t_3 is later than t_1 and t_2, cf. the *arrows*

occurs parallel to the imaginary axis from time t_0 to time $t_0 - i\beta$. Such a complex time contour is originally due to Keldysh [59], and we refer to it as the contour $\mathscr{C}$. For illustration of the round-trip propagation path, see Fig. 2.2.

On the Keldysh contour[9], we can define a generalized time-ordering operator $\hat{T}_{\mathscr{C}}$, which works chronologically (antichronologically) on the upper (lower) branch of the contour and arranges imaginary times which originate from the vertical branch behind purely real times. For a contour-ordered product of operators $\hat{A}_{1,\mathrm{H}}(t_1)\ldots\hat{A}_{n,\mathrm{H}}(t_n)$ which commute pairwise at equal times, we then have $(t_1,\ldots t_n \in \mathscr{C})$,

$$\hat{T}_{\mathscr{C}}\left\{\hat{A}_{1,\mathrm{H}}(t_1)\ldots\hat{A}_{n,\mathrm{H}}(t_n)\right\} = \sum_{\mathscr{P}} \theta_{\mathscr{C}}(t_{\mathscr{P}(1)} - t_{\mathscr{P}(2)})\ldots\theta_{\mathscr{C}}(t_{\mathscr{P}(n-1)} - t_{\mathscr{P}(n)}) \times \hat{A}_{\mathscr{P}(1),\mathrm{H}}(t_{\mathscr{P}(1)})\ldots\hat{A}_{\mathscr{P}(n),\mathrm{H}}(t_{\mathscr{P}(n)}), \tag{2.10}$$

where $\theta_{\mathscr{C}}(t - t')$ is the contour step function that equals one for t later than t' on $\mathscr{C}$ and zero otherwise, cf. the arrows in Fig. 2.2.

We now can refine Eq. (2.9) as follows,

$$\langle\hat{A}\rangle(t) = \frac{1}{Z_0}\mathrm{Tr}\left\{\hat{T}_{\mathscr{C}}\exp\left(-\frac{\mathrm{i}}{\hbar}\int_{\mathscr{C}}\mathrm{d}\bar{t}\,\hat{H}(\bar{t})\right)\hat{A}_{\mathrm{S}}|_t\right\} = \frac{1}{Z_0}\mathrm{Tr}\{\hat{U}_{\mathscr{C}}\hat{A}_{\mathrm{S}}|_t\} \tag{2.11}$$

with the generalized time-evolution operator $\hat{U}_{\mathscr{C}}$.

The presence of the Keldysh contour assesses a contour algebra which was described in detail by DuBois [72] and Langreth [73] and which culminates in the application of the Langreth-Wilkins rules [74], see Table 2.1.

2.1.2 One-Particle Nonequilibrium Green's Function

The contour-ordered, one-particle nonequilibrium Green's function (1pNEGF) is defined according to (for simplicity, we drop subscripts H and S which indicate the Heisenberg or Schrödinger picture),

[9] Sometimes, $\mathscr{C}$ is called Schwinger-Keldysh contour.

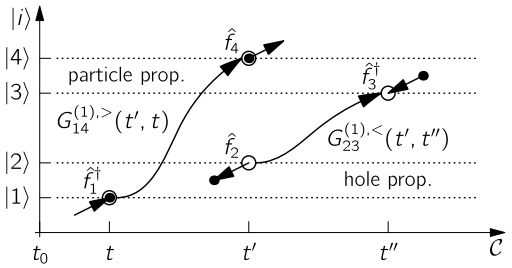

Fig. 2.3 The one-particle nonequilibrium Green's functions (correlation functions) $G^{(1),>}$ and $G^{(1),<}$ correspond, respectively, to the propagation of a "particle" and a "hole". The propagation paths are indicated by *curved arrows*

$$
\begin{aligned}
G_{ij}^{(1)}(t,t') &= -\frac{\mathrm{i}}{\hbar}\langle \hat{T}_{\mathscr{C}}\, \hat{f}_i(t)\hat{f}_j^\dagger(t')\rangle \\
&= \theta_{\mathscr{C}}(t-t')G_{ij}^{(1),>}(t,t') + \theta_{\mathscr{C}}(t'-t)G_{ij}^{(1),<}(t,t'),
\end{aligned}
\tag{2.12}
$$

where the times t and t' are located on the Keldysh contour $\mathscr{C}$, and the lesser and greater components[10] are,

$$
\begin{aligned}
G_{ij}^{(1),>}(t,t') &= -\frac{\mathrm{i}}{\hbar}\langle \hat{f}_i(t)\hat{f}_j^\dagger(t')\rangle, \\
G_{ij}^{(1),<}(t,t') &= \frac{\mathrm{i}}{\hbar}\langle \hat{f}_j^\dagger(t')\hat{f}_i(t)\rangle.
\end{aligned}
\tag{2.13}
$$

In the GCE, the ensemble average $\langle \ldots \rangle$ is evaluated as in Eq. (2.11), i.e.,

$$
G_{ij}^{(1)}(t,t') = -\frac{\mathrm{i}}{\hbar Z_0}\mathrm{Tr}\left\{\hat{U}_{\mathscr{C}}\, \hat{f}_i|_t\, \hat{f}_j^\dagger|_{t'}\right\}. \tag{2.14}
$$

Here, we restrict ourselves to fermions[11] and, furthermore, do not consider "anomalous" Green's functions[12] that are relevant for quantum coherence phenomena such as superfluidity or superconductivity [75–77].

In a quasi-particle picture, the greater component of the 1pNEGF describes the propagation of an added particle whereas the lesser component describes the propagation of a removed particle ("hole"), for illustration see Fig. 2.3. Moreover, the 1pNEGF is directly connected to all one-particle observables, as in the equal-time limit, we recover the 1pRDM (t real and $\varepsilon > 0$),

$$
\rho_{1,ij}(t) = -\mathrm{i}\hbar G_{ij}^{(1),<}(t,t) = -\mathrm{i}\hbar G_{ij}^{(1)}(t,t^+) = -\mathrm{i}\hbar \lim_{\varepsilon\to 0} G_{ij}^{(1)}(t,t+\varepsilon). \tag{2.15}
$$

As an illustration, consider the coordinate representation: With $G^{(1)}(\mathbf{r}t,\mathbf{r}'t') = \sum_{ij}\phi_i^*(\mathbf{r})\phi_j(\mathbf{r}')G_{ij}^{(1)}(t,t')$ for (spin) orbitals $|i\rangle = \phi_i(\mathbf{r})$, the total spatial and current density are given by (for fermions of mass m and no external vector potential applied),

[10] The greater and lesser components are also called correlation functions.

[11] For bosons, $G^{(1),<}$ carries the opposite spin.

[12] Containing two annihilation or two creation operators.

$$\begin{aligned}\rho_1(\mathbf{r},t) &= -\mathrm{i}\hbar G^{(1)}\big(\mathbf{r}t,\mathbf{r}t^+\big),\\ \mathbf{j}_1(\mathbf{r},t) &= -\mathrm{i}\hbar\left\{\frac{\nabla_{\mathbf{r}}-\nabla_{\mathbf{r}'}}{2m\mathrm{i}}G^{(1)}\big(\mathbf{r}t,\mathbf{r}t'\big)\right\}_{t'=t^+}.\end{aligned} \tag{2.16}$$

Furthermore, we define the spectral function,

$$A_{1,ij}\big(t,t'\big) = \mathrm{i}\hbar\big\{G_{ij}^{(1),>}\big(t,t'\big) - G_{ij}^{(1),<}\big(t,t'\big)\big\}, \tag{2.17}$$

which gives access to the local density of states and the addition, respectively, removal energies.

Instead of the prevailing definition (2.12), also matrix representations of the 1pNEGF have emerged. Useful 2 by 2 matrix notations cover only real-time arguments and are known from Keldysh theory. Thereby, different representations are connected by a linear transformation called "Keldysh rotation", see Ref. [74]. A common representation is (omitting the arguments),

$$\mathbf{G}_{2\times2}^{(1)} = \begin{bmatrix} G^{(1),\mathrm{R}} & G^{(1),<} \\ 0 & G^{(1),\mathrm{A}} \end{bmatrix}, \tag{2.18}$$

where the retarded (R) and advanced (A) Green's functions are given by,

$$G^{(1),\mathrm{R/A}}\big(t,t'\big) = \pm\theta_{\mathscr{C}}\big(\pm\big[t-t'\big]\big)\big\{G^{(1),>}\big(t,t'\big) - G^{(1),<}\big(t,t'\big)\big\}. \tag{2.19}$$

Allowing also for imaginary time arguments, we can extend Eq. (2.18) to a 3 by 3 matrix [78, 79], as there are generally nine possibilities to distribute the arguments along the three contour branches (a), (b) and (c) of Fig. 2.2:

$$\mathbf{G}_{3\times3}^{(1)} = \begin{bmatrix} G^{(1),\mathrm{c}} & G^{(1),<} & G^{(1),\rceil} \\ G^{(1),>} & G^{(1),\mathrm{a}} & G^{(1),\rceil} \\ G^{(1),\lceil} & G^{(1),\lceil} & G^{(1),\mathrm{M}} \end{bmatrix}. \tag{2.20}$$

Here, the causal (c) and anticausal (a) Green's functions are defined by,

$$G^{(1),\mathrm{c/a}}\big(t,t'\big) = \theta_{\mathscr{C}}\big(\pm\big[t-t'\big]\big)G^{(1),>}\big(t,t'\big) + \theta_{\mathscr{C}}\big(\pm\big[t'-t\big]\big)G^{(1),<}\big(t,t'\big), \tag{2.21}$$

and $G^{(1),\mathrm{M}}(t,t')$ denotes the Matsubara Green's function for which t and t' are on the imaginary track of $\mathscr{C}$. Further, the mixed Green's function $G^{(1),\rceil}$ (respectively, $G^{(1),\lceil}$) takes a real time as first (second) argument and an imaginary time as second (first) argument. As one generally does not distinguish the origin of the real-time arguments in $G^{(1),\rceil}$ and $G^{(1),\lceil}$, the symbols $\rceil$ ($\lceil$) are quite intuitive when reading them from left to right [80].

Note that both matrix representations, (2.18) and (2.20), are overcomplete because not all components are independent. Regarding the 3 by 3 matrix, either the four components $G^{(1),\mathrm{M}}$, $G^{(1),\lceil}$, $G^{(1),<}$ and $G^{(1),>}$ or $G^{(1),\mathrm{M}}$, $G^{(1),\lceil}$, $G^{(1),\mathrm{c}}$ and $G^{(1),\mathrm{a}}$ define a linear independent subset[13].

[13] Provided the system is in a nonequilibrium state. In the case of a 2 by 2 matrix, there are only two independent components, $G^{(1),>}$ and $G^{(1),<}$.

We collect some useful relations[14] (t_0 real, $\tau, \tau' \in [-\beta, 0]$):

$$\begin{aligned}
G_{ij}^{(1),>}(t,t) - G_{ij}^{(1),<}(t,t) &= -\frac{\mathrm{i}}{\hbar}\delta_{ij} \quad \text{(at equal times!)}, \\
G_{ij}^{(1)}\big(t_0 - \mathrm{i}\beta, t'\big) &= -G_{ij}^{(1)}\big(t_0, t'\big) \quad \text{(a)}, \\
G_{ij}^{(1)}(t, t_0) &= -G_{ij}^{(1)}(t, t_0 - \mathrm{i}\beta) \quad \text{(b)}, \\
G_{ij}^{(1),\mathrm{M}}\big(t_0 - \mathrm{i}0, t_0 - \mathrm{i}0^+\big) &= G_{ij}^{(1),<}(t_0, t_0) \quad \text{(c)}, \\
G_{ij}^{(1),\mathrm{M}}\big(t_0 - \mathrm{i}\tau, t_0 - \mathrm{i}\tau'\big) &= G_{ij}^{(1),\lceil}\big(t_0 - \mathrm{i}\big(\tau - \tau'\big), t_0\big) \quad \text{(d)}, \\
G_{ij}^{(1),\gtrless}\big(t, t'\big) &= -\big[G_{ji}^{(1),\gtrless}\big(t', t\big)\big]^*, \\
G_{ij}^{(1),\lceil}\big(t_0 - \mathrm{i}\tau, t'\big) &= \big[G_{ji}^{(1),\rceil}\big(t', t_0 - \mathrm{i}(\beta - \tau)\big)\big]^*.
\end{aligned} \tag{2.22}$$

In Eq. (2.22)(a) to (d), the system's Hamiltonian is time independent for times $t, t' \leq t_0$, and we assume a thermodynamic equilibrium with temperature β^{-1}. Further, in a matrix representation regarding the basis indices i and j, the last two properties read,

$$\begin{aligned}
G^{(1),\gtrless}\big(t, t'\big) &= -\big[G^{(1),\gtrless}\big(t', t\big)\big]^\dagger, \\
G^{(1),\lceil}\big(t_0 - \mathrm{i}\tau, t'\big) &= \big[G^{(1),\rceil}\big(t', t_0 - \mathrm{i}(\beta - \tau)\big)\big]^\dagger.
\end{aligned} \tag{2.23}$$

2.2 Equations of Motion

For the derivation of equations of motion for the 1pNEGF, we first consider its time derivative in terms of the greater and lesser components,

$$\begin{aligned}
\frac{\partial}{\partial t} G_{ij}^{(1)}\big(t, t'\big) = \delta_{\mathscr{C}}\big(t - t'\big)\big\{G_{ij}^{(1),>}\big(t, t'\big) - G_{ij}^{(1),<}\big(t, t'\big)\big\} \\
+ \theta_{\mathscr{C}}\big(t - t'\big)\frac{\partial}{\partial t} G_{ij}^{(1),>}\big(t, t'\big) + \theta_{\mathscr{C}}\big(t' - t\big)\frac{\partial}{\partial t} G_{ij}^{(1),<}\big(t, t'\big).
\end{aligned} \tag{2.24}$$

Due to the contour delta function, the difference between $G^{(1),>}$ and $G^{(1),<}$ in the first line will be evaluated only at equal times which gives rise to a factor $-\frac{\mathrm{i}}{\hbar}\delta_{ij}$, cf. Eq. (2.22). Explicitly writing out the second line yields with Eq. (2.13),

[14] Properties (a) and (b) are sometimes called Kubo-Martin-Schwinger (KMS) conditions and follow from Eq. (2.14) under the cyclic property of the trace. For bosons, the antiperiodicity turns into periodicity. In expression (c), the second time argument on the l.h.s. is infinitesimally larger on $\mathscr{C}$ than the first one.

$$
\begin{aligned}
&\mathrm{i}\hbar\frac{\partial}{\partial t}G^{(1)}_{ij}(t,t') \\
&\quad=\delta_{\mathscr{C}}(t-t')\delta_{ij} \\
&\qquad+\theta_{\mathscr{C}}(t-t')\left\langle\left\{\frac{\partial}{\partial t}\hat{f}_i(t)\right\}\hat{f}^{\dagger}_j(t')\right\rangle-\theta_{\mathscr{C}}(t'-t')\left\langle\hat{f}^{\dagger}_j(t')\left\{\frac{\partial}{\partial t}\hat{f}_i(t)\right\}\right\rangle, \qquad (2.25)
\end{aligned}
$$

where the dynamics of the annihilation operators is given by the Heisenberg equation (cf. Eq. (2.7)),

$$
\mathrm{i}\hbar\frac{\partial}{\partial t}\hat{f}_i(t)=\left[\hat{f}_i(t),\hat{H}(t)\right]_-. \qquad (2.26)
$$

Taking advantage of the relations in Eq. (A.11) of Appendix A, we readily evaluate the commutator in Eq. (2.26) as (summation over j', k and l is implied),

$$
\mathrm{i}\hbar\frac{\partial}{\partial t}\hat{f}_i(t)=\langle i|h^{(1)}|k\rangle\,\hat{f}_k(t)+\langle ij'|w^{(2)}|kl\rangle\,\hat{f}^{\dagger}_{j'}(t)\,\hat{f}_l(t)\,\hat{f}_k(t). \qquad (2.27)
$$

It follows[15],

$$
\begin{aligned}
\mathrm{i}\hbar\frac{\partial}{\partial t}G^{(1)}_{ij}(t,t')&=\delta_{\mathscr{C}}(t-t')\delta_{ij} \\
&\quad-\frac{\mathrm{i}}{\hbar}\langle i|h^{(1)}|k\rangle\left\{\theta_{\mathscr{C}}(t-t')\left\langle\hat{f}_k(t)\hat{f}^{\dagger}_j(t')\right\rangle-\theta_{\mathscr{C}}(t'-t)\left\langle\hat{f}^{\dagger}_j(t')\hat{f}_k(t)\right\rangle\right\} \\
&\quad-\frac{\mathrm{i}}{\hbar}\langle ij'|w^{(2)}|kl\rangle\left\{\theta_{\mathscr{C}}(t-t')\left\langle\hat{f}^{\dagger}_{j'}(t)\hat{f}_l(t)\hat{f}_k(t)\hat{f}^{\dagger}_j(t')\right\rangle\right. \\
&\quad\left.-\theta_{\mathscr{C}}(t'-t)\left\langle\hat{f}^{\dagger}_j(t')\hat{f}^{\dagger}_{j'}(t)\hat{f}_l(t)\hat{f}_k(t)\right\rangle\right\}. \qquad (2.28)
\end{aligned}
$$

While in the second term on the r.h.s. we can resubstitute the 1pNEGF $G^{(1)}_{kj}(t,t')$, the last term is more complicated involving averages over four operators. In order to identify these terms with the contour-ordered two-particle nonequilibrium Green's function[16] (2pNEGF),

$$
G^{(2)}_{ij,kl}(t,t';\bar{t},\bar{t}')=\left(-\frac{\mathrm{i}}{\hbar}\right)^2\left\langle\hat{T}_{\mathscr{C}}\hat{f}_i(t)\hat{f}_j(t')\hat{f}^{\dagger}_l(\bar{t}')\hat{f}^{\dagger}_k(\bar{t})\right\rangle, \qquad (2.29)
$$

we introduce the generalized (two-time but instantaneous) two-body interaction,

$$
w^{(2)}(t,t')=\delta_{\mathscr{C}}(t-t')w^{(2)}, \qquad (2.30)
$$

to be evaluated on the contour $\mathscr{C}$. Then, Eq. (2.28) becomes,

$$
\begin{aligned}
\mathrm{i}\hbar\frac{\partial}{\partial t}G^{(1)}_{ij}(t,t')&=\delta_{\mathscr{C}}(t-t')\delta_{ij}+\langle i|h^{(1)}|k\rangle G^{(1)}_{kj}(t,t') \\
&\quad-\frac{\mathrm{i}}{\hbar}\int_{\mathscr{C}}\mathrm{d}\bar{t}\,\langle ij'|w^{(2)}(t-\bar{t})|kl\rangle\left\{\theta_{\mathscr{C}}(t-t')\left\langle\hat{f}^{\dagger}_{j'}(\bar{t})\hat{f}_l(\bar{t})\hat{f}_k(t)\hat{f}^{\dagger}_j(t')\right\rangle\right. \\
&\quad\left.-\theta_{\mathscr{C}}(t'-t)\left\langle\hat{f}^{\dagger}_j(t')\hat{f}^{\dagger}_{j'}(\bar{t})\hat{f}_l(\bar{t})\hat{f}_k(t)\right\rangle\right\}. \qquad (2.31)
\end{aligned}
$$

[15] Again, the notation implies summation over all repeatedly occurring indices.

[16] In the language of quasi-particles, the 2pNEGF is a "particle-hole" propagator.

2.2.1 Keldysh-Kadanoff-Baym Equations

With the action of the time-ordering operator $\hat{T}_{\mathscr{C}}$ (recall Eq. (2.10) in Sect. 2.1), we identify the bracket in the last term of Eq. (2.31) including a prefactor of $-\hbar^{-2}$ as the 2pNEGF $G^{(2)}_{lk,jj'}(t,\bar{t},t'\bar{t}^{+})$, where $\bar{t}^{+}$ denotes the limit from above on the contour. The resulting equation determines the dynamics of the one-particle nonequilibrium Green's function with respect to the first time argument t. Starting in Eq. (2.24) with the time derivative with respect to t', we can derive a similar equation for $\frac{\partial}{\partial t'}G^{(1)}_{ij}(t,t')$.

Together, these two equations then form the equations of motion for the 1pNEGF, known as the two-time Keldysh-Kadanoff-Baym equations (KBEs)[17] [28]:

$$\begin{aligned}
&\left\{i\hbar\frac{\partial}{\partial t}\delta_{ik}-\langle i|h^{(1)}(t)|k\rangle\right\}G^{(1)}_{kj}(t,t')\\
&\quad=\delta_{\mathscr{C}}(t-t')\delta_{ij}-\mathrm{i}\hbar\int_{\mathscr{C}}\mathrm{d}\bar{t}\,\langle ij'|w^{(2)}(t-\bar{t})|kl\rangle G^{(2)}_{lk,jj'}(t,\bar{t};t',\bar{t}^{+}),\\
&G^{(1)}_{ik}(t,t')\left\{-i\hbar\frac{\partial}{\partial t'}\delta_{kj}-\langle k|h^{(1)}(t')|j\rangle\right\}\\
&\quad=\delta_{\mathscr{C}}(t-t')\delta_{ij}-\mathrm{i}\hbar\int_{\mathscr{C}}\mathrm{d}\bar{t}\,G^{(2)}_{li,kj'}(t,\bar{t};t',\bar{t}^{+})\langle kj'|w^{(2)}(t'-\bar{t})|jl\rangle.
\end{aligned}\tag{2.32}$$

A few remarks are in order:

(i) The KBEs are a set of coupled (non-Markovian[18]) integro-differential equations and are valid for imaginary and real times defined on the round-trip Keldysh contour $\mathscr{C}$. Note that the second equation in (2.32) is just the adjoint of the first one with the times interchanged, i.e., $t \leftrightarrow t'$.

(ii) The boundary (respectively, initial) conditions for the KBEs are given by the Kubo-Martin-Schwinger (KMS) relations formulated as properties (a) and (b) in Eq. (2.22), cf. [57, 81]. If the equilibrium Matsubara Green's function of the system is known, sufficient KMS conditions are expressions (c) and (d) in Eq. (2.22).

(iii) The KBEs in the form of Eq. (2.32) are not closed, i.e., they do not uniquely define the 1pNEGF without further knowledge. Instead, each KBE requires the 2pNEGF which in turn satisfies the Bethe-Salpeter equation, cf. Refs. [82, 83]. Generally, the equation of motion for $G^{(n)}$ $(n \geq 2)$ requires information about $G^{(n-1)}$ and $G^{(n+1)}$, cf. Refs. [83, 84]. From this point of view, the KBEs represent only the first equations of a complete hierarchy of equations of motion for the NEGFs. This hierarchy is known as the Martin-Schwinger (MS) hierarchy [57].

[17] Summation over j, k and l is implied. For bosons, the contour integrals in the KBEs take a prefactor of $+\mathrm{i}\hbar$.

[18] This means they involve a time integral that reflects memory effects.

(iv) In the special case of equal time arguments, $t = t'$, the MS hierarchy reduces to the BBGKY (Bogolyubov-Born-Green-Kirkwood-Yvon) hierarchy for the reduced density operators, cf., e.g., Ref. [11]. The special case of the dynamics of single-time quantities will be studied in Sect. 4.2.3.

In order to transform the KBEs (2.32) into a closed form avoiding the MS hierarchy, we have to express the 2pNEGF in terms of the 1pNEGF. However, in the presence of correlations, this can be done only by summing over an infinite number of contributions. For this reason, we generally have to resort to approximations when dealing with nonequilibrium Green's functions. Highly useful expansions are provided by many-body perturbation theory (MBPT). To give details in this regard and to cover topics such as "self-consistency" and "conserving approximations" is the task of Sect. 2.3.

Formally, we can rewrite the contour integral in the KBEs as a convolution and include all interaction effects into a one-particle self-energy[19] (1pSE) $\Sigma^{(1)}$:

$$-\mathrm{i}\hbar \int_{\mathscr{C}} \mathrm{d}\bar{t}\, \langle i j' | w^{(2)}(t-\bar{t}) | k l \rangle G^{(2)}_{lk,jj'}\big(t,\bar{t};t',\bar{t}^{+}\big) = \int_{\mathscr{C}} \mathrm{d}\bar{t}\, \Sigma^{(1)}_{ik}(t,\bar{t}) G^{(1)}_{kj}\big(\bar{t},t'\big), \tag{2.33}$$

$$\Sigma^{(1)}_{ij}\big(t,t'\big) = \Sigma^{(1)}_{ij}\big[G^{(1)}, w^{(2)}\big]\big(t,t'\big).$$

In the course of this, the self-energy becomes a functional of the 1pNEGF and the generalized two-body interaction $w^{(2)}$. Often one distinguishes between the regular ("time-diagonal" or "time-local") part of the self-energy $\Sigma^{(1)}_{\mathrm{reg}}(t,t') \propto \delta_{\mathscr{C}}(t-t')$ and the irregular part $\Sigma^{(1)}_{\mathrm{cor}}(t,t')$. Whereas for the former the KBEs are trivial to solve as they become Markovian (the contour integral vanishes), the latter keeps the non-Markovian structure and accounts for memory effects, i.e., correlations.

Using, e.g., the matrix representation of Eq. (2.18), the KBEs can also be written in form of a Dyson equation (we drop the label "2×2" for the Green's functions),

$$\mathbf{G}^{(1)} = \mathbf{G}^{(1)}_0 + \mathbf{G}^{(1)}_0 \Sigma^{(1)}_{2\times 2} \mathbf{G}^{(1)}, \tag{2.34}$$

where $\mathbf{G}^{(1)}_0$ denotes the 1pNEGF of the ideal, non-interacting system. The self-energy matrix $\Sigma^{(1)}_{2\times 2}$ has the same components as $\mathbf{G}^{(1)}$ and $\mathbf{G}^{(1)}_0$ in Eq. (2.18) and acts as integration kernel. Further, the product in Eq. (2.34) involves by definition the integration over two intermediate time variables. For two functions $\mathbf{A}$ and $\mathbf{B}$ in Keldysh space[20], it is,

$$\{\mathbf{AB}\}\big(t,t'\big) = \int_{\mathscr{C}} \mathrm{d}\bar{t}\, \mathbf{A}(t,\bar{t})\mathbf{B}\big(\bar{t},t'\big). \tag{2.35}$$

To specify the structure of the (collision) integral on the r.h.s. of Eq. (2.33) in terms of components of the 1pSE and the 1pNEGF, one most easily applies the Langreth-Wilkins rules. A tabular summary of these can be found in Table 2.1. The operations indicated by $\star$ and $\circ$ are defined by ($x, y \in \{\mathrm{A}, \mathrm{R}, >, <, \rceil, \lceil\}$),

[19] We sum over k.

[20] I.e., contour-ordered functions $\mathbf{A}(t,t')$ and $\mathbf{B}(t,t')$ with $t, t' \in \mathscr{C}$.

Table 2.1 Langreth-Wilkins rules for the multiplication and convolution of two contour-ordered functions **A** and **B**. The result **C** is again a function on the Keldysh space and has the indicated components. The operations denoted by $\star$ and $\circ$ are defined by Eqs. (2.36) and (2.37)

	$C(t,t') = A(t,t')B(t',t)$	$C(t,t') = \int_{\mathscr{C}} \mathrm{d}\bar{t}\, A(t,\bar{t})B(\bar{t},t')$
C^{M}	$A^{\mathrm{M}}B^{\mathrm{M}}$	$A^{\mathrm{M}} \star B^{\mathrm{M}}$
$C^{\lceil}$	$A^{\lceil}B^{\rceil}$	$A^{\lceil} \circ B^{\mathrm{A}} + A^{\mathrm{M}} \star B^{\lceil}$
$C^{\rceil}$	$A^{\rceil}B^{\lceil}$	$A^{\mathrm{R}} \circ B^{\rceil} + A^{\rceil} \star B^{\mathrm{M}}$
$C^{>}$	$A^{>}B^{<}$	$A^{\mathrm{R}} \circ B^{>} + A^{>} \circ B^{\mathrm{A}} + A^{\rceil} \star B^{\lceil}$
$C^{<}$	$A^{<}B^{>}$	$A^{\mathrm{R}} \circ B^{<} + A^{<} \circ B^{\mathrm{A}} + A^{\rceil} \star B^{\lceil}$
C^{R}	$A^{\mathrm{R}}B^{>} + A^{>}B^{\mathrm{A}}$	$A^{\mathrm{R}} \circ B^{\mathrm{R}}$
C^{A}	$A^{\mathrm{A}}B^{<} + A^{<}B^{\mathrm{R}}$	$A^{\mathrm{A}} \circ B^{\mathrm{A}}$

$$\left\{A^x \circ B^y\right\}(t,t') = \int_{t_0}^{\infty} \mathrm{d}\bar{t}\, A^x(t,\bar{t})B^y(\bar{t},t'), \tag{2.36}$$

and,

$$\begin{aligned}
\left\{A^{\mathrm{M}} \star B^{\mathrm{M}}\right\}(\tau) &= \int_0^{\beta} \mathrm{d}\bar{\tau}\, A^{\mathrm{M}}(\tau-\bar{\tau})B^{\mathrm{M}}(\bar{\tau}),\\
\left\{A^{\mathrm{M}} \star B^{\lceil}\right\}(t_0 - \mathrm{i}\tau, t) &= \int_0^{\beta} \mathrm{d}\bar{\tau}\, A^{\mathrm{M}}(\tau-\bar{\tau})B^{\lceil}(t_0 - \mathrm{i}\bar{\tau}, t),\\
\left\{A^{\rceil} \star B^{\mathrm{M}}\right\}(t, t_0 - \mathrm{i}\tau) &= \int_0^{\beta} \mathrm{d}\bar{\tau}\, A^{\rceil}(t, t_0 - \mathrm{i}\bar{\tau})B^{\mathrm{M}}(\bar{\tau}-\tau),\\
\left\{A^{\rceil} \star B^{\lceil}\right\}(t,t') &= -\mathrm{i}\int_0^{\beta} \mathrm{d}\bar{\tau}\, A^{\rceil}(t, t_0 - \mathrm{i}\bar{\tau})B^{\lceil}(t_0 - \mathrm{i}\bar{\tau}, t').
\end{aligned} \tag{2.37}$$

2.2.2 Equilibrium Limit. Dyson Equation

The KBEs (2.32) are valid for all times t and t' on the contour $\mathscr{C}$. However, if the Hamiltonian of the system is time independent (note that this is assumed above for times $t, t' \leq t_0$), the only independent matrix component of the Green's function is $G^{(1),\mathrm{M}}$. As a consequence, the contour reduces to its imaginary track, and the KBEs (2.32) with closure (2.33) simplify to the Dyson equation for the Matsubara Green's function[21],

[21] Summation over k is implied.

$$\left\{\mathrm{i}\hbar\frac{\partial}{\partial\tau}\delta_{ik}-\langle i|h^{(1)}|k\rangle\right\}G^{(1),\mathrm{M}}_{kj}(\tau)=\delta(\tau)\delta_{ij}+\int_0^\beta \mathrm{d}\bar{\tau}\;\Sigma^{(1),\mathrm{M}}_{ik}(\tau-\bar{\tau})G^{(1)}_{kj}(\bar{\tau}),\tag{2.38}$$

in which we have applied the transformation,

$$\mathscr{X}_{ij}\big(\tau-\tau'\big)=-\mathrm{i}\hbar\mathscr{X}_{ij}\big(t_0-\mathrm{i}\tau,t_0-\mathrm{i}\tau'\big),\tag{2.39}$$

to the 1pNEGF ($\mathscr{X}=G^{(1),\mathrm{M}}$) and the 1pSE ($\mathscr{X}=\Sigma^{(1),\mathrm{M}}$). In this notation, the time difference $\tau-\tau'$ generally ranges from $-\beta$ to $+\beta$, and the equilibrium 1pRDM is simply,

$$\rho_{1,ij}=G^{(1),\mathrm{M}}_{ij}\big(0^-\big).\tag{2.40}$$

Further, the antiperiodicity properties (a) and (b) of Eq. (2.22) allow us to restrict the solution of Eq. (2.38) to a half interval, e.g., $[-\beta,0]$ which includes the reduced density matrix at the upper interval boundary[22].

If we include the regular part of the self-energy,

$$\Sigma^{(1),\mathrm{M}}_{\mathrm{reg},ij}(\tau)=\delta(\tau)\Sigma^{(1),\mathrm{M}}_{0,ij},\tag{2.41}$$

in an effectively non-interacting Green's function[23] $G^{(1),\mathrm{M}}_0(\tau)$, the Dyson equation attains the form (compare with Eq. (2.34)),

$$\begin{aligned}G^{(1),\mathrm{M}}_{ij}(\tau)&=G^{(1),\mathrm{M}}_{0,ij}(\tau)+\int_0^\beta \mathrm{d}\bar{\tau}\int_0^\beta \mathrm{d}\bar{\bar{\tau}}\;\Sigma^{(1),\mathrm{K}}_{ik}(\bar{\tau}-\bar{\bar{\tau}})G^{(1),\mathrm{M}}_{kj}(\bar{\bar{\tau}}),\\ \Sigma^{(1),\mathrm{K}}_{ij}(\tau)&=\Sigma^{(1),\mathrm{M}}_{ij}(\tau)-\Sigma^{(1),\mathrm{M}}_{\mathrm{reg},ij}(\tau).\end{aligned}\tag{2.42}$$

It is important to note that here (aside from $w^{(2)}$) the self-energy $\Sigma^{(1),\mathrm{M}}_0$ is strictly a functional of the effectively non-interacting Green's function, whereas $\Sigma^{(1),\mathrm{M}}(\tau)$ depends on the full Green's function and includes, both, a regular and an irregular part.

If the effectively non-interacting Green's function $G^{(1),\mathrm{M}}_0(\tau)$ is known, Eq. (2.42) can be solved by iteration starting from setting $G^{(1),\mathrm{M}}(\tau)=G^{(1),\mathrm{M}}_0(\tau)$ on the r.h.s. Eventually, a self-consistent Matsubara Green's function is reached. Together with transformation (2.39) and properties (c) and (d) of Eq. (2.22), this solution serves as a proper initial condition for the real-time propagation of the 1pNEGF. This means that, in this case, the many-body system will remain stationary in time as long as no external field is applied and the same "conserving" approximation is used for the self-energy, cf. Sect. 2.3.1.

---

[22] Sometimes, $G^{(1),\mathrm{M}}(\tau)$ is considered on the symmetric interval $[-\frac{\beta}{2},\frac{\beta}{2}]$, see, e.g., [85].

[23] The corresponding Dyson equation is obtained by replacing the one-particle energy $\langle i|h^{(1)}|j\rangle$ in Eq. (2.38) by $\langle i|h^{(1)}|j\rangle+\Sigma^{(1),\mathrm{M}}_{0,ij}$ and setting the integration kernel to zero. Sometimes, one refers to $G^{(1),\mathrm{M}}_0$ as the "undressed" ("bare") Green's function whereas the full Green's function $G^{(1),\mathrm{M}}$ is the "dressed" one.

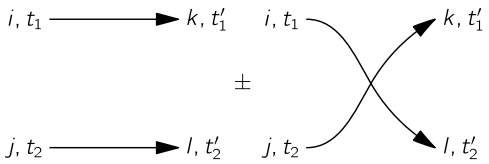

Fig. 2.4 Hartree-Fock: the simplest conserving approximation for the two-particle Green's function $G^{(2)}_{ij,kl}(t_1,t_2;t_1',t_2')$, cf. Eq. (2.43). The sign refers to bosons (+) and fermions (−)

2.3 Many-Body Approximations

One of the key problems in solving the Kadanoff-Baym equations (2.32) as well as the Dyson equation (2.38) is the fact that basically exact knowledge of the two-particle Green's function is required due to the presence of the MS hierarchy, cf. Sect. 2.2.1, point (iii). Unfortunately, $G^{(2)}$ is in general unknown. Therefore, we have to perform a truncation of the hierarchy through a many-body approximation (MBA).

The simplest hierarchy decoupling is achieved in the so-called Hartree-Fock (HF) approximation,

$$G^{(2)}_{ij,kl}(t_1,t_2;t_1',t_2') \approx G^{(1)}_{ik}(t_1,t_1')G^{(1)}_{jl}(t_2,t_2') + G^{(1)}_{il}(t_1,t_2')G^{(1)}_{jk}(t_2,t_1'). \quad (2.43)$$

For plasmas, it leads to a quantum mechanical version of the Vlasov equation [83]. In terms of one-particle propagators (representable by arrows) we can illustrate Eq. (2.43) as shown in Fig. 2.4.

Inserting the HF approximation for $G^{(2)}$ into the first KBE, we obtain (for fermions),

$$\begin{aligned}\left\{\mathrm{i}\hbar\frac{\partial}{\partial t}\delta_{ik} - \langle i|h^{(1)}(t)|k\rangle\right\}G^{(1)}_{kj}(t,t') \\ = \delta_{\mathscr{C}}(t-t')\delta_{ij} - \mathrm{i}\hbar\int_{\mathscr{C}}\mathrm{d}\bar{t}\,\langle ij'|w^{(2)}(t-\bar{t})\langle kl|\{G^{(1)}_{lj}(t,t')G^{(1)}_{kj'}(\bar{t},\bar{t}^+) \\ - G^{(1)}_{il}(t,\bar{t}^+)G^{(1)}_{kj}(t',\bar{t})\},\end{aligned} \quad (2.44)$$

where we sum over j', k and l. If we express the integral on the r.h.s. in the form of Eq. (2.33) using a 1pSE, we easily verify that,

$$\Sigma^{(1),\mathrm{HF}}_{ij}(t,t') = \Sigma^{(1),\mathrm{H}}_{ij}(t,t') + \Sigma^{(1),\mathrm{F}}_{ij}(t,t'), \quad (2.45)$$

with (retaining the generalized two-body interaction),

$$\begin{aligned}\Sigma^{(1),\mathrm{H}}_{ij}(t,t') &= -\mathrm{i}\hbar\delta_{\mathscr{C}}(t-t')\int_{\mathscr{C}}\mathrm{d}\bar{t}\,\langle ij|w^{(2)}(t-\bar{t})|kl\rangle G^{(1)}_{kl}(\bar{t},\bar{t}^+), \\ \Sigma^{(1),\mathrm{F}}_{ij}(t,t') &= \mathrm{i}\hbar\langle il|w^{(2)}(t^+-t')|kj\rangle G^{(1)}_{kl}(t,t').\end{aligned} \quad (2.46)$$

The first (second) term is the Hartree (Fock) self-energy, whereby the Fock contribution accounts for exchange effects, i.e., for the Pauli exclusion principle in the case of fermions. Moreover, as $w^{(2)}(t-t')$ involves a contour delta function, we directly observe that the HF approximation leads to a regular (time-local) self-energy and,

thus, neglects correlation effects. Improvements of Eq. (2.43) beyond Hartree-Fock are obtained by vertex corrections, e.g., [86], and will be discussed in the following. An important necessary criterion for the construction of approximations is that they retain the symmetries and conservation laws of the original (exact) Hamiltonian.

2.3.1 Requirements for a Conserving Scheme

If we analyze the HF approximation of Eq. (2.43), we realize that the approximate 2pNEGF obeys a specific symmetry: It is invariant under the simultaneous exchange of the first and the second pair of (spatial and temporal) arguments. Also, we find that, when applying the HF approximation to the KBEs (2.32), the system's total energy, particle number and momentum are preserved[24]. For this reason, HF is called a "conserving" approximation. In this regard, we note that the 1pNEGF allows us to determine the total energy by (we sum over i and j, i.e., take the trace),

$$\langle \hat{H} \rangle(t) = -\mathrm{i}\hbar G_{ij}^{(1)}\left(t, t^{+}\right)\langle j|h^{(1)}(t)|i\rangle - \frac{\mathrm{i}\hbar}{2}\int_{\mathscr{C}} \mathrm{d}\bar{t}\; \Sigma_{ij}^{(1)}(t,\bar{t})G_{ji}^{(1)}\left(\bar{t}, t^{+}\right). \quad (2.47)$$

The equilibrium limit of this is,

$$\langle \hat{H} \rangle = G_{ij}^{(1)\mathrm{M}}\left(0^{-}\right)\langle j|h^{(1)}|i\rangle + \frac{1}{2}\int_{0}^{\beta} \mathrm{d}\tau\; \Sigma_{ij}^{(1),\mathrm{M}}(-\tau)G_{ji}^{(1),\mathrm{M}}(\tau). \quad (2.48)$$

In fact, it has been shown by Baym [87] that the symmetry of $G^{(2)}$ in Eq. (2.43) is directly linked to important conservation laws and the preservation of particle number. More precisely, an arbitrary MBA is automatically conserving if,

(i) the approximate 1pNEGF simultaneously satisfies the two KBEs in the form of Eq. (2.32), and
(ii) the approximation for $G^{(2)}$ is in line with the symmetry,

$$G_{ij,kl}^{(2)}\left(t_1, t_2; t_1^{+}, t_2^{+}\right) = G_{ji,lk}^{(2)}\left(t_2, t_1; t_2^{+}, t_1^{+}\right). \quad (2.49)$$

Conditions (i) and (ii) represent important criteria for the development of self-consistent solutions of the KBEs beyond the HF level. Condition (ii) is simple to verify if the approximate dependence of $G^{(2)}$ on $G^{(1)}$ is known. On the other hand, a condition equivalent to (ii) can be formulated for the one-particle self-energy, cf. the discussion on "Φ-derivable" approximations in the following subsection.

2.3.2 Perturbation Expansions

There exist at least two ways of generating perturbative solutions of the Kadanoff-Baym equations: Either one can apply an iterative procedure using the integral ver-

[24] For an analysis of conservation laws, we refer to Ref. [28].

sion of the equations of motion for $G^{(1)}$ (Dyson's equation) or one can directly apply self-consistent approximations to the self-energy.

First, we will review the iterative procedure. To this end, we start from taking the functional derivative of the 1pNEGF with respect to the one-particle potential energy $v^{(1)}(t)$. Working out the derivative of time-ordered products, cf. Appendix B.1, we can write (omitting spatial and spin degrees of freedom),

$$\frac{\delta G^{(1)}(t,t')}{\delta v^{(1)}(\bar{t})} = G^{(1)}(t,t')G^{(1)}(\bar{t},\bar{t}^{+}) - G^{(2)}(t,\bar{t};t'\bar{t}^{+}). \tag{2.50}$$

This identity allows us to express the 2pNEGF in the Kadanoff-Baym equations in terms of $\delta G^{(1)}/\delta v^{(1)}$ [28]. The first equation of motion then reads[25],

$$\begin{aligned}\left\{\mathrm{i}\hbar\frac{\partial}{\partial t} - h^{(1)}(t)\right\}G^{(1)}(t,t') \\ = \delta_{\mathscr{C}}(t-t') - \mathrm{i}\hbar\int_{\mathscr{C}}\mathrm{d}\bar{t}\, w^{(2)}(t-\bar{t})\left\{G^{(1)}(\bar{t},\bar{t}^{+}) - \frac{\delta}{\delta v^{(1)}(\bar{t})}\right\}G^{(1)}(t,t').\end{aligned} \tag{2.51}$$

Unfortunately, Eq. (2.51) is not suited for a straightforward solution. However, it can be converted into an integral equation using the non-interacting Green's function which obeys,

$$\left\{\mathrm{i}\hbar\frac{\partial}{\partial t} - h^{(1)}(t)\right\}G_0^{(1)}(t,t') = \delta_{\mathscr{C}}(t-t'), \tag{2.52}$$

and has the inverse[26] $[G_0^{(1)}]^{-1}(t,t') = \delta_{\mathscr{C}}(t-t')\{\mathrm{i}\hbar\frac{\partial}{\partial t'} - h^{(1)}(t')\}$. Using Eqs. (2.50) and (2.52), we obtain,

$$\begin{aligned}G^{(1)}(t,t') = G_0^{(1)}(t,t') - \mathrm{i}\hbar\int_{\mathscr{C}}\mathrm{d}\bar{t}\int_{\mathscr{C}}\mathrm{d}\bar{\bar{t}}\, G^{(1)}(t,\bar{t})w^{(2)}(\bar{t}-\bar{\bar{t}}) \\ \times\left\{G^{(1)}(\bar{\bar{t}},\bar{\bar{t}}^{+}) + \frac{\delta}{\delta v^{(1)}(\bar{\bar{t}})}\right\}G^{(1)}(\bar{t},t'),\end{aligned} \tag{2.53}$$

which is a formal solution of Eq. (2.51) and satisfies the KMS conditions.

Equation (2.53) is the starting point for expanding the 1pNEGF in a power series regarding the interaction $w^{(2)}$. The individual contributions are obtained by iteration. While the zeroth order is just $G^{(1)} = G_0^{(1)}$, the first-order expression follows from substituting the non-interacting Green's function on the r.h.s. yielding,

$$\begin{aligned}G^{(1)}(t,t') = G_0^{(1)}(t,t') - \mathrm{i}\hbar\int_{\mathscr{C}}\mathrm{d}\bar{t}\int_{\mathscr{C}}\mathrm{d}\bar{\bar{t}}\, G_0^{(1)}(t,\bar{t})w^{(2)}(\bar{t}-\bar{\bar{t}}) \\ \times\left\{G_0^{(1)}(\bar{\bar{t}},\bar{\bar{t}}^{+}) + \frac{\delta}{\delta v^{(1)}(\bar{\bar{t}})}\right\}G_0^{(1)}(\bar{t},t').\end{aligned} \tag{2.54}$$

[25] Note, that $h^{(1)}(t) = t^{(1)} + v^{(1)}(t)$.

[26] The inverse Green's function is defined as $\int_{\mathscr{C}}\mathrm{d}\bar{t}\,[G^{(1)}]^{-1}(t,\bar{t})G^{(1)}(\bar{t},t') = \delta_{\mathscr{C}}(t-t')$.

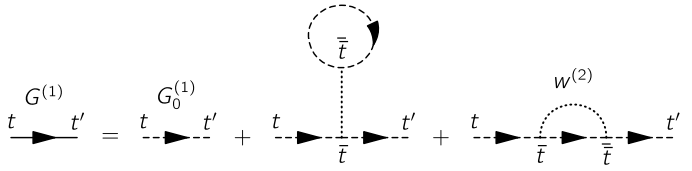

Fig. 2.5 Diagrammatic representation of the first-order iteration result of Eq. (2.56) leading to the Hartree-Fock (HF) approximation. The (non-)interacting 1pNEGF is indicated by *solid* (*dashed*) *arrows*. The *dotted lines* mark the generalized two-body interaction potential $w^{(2)}$

In contrast to Eq. (2.53), the functional derivative is here simple to evaluate[27]:

$$\frac{\delta G_0^{(1)}(t,t')}{\delta v^{(1)}(\bar{t})} = G_0^{(1)}(t,\bar{t})G_0^{(1)}(\bar{t},t'). \tag{2.55}$$

Hence, in the first-order approximation (in $w^{(2)}$), the KBEs obtain the integral form,

$$\begin{aligned} G^{(1)}(t,t') = G_0^{(1)}(t,t') - \mathrm{i}\hbar \int_{\mathscr{C}} \mathrm{d}\bar{t} \int_{\mathscr{C}} \mathrm{d}\bar{\bar{t}}\; G_0^{(1)}(t,\bar{t}) w^{(2)}(\bar{t}-\bar{\bar{t}}) \\ \times \left\{ G_0^{(1)}(\bar{\bar{t}},\bar{\bar{t}}^+) G_0^{(1)}(\bar{t},t') - G_0^{(1)}(\bar{t},\bar{\bar{t}}^+) G_0^{(1)}(\bar{\bar{t}},t') \right\}. \end{aligned} \tag{2.56}$$

Comparing the last part of the integrand in Eq. (2.56) to Eq. (2.44), we find that the solution of first order is just the HF approximation expanded to first order in the interaction, cf. Fig. 2.5. Substituting $G^{(1)}$ for $G_0^{(1)}$ in the brackets leads to the full HF approximation.

In order to generate higher-order contributions, we reinsert Eq. (2.56) into the initial equation (2.53) and replace the derivative with respect to $v^{(1)}$ again by Eq. (2.55). Doing so, most of the terms in second order just originate from iterating the Hartree-Fock equation. The additional ones are counted among the lowest-order terms of a many-body approximation beyond Hartree-Fock (the second Born approximation). We note that the exact 1pNEGF follows from accounting for all topologically distinct connected diagrams, for a discussion see, e.g., Ref. [28].

Often, only summations of infinite classes of terms have reasonable convergence properties. Therefore, an expansion of $G^{(1)}$ in powers of $w^{(2)}$ and $G_0^{(1)}$ is not really practical. To overcome this bottleneck, it is a great advantage, that sums of infinite classes are equivalently obtained by expanding the 1pSE in terms of $w^{(2)}$ and the full, interacting 1pNEGF. Such an approach leads to a self-consistent approximation and, potentially, is conserving (compare with Sect. 2.3.1).

The starting points are the following equations for the 1pSE and the derivative $\delta G^{(1)}/\delta v^{(1)}$ of Eq. (2.50), which generate higher-order approximations by iterative use[28]:

[27] The result follows from evaluating $\frac{\delta}{\delta v^{(1)}(\bar{\bar{t}})} \int_{\mathscr{C}} \mathrm{d}\bar{t}\, [G_0^{(1)}]^{-1}(t,\bar{t}) G_0^{(1)}(\bar{t},t') = 0$ under the product rule, multiplying by $G_0^{(1)}$ from the left, integrating over a second time variable and using the definition of the inverse $[G_0^{(1)}]^{-1}$ as defined below Eq. (2.52).

[28] For the derivations, see Appendix B.2 and Refs. [88, 89].

$$\Sigma^{(1)}(t,t') = \mathrm{i}\hbar w^{(2)}(t^+ - t')G^{(1)}(t,t') - \mathrm{i}\hbar\delta_{\mathscr{C}}(t-t')\int_{\mathscr{C}} \mathrm{d}\bar{t}\, w^{(2)}(t-\bar{t})G^{(1)}(\bar{t},\bar{t}^+) + \mathrm{i}\hbar\int_{\mathscr{C}}\mathrm{d}\bar{t}\int_{\mathscr{C}}\mathrm{d}\bar{\bar{t}}\, G^{(1)}(t,\bar{t})w^{(2)}(\bar{t}^+ - \bar{\bar{t}})\frac{\delta\Sigma^{(1)}(\bar{t},t')}{\delta v^{(1)}(\bar{\bar{t}})}, \quad (2.57)$$

$$\frac{\delta G^{(1)}(t,t')}{\delta v^{(1)}(\bar{t})} = G^{(1)}(t,\bar{t})G^{(1)}(\bar{t},t') + \int_{\mathscr{C}}\mathrm{d}t_1\int_{\mathscr{C}}\mathrm{d}t_2\, G^{(1)}(t,t_1)\frac{\delta\Sigma^{(1)}(t_1,t_2)}{\delta v^{(1)}(\bar{t})}G^{(1)}(t_2,t'). \quad (2.58)$$

Neglecting the derivative $\delta\Sigma^{(1)}/\delta v^{(1)}$ on the r.h.s., we arrive again at the HF approximation for the self-energy, i.e., we get $\Sigma^{(1),\mathrm{HF}}$ which is regular and of first order in the interaction, compare with Eqs. (2.45) and (2.46).

The first iteration of Eq. (2.57) yields [88, 89],

$$\Sigma^{(1)}(t,t') = \Sigma^{(1),\mathrm{HF}} + \mathrm{i}\hbar\int_{\mathscr{C}}\mathrm{d}\bar{t}\int_{\mathscr{C}}\mathrm{d}\bar{\bar{t}}\, G^{(1)}(t,\bar{t})w^{(2)}(\bar{t}^+ - \bar{\bar{t}}) \times \frac{\delta}{\delta v^{(1)}(\bar{\bar{t}})}\left\{\Sigma^{(1),\mathrm{HF}}(\bar{t},t') + \mathrm{i}\hbar\int_{\mathscr{C}}\mathrm{d}t_1\int_{\mathscr{C}}\mathrm{d}t_2\, G^{(1)}(\bar{t},t_1)w^{(2)}(\bar{t}^+,t_2)\frac{\delta\Sigma^{(1)}(t_1,t')}{\delta v^{(1)}(t_2)}\right\}, \quad (2.59)$$

where the derivative $\delta\Sigma^{(1),\mathrm{HF}}/\delta v^{(1)}$ evaluates with Eq. (2.46) and Eq. (2.58) to,

$$\begin{aligned}\frac{\delta\Sigma^{(1),\mathrm{HF}}(\bar{t},t')}{\delta v^{(1)}(\bar{\bar{t}})} &= \mathrm{i}\hbar\frac{\delta G^{(1)}(\bar{t},t')}{\delta v^{(1)}(\bar{\bar{t}})}w^{(2)}(\bar{t}^+,t') - \mathrm{i}\hbar\int_{\mathscr{C}}\mathrm{d}t_1\, w^{(2)}(t',t_1)\frac{\delta G^{(1)}(t_1,t_1^+)}{\delta v^{(1)}(\bar{\bar{t}})} \\ &= \mathrm{i}\hbar G^{(1)}(\bar{t},\bar{\bar{t}})G^{(1)}(\bar{\bar{t}},t')w^{(2)}(\bar{t}^+ - \bar{\bar{t}}) - \mathrm{i}\hbar\delta_{\mathscr{C}}(\bar{t}-t')\int_{\mathscr{C}}\mathrm{d}t_1\, w^{(2)}(t'-t_1)G^{(1)}(t_1,\bar{\bar{t}})G^{(1)}(\bar{\bar{t}},t_1^+) \\ &\quad + (\mathrm{i}\hbar)\times\mathrm{terms}\left\{w^{(2)}, G^{(1)}, \frac{\delta\Sigma^{(1)}}{\delta v^{(1)}}\right\}. \end{aligned} \quad (2.60)$$

Inserting Eq. (2.59) in Eq. (2.60), we obtain the result,

$$\Sigma^{(1)}(t,t') = \Sigma^{(1),2\mathrm{B}}(t,t') + (\mathrm{i}\hbar)^2\times\mathrm{terms}\left\{w^{(2)}, G^{(1)}, \frac{\delta\Sigma^{(1)}}{\delta v^{(1)}}\right\},$$

where we have introduced the second Born (2B) self-energy as,

$$\begin{aligned}&\Sigma^{(1),2\mathrm{B}}(t,t') - \Sigma^{(1),\mathrm{HF}}(t,t') \\ &= (\mathrm{i}\hbar)^2\int_{\mathscr{C}}\mathrm{d}\bar{t}\int_{\mathscr{C}}\mathrm{d}\bar{\bar{t}}\, G^{(1)}(t,\bar{t})w^{(2)}(\bar{t}^+ - \bar{\bar{t}})G^{(1)}(\bar{t},\bar{\bar{t}})G^{(1)}(\bar{\bar{t}},t')w^{(2)}(\bar{t}^+ - t') \\ &\quad - (\mathrm{i}\hbar)^2\int_{\mathscr{C}}\mathrm{d}\bar{t}\int_{\mathscr{C}}\mathrm{d}\bar{\bar{t}}\, G^{(1)}(t,t')w^{(2)}(t^+ - \bar{t})w^{(2)}(t' - \bar{\bar{t}})G^{(1)}(\bar{\bar{t}},\bar{t})G^{(1)}(\bar{t},\bar{\bar{t}}^+). \end{aligned} \quad (2.61)$$

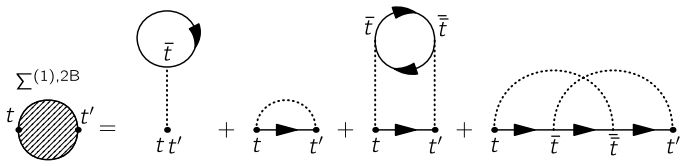

Fig. 2.6 Diagrammatic representation of the second Born self-energy $\Sigma^{(1),2B}(t,t')$ including terms of first and second order in $w^{(2)}$. The first two diagrams refer to the Hartree and the Fock (exchange) contribution, cf. Fig. 2.5

The many-body approximation (2.61) is known as the 2B approximation and is the simplest one that accounts for correlations. Diagrammatically, it is shown in Fig. 2.6. In the numerical results presented below, we will restrict ourselves to the 2B approximation. We note for completeness that other familiar, more advanced approximations for the one-particle self-energy such as the GW or T-matrix approximation (TM) include higher-order terms obtained in the subsequent iteration(s).

Concerning the derivation above, the question remains whether the obtained 2B self-energy leads to a conserving scheme, i.e., aside from the HF part which has already been discussed earlier. Interestingly, it turns out that 2B is indeed fully conserving. This is due to the fact that $\Sigma^{(1),2B}$ can be derived from a generating thermodynamic potential Φ [90]. In general, a conserving self-energy is obtained by removing propagator lines in all possible ways in the diagrammatic power series expansion of the Luttinger-Ward functional (LWF) $\Phi = \ln\langle S_{\mathscr{C}}\rangle$, i.e., calculating,

$$\Sigma^{(1)}(t,t') = \frac{\delta\Phi[G^{(1)}, w^{(2)}]}{\delta G^{(1)}(t',t)}. \tag{2.62}$$

Here, in the LWF, $S_{\mathscr{C}}$ means the generalized S-matrix,

$$S_{\mathscr{C}} = \hat{T}_{\mathscr{C}} \exp\left[-\frac{\mathrm{i}}{2\hbar}\int_{\mathscr{C}} \mathrm{d}t \int_{\mathscr{C}} \mathrm{d}t'\, w^{(2)}(t-t')\,\hat{f}^{\dagger}(t)\,\hat{f}^{\dagger}(t')\,\hat{f}(t')\,\hat{f}(t)\right]. \tag{2.63}$$

An approximation derived from Eq. (2.62) is often called "Φ-derivable" and fully satisfies the requirements of a conserving approximation given in Sect. 2.3.1. For details and examples on how to perform the diagrammatic expansion of the LWF under the relevant Feynman rules before evaluating $\delta\Phi/\delta G^{(1)}$, the reader is referred to Ref. [91]. An explicit formula for Φ including prefactors and the topologically distinct diagrams can be found, e.g., in [92].

2.4 Quantum Kinetic Equations for Single-Time Quantities

In many practical situations, the presence of the over-time-expanding memory kernel (i.e., the retardation) in the KBEs inhibits a successful two-time propagation of the 1pNEGF or limits it to a certain maximum time. Only for "increasingly smooth"

kernels[29] efficient solvers exist that do not rely *a priori* on massive parallelization, e.g., Ref. [93]. On the other hand, much information about the considered quantum many-body system is already contained in the 1pRDM $\rho_1(t)$, which is a single-time quantity. Therefore, it is reasonable to ask the question of whether it is possible to derive quantum kinetic equations which are based solely on one time variable.

Mathematically, this poses the question of how to reconstruct two-time quantities in the KBEs from single-time (or time-diagonal) ones. In this section, we review such a reconstruction scheme based on the early works of Lipavský et al., Ref. [23]. It demonstrates that there indeed exists an exact relation between the two-time correlation functions and the 1pRDM (or phase-space distribution function). As a direct implication, the reconstruction theorem will lead over to the generalized Kadanoff-Baym ansatz (GKBA) which generates the time-diagonal limit of the KBEs though requiring further approximations. Conceptually, the GKBA paves the way for rigorously transforming the KBEs into familiar equations of motion for the Wigner distribution function such as the Boltzmann, Landau or Balescu-Lenard equations, e.g., Ref. [94]. These equations are accurate for slowly varying disturbances and "simple" transport processes. But non-Markovian extensions of these single-time quantum kinetic equations exist as well, see, e.g., [11, 95, 96], and can be derived applying the GKBA.

2.4.1 The Reconstruction Problem for the One-Particle Green's Function

The reconstruction scheme for $G^{(1),\gtrless}(t,t')$ (at $t \neq t'$) as introduced in the original publication (see Ref. [23]) is somewhat subtle, and also reviews of the same authors (see, e.g., Refs. [24–26]) include some nested elaborations. For this reason, we present a detailed derivation below which hopefully will be more clear to the reader. For simplicity, we again drop any indices that refer to spin or spatial degrees of freedom. Also, we focus on the lesser matrix component of the Green's function. The reconstruction of the greater component is carried out in the same manner.

First of all, we define two auxiliary functions,

$$\begin{aligned} G_{\mathrm{R}}^{(1),<}(t,t') &= \theta_{\mathscr{C}}(t-t')G^{(1),<}(t,t'), \\ G_{\mathrm{A}}^{(1),<}(t,t') &= -\theta_{\mathscr{C}}(t'-t)G^{(1),<}(t,t'), \end{aligned} \tag{2.64}$$

which must not be confused with the usual retarded and advanced Green's functions and allow us to recover the full lesser correlation function from $G^{(1),<}(t,t') = G_{\mathrm{R}}^{(1),<}(t,t') - G_{\mathrm{A}}^{(1),<}(t,t')$. In particular, $[G_{\mathrm{R}}^{(1),<}(t,t')]^\dagger = G_{\mathrm{A}}^{(1),<}(t',t)$. Second, we evaluate the time derivative,

[29] Evoked by the time dependence of the 1pNEGF and (or) the 1pSE.

$$\mathrm{i}\hbar\frac{\partial}{\partial t}G_{\mathrm{R}}^{(1),<}(t,t') = \mathrm{i}\hbar\delta_{\mathscr{C}}(t-t')G^{(1),<}(t,t') + \mathrm{i}\hbar\theta_{\mathscr{C}}(t-t')\frac{\partial}{\partial t}G^{(1),<}(t,t'). \tag{2.65}$$

Third, we summarize some important relations for the inverse of the retarded, advanced and non-interacting Green's functions (note that the short-hand notation $AB|_{(t,t')}$ includes the contour integral $\int_{\mathscr{C}}\mathrm{d}\bar{t}\,A(t,\bar{t})B(\bar{t},t')$),

$$\begin{aligned}
\left[G^{(1),\mathrm{R/A}}\right]^{-1}(t,t') &= \left[G_0^{(1)}\right]^{-1}(t,t') - \Sigma^{(1),\mathrm{R/A}}(t,t'),\\
\left[G_0^{(1)}\right]^{-1}G_0^{(1),\gtrless}\big|_{(t,t')} &= G_0^{(1),\gtrless}\left[G_0^{(1)}\right]^{-1}\big|_{(t,t')} = 0,\\
\left[G^{(1),\mathrm{R}}\right]^{-1}G^{(1),\gtrless}\big|_{(t,t')} &= \Sigma^{(1),\gtrless}G^{(1),\mathrm{A}}\big|_{(t,t')}.
\end{aligned} \tag{2.66}$$

Our goal is now to express the two-time functions of Eq. (2.64) in terms of the density matrix. We treat both expressions separately (comments on notations and transformations made are given below Eq. (2.67) and Eq. (2.68)):

(i) For $G_{\mathrm{R}}^{(1),<}$, we consider,

$$\begin{aligned}
&\left[G^{(1),\mathrm{R}}\right]^{-1}G_{\mathrm{R}}^{(1),<}\big|_{(t,t')}\\
&= \left\{\left[G_0^{(1)}\right]^{-1} - \Sigma^{(1),\mathrm{R}}\right\}G_{\mathrm{R}}^{(1),<}\big|_{(t,t')}\\
&\overset{(a)}{=} \mathrm{i}\hbar\delta_{\mathscr{C}}(t-t')G^{(1),<}(t,t')\\
&\quad + \theta_{\mathscr{C}}(t-t')\int_{\mathscr{C}}\mathrm{d}\bar{t}\,\theta_{\mathscr{C}}(\bar{t}-t')\left[G_0^{(1)}\right]^{-1}(t,\bar{t})G^{(1),<}(\bar{t},t')\\
&\quad - \Sigma^{(1),\mathrm{R}}G_{\mathrm{R}}^{(1),<}\big|_{(t,t')}\\
&\overset{(b)}{=} \mathrm{i}\hbar\delta_{\mathscr{C}}(t-t')G^{(1),<}(t,t')\\
&\quad + \theta_{\mathscr{C}}(t-t')\int_{\mathscr{C}}\mathrm{d}\bar{t}\,\theta_{\mathscr{C}}(\bar{t}-t')\left[G^{(1),\mathrm{R}}\right]^{-1}(t,\bar{t})G^{(1),<}(\bar{t},t')\\
&\quad + \theta_{\mathscr{C}}(t-t')\int_{\mathscr{C}}\mathrm{d}\bar{t}\,\theta_{\mathscr{C}}(\bar{t}-t')\Sigma^{(1),\mathrm{R}}(t,\bar{t})G^{(1),<}(\bar{t},t')\\
&\quad - \Sigma^{(1),\mathrm{R}}G_{\mathrm{R}}^{(1),<}\big|_{(t,t')}\\
&\overset{(c)}{=} \mathrm{i}\hbar\delta_{\mathscr{C}}(t-t')G^{(1),<}(t,t')\\
&\quad + \theta_{\mathscr{C}}(t-t')\int_{\mathscr{C}}\mathrm{d}\bar{t}\,\Sigma^{(1),<}(t,\bar{t})G^{(1),\mathrm{A}}(\bar{t},t')\\
&\quad - \theta_{\mathscr{C}}(t-t')\int_{\mathscr{C}}\mathrm{d}\bar{t}\,\theta_{\mathscr{C}}(t'-\bar{t})\left[G^{(1),\mathrm{R}}\right]^{-1}(t,\bar{t})G^{(1),<}(\bar{t},t')\\
&\overset{(d)}{=} \mathrm{i}\hbar\delta_{\mathscr{C}}(t-t')G^{(1),<}(t,t')\\
&\quad + \theta_{\mathscr{C}}(t-t')\int_{\mathscr{C}}\mathrm{d}\bar{t}\,\theta_{\mathscr{C}}(t'-\bar{t})\Sigma^{(1),<}(t,\bar{t})G^{(1),\mathrm{A}}(\bar{t},t')\\
&\quad + \theta_{\mathscr{C}}(t-t')\int_{\mathscr{C}}\mathrm{d}\bar{t}\,\theta_{\mathscr{C}}(t'-\bar{t})\Sigma^{(1),\mathrm{R}}(t,\bar{t})G^{(1),<}(\bar{t},t').
\end{aligned} \tag{2.67}$$

The transformations carried out in Eq. (2.67) are as follows:

(a) This equality is obtained by using the definition of the inverse Green's function $[G_0^{(1)}]^{-1}(t,t') = \delta_{\mathscr{C}}(t-t')\{\mathrm{i}\hbar\frac{\partial}{\partial t'} - h^{(1)}(t')\}$ together with Eq. (2.65).

(b) Here, we reinsert the expression for $[G_0^{(1)}]^{-1}$ in terms of the retarded Green's function and the retarded self-energy (first line of Eq. (2.66)). By definition, the last two terms involving $\Sigma^{(1),\mathrm{R}}$ on the r.h.s. are equal and cancel.

(c) Use the third identity in Eq. (2.66). The last term with negative sign corrects for the presence of the step function.

(d) This is the result of again writing out the inverse $[G^{(1),\mathrm{R}}]^{-1}$ and noting that $\int_{\mathscr{C}} \mathrm{d}\bar{t}\,\theta_{\mathscr{C}}(t'-\bar{t})[G_0^{(1)}]^{-1}(t,\bar{t})G^{(1),<}(\bar{t},t')$ evaluates to zero (cf. Eq. (2.66)). The inclusion of the step function into the second line is consistent with the definition of the advanced Green's function, see Eq. (2.19).

(ii) For $G_{\mathrm{A}}^{(1),<}$, we consider,

$$
\begin{aligned}
&G_{\mathrm{A}}^{(1),<}\big[G^{(1),\mathrm{A}}\big]^{-1}|_{(t,t')} \\
&\overset{(*)}{=} \Big\{\big[G_0^{(1)}\big]^{-1} - \Sigma^{(1),\mathrm{A}}\Big\}^{\dagger}\big[G_{\mathrm{A}}^{(1),<}\big]^{\dagger}\big|^{\dagger}_{(t',t)} \\
&\overset{(a)}{=} \mathrm{i}\hbar\delta_{\mathscr{C}}\big(t'-t\big)G^{(1),<}\big(t,t'\big) \\
&\quad + \theta_{\mathscr{C}}\big(t-t'\big)\int_{\mathscr{C}}\mathrm{d}\bar{t}\,\theta_{\mathscr{C}}(\bar{t}-t)\big[G_0^{(1)}\big]^{-1}\big(t',\bar{t}\big)G^{(1),<}(\bar{t},t)\Big|^{\dagger} \\
&\quad - \Sigma^{(1),\mathrm{R}}G_{\mathrm{R}}^{(1),<}\big|^{\dagger}_{(t,t')} \\
&\overset{(b)}{=} \mathrm{i}\hbar\delta_{\mathscr{C}}\big(t'-t\big)G^{(1),<}\big(t,t'\big) \\
&\quad + \theta_{\mathscr{C}}\big(t-t'\big)\int_{\mathscr{C}}\mathrm{d}\bar{t}\,\theta_{\mathscr{C}}(\bar{t}-t)\big[G^{(1),\mathrm{R}}\big]^{-1}\big(t',\bar{t}\big)G^{(1),<}(\bar{t},t)\Big|^{\dagger} \\
&\quad + \theta_{\mathscr{C}}\big(t-t'\big)\int_{\mathscr{C}}\mathrm{d}\bar{t}\,\theta_{\mathscr{C}}(\bar{t}-t)\Sigma^{(1),\mathrm{R}}\big(t',\bar{t}\big)G^{(1),<}(\bar{t},t)\Big|^{\dagger} \\
&\quad - \Sigma^{(1),\mathrm{R}}G_{\mathrm{R}}^{(1),<}\big|^{\dagger}_{(t,t')} \\
&\overset{(c)}{=} \mathrm{i}\hbar\delta_{\mathscr{C}}\big(t'-t\big)G^{(1),<}\big(t,t'\big) \\
&\quad + \theta_{\mathscr{C}}\big(t-t'\big)\int_{\mathscr{C}}\mathrm{d}\bar{t}\,\Sigma^{(1),<}\big(t',\bar{t}\big)G^{(1),\mathrm{A}}(\bar{t},t)\Big|^{\dagger} \\
&\quad - \theta_{\mathscr{C}}\big(t-t'\big)\int_{\mathscr{C}}\mathrm{d}\bar{t}\,\theta_{\mathscr{C}}(t-\bar{t})\big[G^{(1),\mathrm{R}}\big]^{-1}\big(t',\bar{t}\big)G^{(1),<}(\bar{t},t)\Big|^{\dagger} \\
&\overset{(d)}{=} \mathrm{i}\hbar\delta_{\mathscr{C}}\big(t'-t\big)G^{(1),<}\big(t,t'\big) \\
&\quad - \theta_{\mathscr{C}}\big(t-t'\big)\int_{\mathscr{C}}\mathrm{d}\bar{t}\,\theta_{\mathscr{C}}(t-\bar{t})G^{(1),\mathrm{R}}(t,\bar{t})\Sigma^{(1),<}\big(\bar{t},t'\big) \\
&\quad - \theta_{\mathscr{C}}\big(t-t'\big)\int_{\mathscr{C}}\mathrm{d}\bar{t}\,\theta_{\mathscr{C}}(t-\bar{t})G^{(1),<}(t,\bar{t})\Sigma^{(1),\mathrm{A}}\big(\bar{t},t'\big). \qquad (2.68)
\end{aligned}
$$

Comments on the transformations:

(*) Here, the notation $AB|_{(t',t)}$ is to be understood as $\int_{\mathscr{C}} \mathrm{d}\bar{t}\, A(\bar{t},t')B(t,\bar{t})$, and $AB|^{\dagger}_{(t',t)}$ denotes $\int_{\mathscr{C}} \mathrm{d}\bar{t}\, B^{\dagger}(t',\bar{t})A^{\dagger}(\bar{t},t)$.

(a) We use that the adjoint of $[G_0^{(1)}]^{-1}(t,t')$ is given by $[G_0^{(1)}]^{-1}(t',t)$ and apply Eqs. (2.64) and (2.65). Note, that $[\Sigma^{(1),\mathrm{A}}(t,t')]^{\dagger} = \Sigma^{(1),\mathrm{R}}(t',t)$.

(b) As in (i), we substitute the expression for the inverse of the non-interacting Green's function. Again, the last two terms on the r.h.s. cancel.

(c), (d) These equalities follow in the same way as points (c) and (d) in Eq. (2.67).

Equations (2.67) and (2.68) almost complete the reconstruction. As the final step, we multiply Eq. (2.67) from the left by $G^{(1),\mathrm{R}}$ and Eq. (2.68) from the right by $G^{(1),\mathrm{A}}$, integrate over another intermediate time coordinate and identify the 1pRDM $\rho_1(t) = -\mathrm{i}\hbar G^{(1),<}(t,t)$. We finally obtain,

$$\begin{aligned} G^{(1),<}(t,t') = &-G^{(1),\mathrm{R}}(t,t')\rho_1(t') \\ &+ \int_{t'}^{t} \mathrm{d}\bar{t} \int_{t_0}^{t'} \mathrm{d}\bar{\bar{t}}\; G^{(1),\mathrm{R}}(t,\bar{t})\Sigma^{(1),<}(\bar{t},\bar{\bar{t}})G^{(1),\mathrm{A}}(\bar{\bar{t}},t') \\ &+ \int_{t'}^{t} \mathrm{d}\bar{t} \int_{t_0}^{t'} \mathrm{d}\bar{\bar{t}}\; G^{(1),\mathrm{R}}(t,\bar{t})\Sigma^{(1),\mathrm{R}}(\bar{t},\bar{\bar{t}})G^{(1),<}(\bar{\bar{t}},t') \\ &+ \rho_1(t)G^{(1),\mathrm{A}}(t,t') \\ &+ \int_{t'}^{t} \mathrm{d}\bar{t} \int_{t_0}^{t'} \mathrm{d}\bar{\bar{t}}\; G^{(1),\mathrm{R}}(t,\bar{t})\Sigma^{(1),<}(\bar{t},\bar{\bar{t}})G^{(1),\mathrm{A}}(\bar{\bar{t}},t') \\ &+ \int_{t'}^{t} \mathrm{d}\bar{t} \int_{t_0}^{t'} \mathrm{d}\bar{\bar{t}}\; G^{(1),<}(t,\bar{t})\Sigma^{(1),\mathrm{A}}(\bar{t},\bar{\bar{t}})G^{(1),\mathrm{A}}(\bar{\bar{t}},t'). \end{aligned} \tag{2.69}$$

A very similar equation is valid for the greater component of the 1pNEGF. The only difference is that we cannot identify the 1pRDM in the non-integral terms (compare with Eq. (2.70)).

2.4.2 The Generalized Kadanoff-Baym Ansatz

The reconstruction (2.69) is exact as long as the exact advanced and retarded propagators are used. However, it has still the form of an integral equation the iterative solution of which is complicated. A simple approximation is to retain only the non-integral terms. This procedure is known as the generalized Kadanoff-Baym ansatz[30] (GKBA) [23]:

[30] Sometimes, it is also called Lipavský ansatz, e.g., [11].

$$G^{(1),\gtrless}(t,t') = -G^{(1),\mathrm{R}}(t,t')\rho_1^{\gtrless}(t') + \rho_1^{\gtrless}(t)G^{(1),\mathrm{A}}(t,t')$$
$$= \frac{i}{\hbar}A(t,t')\{\theta_{\mathscr{C}}(t-t')\rho^{\gtrless}(t') + \theta_{\mathscr{C}}(t'-t)\rho^{\gtrless}(t)\}, \quad (2.70)$$

where,

$$\rho_1^{\gtrless}(t) = -\mathrm{i}\hbar G^{(1),\gtrless}(t,t), \quad (2.71)$$

and $A(t,t')$ denotes the spectral function of Eq. (2.17) [69]. In the limit of equal times, the GKBA is an identity for the lesser and greater correlation function[31], which automatically implies particle number conservation. For other times t and t', the correlation functions explicitly depend on the retarded and advanced propagators. These have to be specified when making practical use of the ansatz as they are again functions of two time variables and, hence, cannot be treated on the same approximation level of MBPT.

In contrast to the common (or original) Kadanoff-Baym ansatz, e.g., [24], where one postulates,

$$G^{(1),<}(t,t') = f\left(\frac{t+t'}{2}\right)\{G^{(1),\mathrm{A}}(t,t') - G^{(1),\mathrm{R}}(t,t')\}, \quad (2.72)$$

with f being the Wigner (distribution) function [28], Eq. (2.70) maintains a causal time structure. It is this causal structure of the GKBA which ensures the conservation of total energy, momentum and density whenever a conserving approximation is used for the self-energy and which allows for applications beyond the quasi-particle picture. Moreover, the GKBA is better suited for dealing with temporally and (or) spatially fast varying perturbations than Eq. (2.72). Details on the implementation of the GKBA, particularly when treating the retarded and advanced propagators on the HF level, are compiled in Sect. 4.2.3.

Applications of the GKBA to spatially homogeneous systems can be found in various fields and include the numerical treatment of ultrafast carrier relaxation in the dense electron gas and (laser) plasmas [63, 97, 98], the study of quantum transport phenomena [61, 99] and quantum diffusion [100]. In this respect, it is often used to connect different time scales studying the crossover from the transient regime to the long-time behavior [101]. Tests of the GKBA against full two-time calculations have been performed in Refs. [97, 102, 103]. In the presence of phonons and laser excitations, the GKBA has been applied to semiconductor electron-hole plasmas in Refs. [104, 105], and to dynamical screening effects of carrier-phonon and carrier-carrier interactions in [106]. For extensions to electrons in quantum dots and wells, see Refs. [107–110]. In addition, the GKBA is discussed in the context of (improved) non-Lorentzian spectral functions [69], and a gauge-invariant formulation of the GKBA can be found in [98] and is used in Refs. [111, 112] for dynamical screening and harmonics generation in dense laser plasmas. An extension of the GKBA to spatially inhomogeneous finite systems has been presented in Ref. [113] and will be discussed in more detail in Sect. 4.2.3.

[31] This is easily verified as the integral in Eq. (2.69) vanishes in that case.

Part III
Computational Methods

Chapter 3
Representations of the Nonequilibrium Green's Function

In this chapter, we are approaching the numerical solution of the Kadanoff-Baym equations which, in general, means to solve a large set of coupled integro-differential equations. First numerical solutions for homogeneous systems have been obtained by Danielewicz [67], Köhler [114] and Schäfer [115, 116].

In contrast to homogeneous quantum many-body systems, where the extent of the memory kernel in the KBEs is numerically not critical, it becomes a limiting factor for full two-time NEGF calculations on inhomogeneous systems. Here, the memory kernel is often not very smooth[1] leading to large storage requirements and allowing for short propagation times only. In response to this fact, which is discussed in greater detail in Sect. 3.1, the question arises how an efficient treatment of non-temporal, i.e., particularly spatial degrees of freedom in the 1pNEGF can be achieved.

An answer to this question leads over to the decision of using either a grid or a basis representation of the nonequilibrium Green's function (cf. Sect. 3.2). Eventually, also a hybrid approach can be preferable. A specific example in this direction is given in Sect. 3.3 based on the finite element-discrete variable representation (FE-DVR). Respective applications on model systems can be found in Chap. 6.

3.1 Numerical Resources

3.1.1 Homogeneous Systems. A Brief Outline

In comparison to inhomogeneous quantum many-body systems, the NEGF description of homogeneous systems, such as nuclear matter, correlated electron gases, (dense) plasmas or interacting charge carriers in semiconductors, is generally simpler. This is due to the fact that the 1pNEGF is a function of only a single space or

[1] This means, that the Green's function (or self-energy) does not decay sufficiently fast when "looking" back into the past from the current time.

K. Balzer, M. Bonitz, *Nonequilibrium Green's Functions Approach to Inhomogeneous Systems*, Lecture Notes in Physics 867,
DOI 10.1007/978-3-642-35082-5_3, © Springer-Verlag Berlin Heidelberg 2013

momentum coordinate, i.e., $G^{(1)}_{ij}(t,t')$ of Eq. (2.12) is replaced by a nonequilibrium Green's function which is diagonal with respect to i and j. In momentum representation, we write $G^{(1)}(\mathbf{p},t,t')$, and the KBEs take the form (m indicates the electron mass),

$$\left\{\mathrm{i}\hbar\frac{\partial}{\partial t}-\frac{\mathbf{p}^2}{2m}\right\}G^{(1)}(\mathbf{p},t,t')=\int_{\mathscr{C}}\mathrm{d}\bar{t}\,\Sigma^{(1)}(\mathbf{p},t,\bar{t})G^{(1)}(\mathbf{p},\bar{t},t'), \tag{3.1}$$

and the adjoint Eq. with $t\leftrightarrow t'$.

If, further, the system under investigation is fully isotropic due to cylindrical (spherical) symmetry in 2D (3D), the 1pNEGF only depends on the modulus $k=|\mathbf{k}|$ of the wave vector ($\mathbf{p}=\hbar\mathbf{k}$). For this reason, the problem becomes essentially one-dimensional[2], and we can discretize the wave number k according to $k_i=i\Delta k$ ($i=0,1,2,\ldots,i_{\max}$) allowing for a maximum momentum $p_{\max}=i_{\max}\hbar\Delta k$. Computationally, $p_{\max}$ is limited by the available memory capacities. In the case of full two-time calculations, typical discretizations account for about 32 to 64 points in k-space, compare with Refs. [117, 118]. If we take 64 k-points and propagate 1000 time steps in, both, t- and t'-direction, the required memory comprises,

$$1000^2\cdot 64\cdot 16\ \text{bytes}\approx 1\ \text{Gigabyte}, \tag{3.2}$$

for the storage of the correlation functions[3].

For homogeneous systems, the integration of the KBEs (3.1) is usually achieved by Runge-Kutta methods[4]. Concerning the computation of irregular parts of the self-energy, it is reported in the work of Köhler et al. (Ref. [117]) that the use of a (2D) 3D Cartesian fast Fourier transform is highly efficient to perform the intermediate momentum integrations. This allows one to effectively study also systems non-isotropic in $\mathbf{p}$-space and investigate, e.g., ultrafast momentum orientation relaxation processes [119]. For a detailed overview on the numerics, see Refs. [114] and [118]. We emphasize, that especially Ref. [118] includes many comprehensive visualizations of the real and imaginary part of the two-time 1pNEGF $G^{(1)}(\mathbf{p},t,t')$ and of the spectral function $A(\mathbf{p},t,t')$ under various nonequilibrium conditions.

To give a specific example let us consider an interacting electron gas or, in other words, a one-component electron plasma with a homogeneous positive background. Such a model is of fundamental relevance in plasma [83] and semiconductor physics [61]. For a GaAs system, cf. Refs. [118, 120], Fig. 3.1 shows the temporal evolution of the momentum distribution $f(k,t)=-\mathrm{i}\hbar G^{(1)}(\hbar k,t,t)$ as function of the wave number k when we start propagating the 1pNEGF from a highly nonequilibrium initial state, e.g., created by an external laser field. In the case shown, the initial state is ideal, i.e., it corresponds to the non-interacting electron gas. Following the time evolution, we observe that, in the presence of electron-electron interactions,

[2] Aside from the generic two-time structure.

[3] Note, that the correlation functions are in general complex. Assuming double precision, we need 16 bytes for a single complex number.

[4] Potentially, including an adaptive time step size.

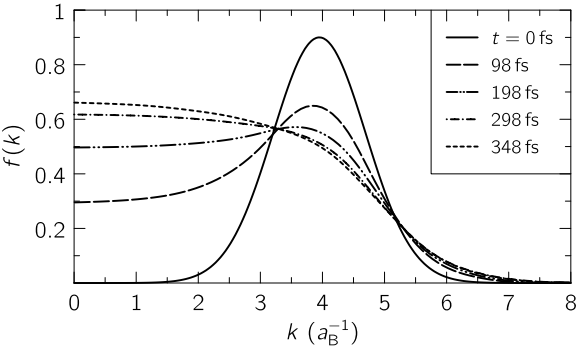

Fig. 3.1 Time-evolution of the distribution function $f(k,t)$ of an initially non-correlated electron gas in GaAs in 2B approximation (density: $n = 10^{18}$ cm^{-3}, temperature: $T = 290$ K). The initial distribution is Gaussian: $f_0 \mathrm{e}^{-(k-k_0)^2/\sigma_k^2}$ with $f_0 = 0.9$, $k_0 = 3.95 a_\mathrm{B}^{-1}$, $\sigma_k = 1.06 a_\mathrm{B}^{-1}$ and the Bohr radius $a_\mathrm{B} = 4\pi\varepsilon\varepsilon_0\hbar^2/(m^* e^2)$. Figure after Ref. [120]

the initial Gaussian distribution relaxes within a few hundred femtoseconds to a stationary equilibrium distribution. As the integral over all wave numbers k increases with time, it is clear that also the kinetic energy of the system increases and hence the system heats up during equilibration. However, we note that the final distribution is not a Fermi-distribution but only Fermi-like due to the correlations treated in 2B approximation. The equilibration and correlation times are proportional to the inverse plasma frequency $\omega_\mathrm{pl} = (ne^2/(\varepsilon\varepsilon_0 m^*))^{1/2}$ where m^* is the effective electron mass and ε denotes the material dielectric constant[5].

For the short-time dynamics of a many-body system, the proper choice of the initial condition is essential. In the previous example, where electrons are excited by a laser pulse into the previously empty conduction band of a semiconductor, it is reasonable to assume that these electrons are initially uncorrelated. In other cases, the neglect of initial correlations (IC) may however be a too dramatic simplification. In general, they must be included in the KBEs. A general non-perturbative approach to ICs is subject of Refs. [70, 71, 121] and leads to additional collision terms in the KBEs[6] involving an extra self-energy $\Sigma^{(1)}_\mathrm{in}(\mathbf{p}, t, t')$ in Eq. (3.1). This concept is valid for arbitrary equilibrium as well as nonequilibrium initial states. As a consequence, if the electron gas discussed in Fig. 3.1 would be prepared in an over-correlated initial state, we would observe the opposite effect, namely, cooling—compare with Ref. [121]. Moreover, applications to plasma oscillations and the dynamic structure factor including ICs can be found in Ref. [122].

[5] In Coulomb systems, the correlation time is typically of the order of $\tau_\mathrm{cor} \approx 2\pi/|\omega_\mathrm{pl}|$. At weak coupling, the relaxation time of the Wigner distribution is typically significantly larger, $\tau_\mathrm{rel} \gg \tau_\mathrm{cor}$ [11, 95, 123].

[6] The resulting equations of motion for the 1pNEGF are sometimes called "generalized" Kadanoff-Baym equations, e.g., [121, 124].

Finally, generalizations of Eq. (3.1) are obtained in the context of intra- and interband Kadanoff-Baym equations which, e.g., describe the electron (or hole) dynamics in the conduction and the valence band of a semiconductor (see, e.g., Refs. [103, 125] and references therein) and extend standard Bloch equation approaches [61] to a two-time description.

3.1.2 Inhomogeneous Systems. Computer Memory as Limiting Factor

For spatially inhomogeneous systems, the computational limits—placed by the memory kernel of the KBEs—are reached much sooner, i.e., at comparably smaller grid or basis sizes than for homogeneous systems. This is due to the quadratic scaling of the effort regarding spin and (or) spatial coordinates. Whereas for homogeneous systems, the 1pNEGF $G^{(1)}_{ij}(t,t')$ is diagonal ($\propto \delta_{ij}$), it is generally not for inhomogeneous systems. On top of that, finite and, especially, confined systems often show strong density modulations the resolution of which requires fine grids or large basis sizes to ensure adequate convergence of the relevant observables.

For a comparison with Eq. (3.2) of Sect. 3.1.1, let us assume the same number of 1000 time steps for the two-time propagation of the nonequilibrium Green's function and a slightly larger spatial discretization which involves 90 spin orbitals. The resulting memory for the correlation functions is then,

$$1000^2 \cdot 90^2 \cdot 16 \text{ bytes} \approx 130 \text{ Gigabyte}. \tag{3.3}$$

This means a more than two orders of magnitude larger storage requirement for the 1pNEGF than delineated in Eq. (3.2) and well exemplifies the increased numerical effort when propagating the Green's function in real-time for inhomogeneous quantum systems[7].

Anyhow, as the memory requirements of Eq. (3.3) are way beyond the capabilities of typical desktop computers, a serial time-propagation code must be run on multiprocessor machines or clusters with a shared-memory setup. To make calculations efficient with respect to runtime[8] and average (single or total) processor load, one, in addition, has to address high-performance computing strategies such as a proper parallelization, see Sect. 4.2.1.

3.2 Grid versus Basis Representations for Inhomogeneous Systems

As outlined above, the 1pNEGF has off-diagonal elements for inhomogeneous systems. The KBEs have, therefore, the form of the multi-band (or multi-level) version

[7] In the presence of correlations, that is beyond the HF level.

[8] Note that the runtime itself can be a bottleneck at large memory consumption as we have to account for matrix instead of scalar multiplications.

outlined at the end of Sect. 3.1.1, but with the number of "bands" usually being comparatively large.

If we represent the 1pNEGF on a spatial grid, i.e., replace,

$$G_{ij}^{(1)}(t,t') \to G^{(1)}(\mathbf{r}_i t, \mathbf{r}_j t'), \tag{3.4}$$

the required mesh has dimension $2 \cdot d$ where d is the dimensionality of the considered problem. Including both time variables, the Green's function is then a $(2 \cdot d + 2)$-dimensional object which is difficult to operate with even in 1D ($d = 1$). This becomes obvious, when we compare it to a (one-) two-particle wave function in 1D (2D) which has a dimension of 3 lacking the additional time variable present in the nonequilibrium Green's function. Therefore, although grid methods are simple to implement numerically and just require low-order, finite-difference estimates for differential operators, grid-based KBE solvers are essentially more complex than common codes that propagate wave functions according to the time-dependent Schrödinger equation. We note that the explicit inclusion of the electron spin would further increase the complexity by a factor of 4. On top of that, as one has to account for non-Markovian effects, NEGF calculations must be placed on the same level as sophisticated Kohn-Sham approaches in time-dependent density functional theory (TDDFT) which use non-adiabatic exchange-correlation kernels, e.g., Refs. [126–128].

Of course, there may exist situations where, for example, angular degrees of freedom can be integrated out or symmetries can be exploited, such that the problem is reduced in dimensionality. However, grid methods perform, in general, poorly in the description of bound (or localized) states which are characteristic for inhomogeneous systems. Here, small mesh spacings are indispensable. In this regard, one rather would prefer an expansion of the 1pNEGF in terms of spatial one-particle orbitals $\chi_i(\mathbf{r})$ such as eigenfunctions of the confinement potential, i.e.,

$$G^{(1)}(\mathbf{r}t, \mathbf{r}'t') = \sum_{ij} \chi_i^*(\mathbf{r}) \chi_j(\mathbf{r}') G_{ij}^{(1)}(t,t'). \tag{3.5}$$

From the computational point of view, it is vital that the basis functions are sufficiently simple such that matrix elements of one- and two-body operators can readily be computed. In addition, observables should converge as fast as possible with the basis dimension.

In fact, there exist many approaches to generate an adequate (one-particle) basis which is quadratically integrable[9] and complete. The simplest one is certainly to diagonalize the time-independent part of the system's ideal, single-particle Hamiltonian. The corresponding eigenfunctions form a well-defined basis and, generally, allow for a good description of systems that are close to the ground state or equilibrium and are weakly interacting. On the other hand, this approach breaks down if strong external driving forces (leading to fragmentation) are involved and an accurate modeling of continuum (final) states is necessary. Advanced representations can

[9] Quadratic integrability is required to well-define operator matrix elements.

be derived from effective Hamiltonians or pseudopotentials and are better adapted to the many-body problem. These include, e.g., the use of HF and Kohn-Sham orbitals [68, 129] which originate from self-consistent field methods [35] and DFT within the local-density approximation (LDA) [128], respectively.

For simulations of atomic and molecular systems, often a highly localized basis is chosen if the excitation dynamics is such that ionization processes can be neglected. Such a representation can basically be constructed from any bound, atomic (molecular) orbitals and their linear combinations. However, the most common approaches use Gauss- or Slater-type functions (i.e., Gauss- or Slater-type orbitals) which are centered on the individual atoms. For respective NEGF calculations, we refer to the work of van Leeuwen, Dahlen and Stan in Refs. [68, 92, 130–132]. More sophisticated strategies include, e.g., polarized atomic orbitals where functions with different angular momenta are being mixed [133].

Extensions to periodic and condensed matter systems must conform with Bloch's theorem and involve delocalized states (Bloch functions) such as plane waves. However, also here, it is possible to introduce localized orbitals. A promising approach is the concept of maximally localized Wannier functions, e.g., Refs. [134, 135] and references therein, which are the solid-state equivalent of localized molecular orbitals. Typically, these follow from LDA band states in the case of not too strong interactions. Furthermore, a successful strategy is the derivation of effective lattice Hamiltonians starting from Bloch or Wannier functions, see, e.g., Refs. [136, 137] for an overview and Sect. 6 for some basic NEGF applications.

Eventually, it may be useful to map even a non-lattice quantum system onto an equivalent system the Hamiltonian of which has the form of a lattice system. Doing so can be beneficial at least in two aspects:

(i) it may improve the convergence of relevant observables regarding the basis size, and (or)
(ii) it may allow for sparse representations of operator matrix elements.

Following (i) and (or) (ii), the numerical solution of the KBEs should be easier. Concerning point (ii), especially a sparse representation (e.g., a high degree of diagonality) of the binary interaction is desirable as it can drastically simplify the self-energies and, in addition, the collision integrals of the KBEs, compare with Sects. 3.3.3 and 3.3.4. Moreover, it may be the case that long-range interactions, such as the contributions beyond next-neighbor interaction in the Hubbard model and its variations, cf. [138], can be neglected.

In the following section, we give an example of a very general procedure for mapping a spatially continuous system onto an equivalent lattice system. This procedure is based on finite elements and the discrete variable representation, e.g., Ref. [139], and has the great advantage of offering very simple and analytically determined matrix elements for, both, one- and two-particle operators.

3.3 An Efficient Solution: The Finite Element-Discrete Variable Representation

3.3.1 General Idea and Background

The numerical solution of (non-)linear partial differential equations (PDEs) usually requires small mesh spacings as typically rather low-order finite-difference methods are applied to approximate linear differential operators. If the solution of the PDE is, on the other hand, expanded in function space such that we deal with a matrix equation for the coefficients, often large dimensions are necessary to obtain adequate accuracy. In addition, the computation of the matrices can itself be elaborate.

In this dilemma, the finite element-discrete variable representation (FE-DVR) opens a hybrid approach combining favorable aspects of, both, (spatial) grids and basis expansions, cf. Ref. [140]. The main idea is to divide the coordinate space into fixed domains in each of which a purely local, so-called DVR basis is employed to describe local variations. In the course of this, the basis itself relies on a subordinate grid that is connected[10] to a set of interpolating polynomials. Regarding quantum mechanics, the great advantage of the FE-DVR is a sparse representation of local and non-local one- as well as two-particle operators, see Sect. 3.3.3.

One ingredient of the FE-DVR, the discrete variable representation, has been widely used in quantum chemistry, e.g., [141, 142]. In combination with finite elements, it has become more and more popular in the recent decade in the context of numerically solving the one- and two-particle time-dependent Schrödinger equation (TDSE). Pioneering work along this line is due to Rescigno and McCurdy, cf. Ref. [139], as well as Schneider, cf. Ref. [143]. Respective applications are widespread and include, e.g., the description of scattering problems in combination with time-dependent close coupling [144], the determination of bound and continuum states as well as the strong-field photoionization cross sections of the hydrogen molecular ion [145, 146] and approaches to molecular hydrogen (i.e., two electrons) [147], and ions in circularly polarized laser fields [148]. Moreover, combined FE and DVR schemes are, to date, also used in multiconfiguration time-dependent Hartree-Fock (MCTDHF) and configuration interaction (CI) calculations, see, e.g., Refs. [17, 149] and references therein.

Aside from simple and analytically accessible matrix elements, one of the key properties of the FE-DVR regarding the time evolution of a (many-body) wave function is its potential for a highly effective TDSE-code parallelization. To this end, one applies the real-space product ansatz discussed in Ref. [150]. On the other hand, when applied to NEGF calculations, the main advantage will be the sparse representation, cf. Sects. 3.3.3 and 3.3.4. Applications to model atoms and molecules can be found in Chap. 6.

In the following, we introduce the FE-DVR approach in one spatial dimension. The generalization to higher dimensionality is straightforward using product states in Cartesian space, cf., e.g., Ref. [143].

[10] Similar to methods using B-splines.

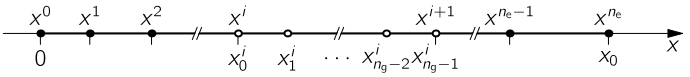

Fig. 3.2 One-dimensional simulation box $\mathscr{S} = [0, x_0]$ as discretized in the finite element-discrete variable representation (FE-DVR). Each finite element $[x^i, x^{i+1}]$ is subdivided by n_g *generalized Gauss-Lobatto* points defined along Eqs. (3.8) and (3.9)

3.3.2 Construction of the FE-DVR Basis

For a one-dimensional simulation box $\mathscr{S} = [0, x_0]$, we consider its partitioning into finite elements $[x^i, x^{i+1}]$ where $(i = 0, 1, \ldots, n_e - 1)$,

$$\begin{aligned} x^0 < x^1 < x^2 < \cdots < x^{n_e-1} < x^{n_e}, \\ x^0 = 0, \qquad x^{n_e} = x_0, \end{aligned} \tag{3.6}$$

and n_e denotes the number of sub-intervals, see Fig. 3.2.

An accurate, pointwise representation of a function $g(x)$ within each sub-interval can be obtained from a quadrature rule that uses interpolating functions to approximate definite integrals. In our case, we take the Gauss-Lobatto quadrature as a starting point. It estimates an integral over the interval $[-1, 1]$ as (n_g abscissas),

$$\int_{-1}^{+1} \mathrm{d}x\, g(x) \approx \sum_{m=0}^{n_g-1} w_m g(x_m), \tag{3.7}$$

and is exact for polynomials of maximum degree $2n_g - 1$. The integration points x_m and weights w_m are defined by[11] $(m = 0, 1, \ldots, n_g - 1)$,

$$\begin{aligned} &\left.\frac{\mathrm{d}L_{n_g-1}(x)}{\mathrm{d}x}\right|_{x=x_m} = 0, \\ &w_m = \begin{cases} \frac{2}{n_g(n_g-1)}, & m = 0, n_g - 1, \\ \frac{2}{n_g(n_g-1)\{L_{n_g-1}(x_m)\}^2}, & \text{otherwise}, \end{cases} \end{aligned} \tag{3.8}$$

with the Legendre polynomial $L_{n_g-1}(x)$. For a collection of numerical values for x_m and w_m, see, e.g., Ref. [151].

The extension of Eq. (3.7) to an arbitrary interval $[x^i, x^{i+1}]$ is mediated by a linear transformation and leads to the *generalized Gauss-Lobatto* (GGL) points [139],

$$x_m^i = \frac{1}{2}\left\{\left(x^{i+1} - x^i\right)x_m + \left(x^{i+1} + x^i\right)\right\}, \tag{3.9}$$

and the associated weights,

[11] As the roots of Legendre polynomials are symmetric about $x = 0$, the same symmetry applies to the Gauss-Lobatto points (weights) x_m (w_m).

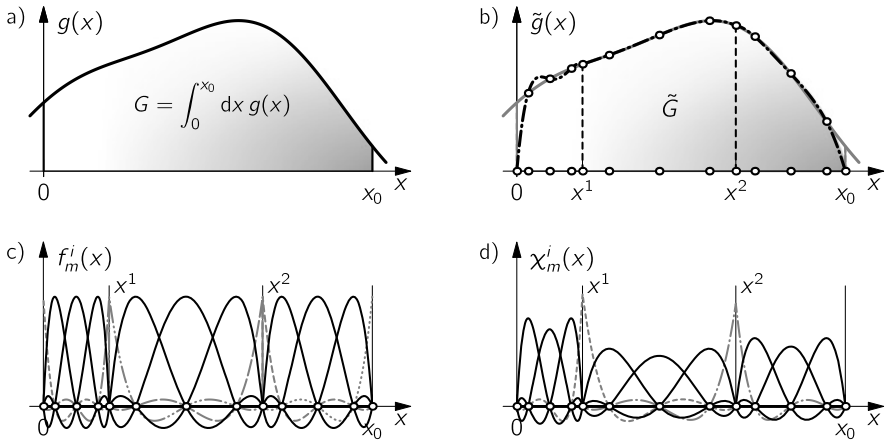

Fig. 3.3 (**a**) Integration of a function $g(x)$ (*solid line*) and (**b**) its approximate $\tilde{g}(x)$ (*dash-dotted line*) according to Eq. (3.11) for $n_\mathrm{e} = 3$ elements, $n_\mathrm{g} = 5$ generalized Gauss-Lobatto points per element, and the constraint $\tilde{g}(0) = \tilde{g}(x_0) = 0$. Panel (**c**) shows the corresponding Lobatto shape functions $f_m^i(x)$ of Eq. (3.12), and panel (**d**) indicates the normalized FE-DVR basis functions $\chi_m^i(x)$, cf. Eq. (3.16). Neglecting the first and the last DVR function in the construction, the basis has dimension $n_\mathrm{b} = 11$. Note that each of the two bridge functions (*gray dashed lines*) extends over two adjacent finite elements to guarantee spatial continuity

$$w_m^i = \frac{1}{2} w_m \left(x^{i+1} - x^i \right). \tag{3.10}$$

Here, the superscript i refers to the i-th element of the simulation box partitioning (3.6), compare with Fig. 3.2.

Computationally, an integral over the entire simulation box $\mathscr{S}$ can now be performed by successive applications of the quadrature rule. Under the additional constraint of a vanishing integrand at the interval boundaries $x = 0$ and $x = x_0$, we obtain the estimator,

$$G = \int_0^{x_0} \mathrm{d}x\, g(x) = \sum_{i=0}^{n_\mathrm{g}-1} \int_{x^i}^{x^{i+1}} \mathrm{d}x\, g(x) \approx \sum_{i=0}^{n_\mathrm{e}-1} \sum_{m=0}^{n_\mathrm{g}-1} w_m^i g\left(x_m^i\right) = \tilde{G}. \tag{3.11}$$

For an illustration of an integral with $n_\mathrm{e} = 3$ elements and $n_\mathrm{g} = 3$ GGL points, see Fig. 3.3(a) and (b).

For sufficiently smooth functions $g(x)$ in Eq. (3.11), convergence $\tilde{G}(n_\mathrm{e}, n_\mathrm{g}) \to G$ is reached faster by adding finite elements than increasing the maximum order of the interpolating polynomials (increase of n_g). For this reason, the number of GGL points can be kept quite small—typically $n_\mathrm{g} < 10$, cf. Ref. [139]. Moreover, we emphasize that the estimated value may be highly inaccurate if the integrand is not continuously differentiable within $\mathscr{S}$. This fact is related to the Gibbs phenomenon observed in Fourier series.

The interpolating functions behind Eq. (3.11) are usually referred to as DVR or *Lobatto shape functions* (see Refs. [139, 152]) and have the polynomial form,

$$f_m^i(x) = \begin{cases} \prod_{m' \neq m} \frac{x - x_{m'}^i}{x_m^i - x_{m'}^i}, & x^i \leq x \leq x^{i+1}, \\ 0, & \text{otherwise.} \end{cases} \tag{3.12}$$

Figure 3.3(c) shows them for the partitioning introduced in panel (a) and (b), respectively. For further reference, we collect some important properties:

(i) For Lobatto shape functions evaluated at a GGL point $x_{m'}^{i'}$, we have[12],

$$f_m^i\left(x_{m'}^{i'}\right) = \delta_{mm'}^{ii'}, \tag{3.13}$$

(ii) two Lobatto shape functions are orthogonal in the sense of the generalized Gauss-Lobatto quadrature, i.e.,

$$\int_0^{x_0} \mathrm{d}x \, f_m^i(x) f_{m'}^{i'}(x) \overset{(3.11)}{=} \delta_{mm'}^{ii'} w_m^i, \tag{3.14}$$

(iii) the first derivative at a GGL point reads,

$$\left.\frac{\mathrm{d}f_m^i(x)}{\mathrm{d}x}\right|_{x=x_{m'}^{i'}} = \begin{cases} \frac{1}{x_m^i} \prod_{\tilde{m} \neq m,m'} \frac{x_{m'}^i - x_{\tilde{m}}^i}{x_m^i - x_{\tilde{m}}^i}, & m = m', \\ \frac{\delta_{m,n_\mathrm{g}-1} + \delta_{m0}}{2w_m^i}, & \text{otherwise.} \end{cases} \tag{3.15}$$

With Eq. (3.14), the subset of those Lobatto shape functions which are non-zero in element i form locally, i.e., in element i, a complete basis. This basis is called a DVR basis. However, in order to extend it to the whole simulation box $\mathscr{S}$, we must account for the following: As the Lobatto shape functions in adjacent elements are independent of each other (note, there is no overlap), they generally cannot represent a continuous function in the joined space. To resolve this problem, we combine the last function $f_{n_\mathrm{g}-1}^i(x)$ of element i and the first function $f_0^{i+1}(x)$ of element $i+1$ into a single one, cf. the dashed and dash-dotted lines in Fig. 3.3(d). Such a "bridge"-function exhibits the required overlap and, hence, guarantees spatial continuity of any expanded quantity. Moreover, we refrain from including the very first and the very last Lobatto shape function, $f_0^0(x)$ and $f_{n_\mathrm{g}-1}^{n_\mathrm{e}-1}(x)$, in the construction of the basis which is consistent with the boundary condition that any physical quantity vanishes at $x = 0$ and $x = x_0$.

After proper normalization in the sense of the generalized Gauss-Lobatto rule of Eq. (3.11), we arrive at the following FE-DVR basis functions [139]:

$$\chi_m^i(x) = \begin{cases} \frac{f_{n_\mathrm{g}-1}^i(x) + f_0^{i+1}(x)}{\{w_{n_\mathrm{g}-1}^i + w_0^{i+1}\}^{1/2}}, & m = 0 \quad \text{(bridge)}, \\ \frac{f_m^i(x)}{\{w_m^i\}^{1/2}}, & \text{otherwise} \quad \text{(element)}. \end{cases} \tag{3.16}$$

Note that m is now ranging from 0 to $n_\mathrm{g} - 2$, such that the total dimension of the FE-DVR basis is given by,

[12] With the short-hand notation $\delta_{mm'}^{ii'} = \delta_{ii'}\delta_{mm'}$.

$$n_{\mathrm{b}} = n_{\mathrm{e}}(n_{\mathrm{g}} - 1) - 1, \tag{3.17}$$

compare with Fig. 3.3(d).

3.3.3 Matrix Elements of Relevant Energies

As a next step, we, in FE-DVR representation, have to determine the matrix elements of the single-particle energy $h^{(1)}(t) = t^{(1)} + v^{(1)}(t)$ and the binary interaction $w^{(2)}$ because they enter the Kadanoff-Baym equations. For simplicity, we introduce the multi-indices $\mu = (i, m)$, $\nu = (i', m')$, $\bar{\mu} = (\bar{i}, \bar{m})$ and $\bar{\nu} = (\bar{i}', \bar{m}')$, refer to the FE-DVR basis functions as $|\mu\rangle = \chi_m^i(x)$, and compute the matrix elements $h^{(1)}_{\mu\nu}(t) = \langle\mu|h^{(1)(t)}|\nu\rangle$ and $w^{(2)}_{\mu\nu\bar{\mu}\bar{\nu}} = \langle\mu\nu|w^{(2)}|\bar{\mu}\bar{\nu}\rangle$. Computationally, it is convenient to treat the bridge function $\chi_0^i(x)$ as the last basis function in each element i (cf. also Fig. 3.4).

For the single-particle energy, one easily verifies that[13],

$$\begin{aligned} v^{(1)}_{\mu\nu}(t) &= \int_0^{x_0} \mathrm{d}x\, \chi_m^i(x) v^{(1)}(x,t) \chi_{m'}^{i'}(x) \\ &= \delta_{\mu\nu} \tilde{v}^{(1)}_{\mu}(t), \end{aligned} \tag{3.18}$$

where,

$$\tilde{v}^{(1)}_{\mu}(t) = \begin{cases} v^{(1)}(x^i_{n_{\mathrm{g}}-1}, t), & m = 0, \\ v^{(1)}(x^i_m, t), & \text{otherwise.} \end{cases} \tag{3.19}$$

To determine the matrix of the kinetic energy is somewhat more subtle. This is for two reasons: First, the non-locality caused by the differential operator $\partial^2/\partial x^2$ in (m denotes the particle mass),

$$t^{(1)}_{\mu\nu} = -\frac{\hbar^2}{2m} \int_0^{x_0} \mathrm{d}x\, \chi_m^i(x) \frac{\partial^2}{\partial x^2} \chi_m^i(x), \tag{3.20}$$

and, second, the fact that all FE-DVR basis functions have discontinuous derivatives at the element boundaries x^i ($i = 0, 1, \ldots, n_{\mathrm{e}}$), cf. Fig. 3.3(d). Following the derivation of Ref. [139], one has to properly define the second derivative of an FE-DVR basis function under the integral of Eq. (3.20) and obtains the final result:

[13] The same result holds for any other operator that is local in space.

$$t^{(1)}_{\mu\nu} = \frac{1}{2}\begin{cases} \frac{\delta_{ii'}(\tilde{t}^{(1),i}_{n_g-1,n_g-1}+\tilde{t}^{(1),i+1}_{00})+\delta_{i,i'+1}\tilde{t}^{(1),i}_{n_g-1,0}+\delta_{i,i'-1}\tilde{t}^{(1),i'}_{0,n_g-1}}{\{(w^i_{n_g-1}+w^{i+1}_0)(w^{i'}_{n_g-1}+w^{i'+1}_0)\}^{1/2}}, & m=m'=0, \\ \frac{\delta_{ii'}\tilde{t}^{(1),i}_{n_g-1,m'}+\delta_{i,i'-1}\tilde{t}^{(1),i'}_{0m'}}{\{w^i_{n_g-1}+w^{i+1}_0\}^{1/2}}, & m=0, m'>0, \\ \frac{\delta_{ii'}\tilde{t}^{(1),i}_{m,n_g-1}+\delta_{i,i'+1}\tilde{t}^{(1),i}_{m0}}{\{w^i_{m_1}(w^{i'}_{n_g-1}+w^{i'+1}_0)\}^{1/2}}, & m>0, m'=0, \\ \frac{\delta_{ii'}\tilde{t}^{(1),i}_{mm'}}{\{w^i_m w^i_{m'}\}^{1/2}}, & m,m'>0, \end{cases} \tag{3.21}$$

where the quantity $\tilde{t}^{(1)}$ is related to the derivative of Lobatto-shape functions by,

$$\tilde{t}^{(1),i}_{mm'} = \sum_{\bar{m}} w^i_{\bar{m}} \frac{\mathrm{d}f^i_m(x)}{\mathrm{d}x}\bigg|_{x=x^i_{\bar{m}}} \cdot \frac{\mathrm{d}f^i_m(x)}{\mathrm{d}x}\bigg|_{x=x^i_{\bar{m}}}. \tag{3.22}$$

Finally, we consider the matrix elements of the binary interaction $w^{(2)}$ in FE-DVR representation. They are defined by (we use the physicist's notation [36]),

$$w^{(2)}_{\mu\nu,\bar{\mu}\bar{\nu}} = \int_0^{x_0}\mathrm{d}x \int_0^{x_0}\mathrm{d}\bar{x}\, \chi_\mu(x)\chi_{\bar{\mu}}(\bar{x})w^{(2)}(x-\bar{x})\chi_\nu(x)\chi_{\bar{\nu}}(\bar{x}), \tag{3.23}$$

and are symmetric with respect to interchange of $\mu \leftrightarrow \nu$, $\bar{\mu} \leftrightarrow \bar{\nu}$ and pairs $(\mu,\nu) \leftrightarrow (\bar{\mu},\bar{\nu})$. Using Eq. (3.11), we find,

$$w^{(2)}_{\mu\nu,\bar{\mu}\bar{\nu}} = \delta_{\mu\nu}\delta_{\bar{\mu}\bar{\nu}}\tilde{w}^{(2)}_{\mu\nu}, \tag{3.24}$$

with,

$$\tilde{w}^{(2)}_{\mu\nu} = \begin{cases} w^{(2)}(x^i_{n_g-1} - x^{i'}_{n_g-1}), & m=m'=0, \\ w^{(2)}(x^i_{n_g-1} - x^{i'}_{m'}), & m=0,\ m'>0, \\ w^{(2)}(x^i_m - x^{i'}_{n_g-1}), & m>0,\ m'=0, \\ w^{(2)}(x^i_m - x^{i'}_{m'}), & m,m'>0, \end{cases} \tag{3.25}$$

which means, we just have to evaluate the interaction potential for particles located at the relevant GGL points.

With Eqs. (3.18), (3.21) and (3.24), all required matrix elements are analytically known for a given set of Gauss-Lobatto points. Thereby, the potential energy is diagonal and the kinetic energy has a block-diagonal representation[14]. But most important is the result for the binary interaction, cf. Eq. (3.24). Here, the properties of the FE-DVR basis lead to a high degree of diagonality such that the two-particle interaction potential can be represented by an object of the size of a single-particle quantity, see Eq. (3.25). Although the matrix $\tilde{w}^{(2)}_{\mu\nu}$ is generally fully occupied, this means a great advantage, as only few matrix elements have to be precomputed and, in turn, the evaluation of self-energies can drastically be simplified, cf. Sect. 3.3.4. The structure of all relevant matrices are illustrated in Fig. 3.4(a), (b), and (c).

[14] This becomes clear after a thorough analysis of Eg. (3.21).

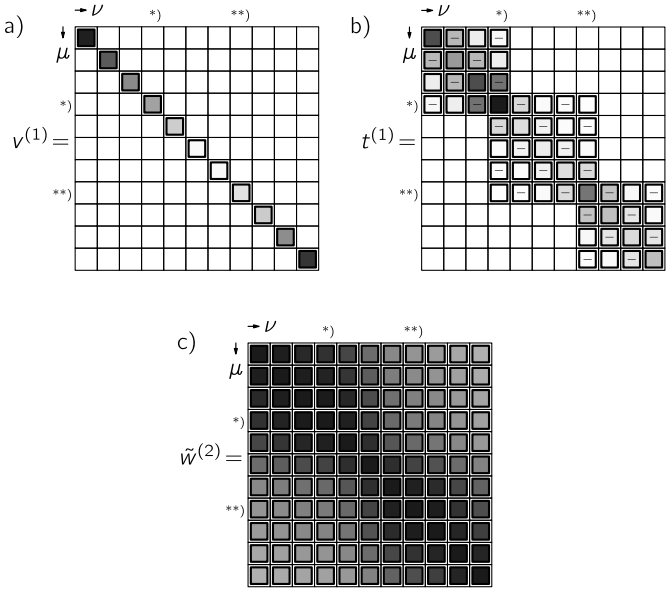

Fig. 3.4 Structure of the matrix of (**a**) the potential and (**b**) the kinetic energy in an FE-DVR basis of dimension $n_b = 11$. The grid parameters are as in Fig. 3.3. Panel (**c**) shows the matrix $\tilde{w}^{(2)}$ for a typical two-body interaction of the form $w^{(2)}(x - x') = [(x - x')^2 + 1]^{-1/2}$. For the potential energy, we have chosen $v^{(1)}(x) = \frac{1}{2}(x - \frac{x_0}{2})^2$. For the kinetic energy, negative matrix elements are marked by a minus sign. In all panels, the matrix elements associated with the first, respectively, the second bridge function are labeled by (*), respectively, (**), and no entry (i.e., no box) means that the corresponding matrix element (μ, ν) is zero

As a final remark, we note that the above results also hold for the case when the number of Lobatto shape functions varies from element to element. For details, we refer to Ref. [143].

3.3.4 First- and Second-Order Self-energies

Using the results of the last Section, we now can give explicit FE-DVR expressions for the HF and 2B self-energies as depicted in Fig. 2.6 of Chap. 2. Since the 1pSE functionally depends upon the 1pNEGF $G^{(1)}$ and the binary interaction $w^{(2)}$, we can use Eq. (3.24) to express it in terms of the reduced quantity $\tilde{w}^{(2)}$ of Eq. (3.25). In the course of this, some summations vanish due to the Kronecker deltas. In the following, we use the same notation as above (see the paragraph preceding Eq. (3.18)) and include a spin degeneracy factor $\xi = 2$ which accounts for double occupancy of states for a closed-shell electron system[15].

[15]For a spin-polarized system, we have $\xi = 1$.

For the (regular) HF self-energy, we obtain (cf. Eqs. (2.45) and (2.46)),

$$\begin{aligned}\Sigma^{(1),\mathrm{HF}}_{\mu\nu}(t,t') &= \delta_{\mathscr{C}}(t-t')\,\Sigma^{(1),\mathrm{HF}}_{\mu\nu}(t)\\ &= \delta_{\mathscr{C}}(t-t')\left\{\Sigma^{(1),\mathrm{H}}_{\mu\nu}(t)+\Sigma^{(1),\mathrm{F}}_{\mu\nu}(t)\right\},\end{aligned} \tag{3.26}$$

with,

$$\begin{aligned}\Sigma^{(1),\mathrm{H}}_{\mu\nu}(t) &= -\mathrm{i}\xi\,\delta_{\mu\nu}\sum_{\bar{\mu}}\tilde{w}^{(2)}_{\mu\bar{\mu}}G^{(1)}_{\bar{\mu}\bar{\mu}}(t,t^+),\\ \Sigma^{(1),\mathrm{F}}_{\mu\nu}(t) &= \mathrm{i}\tilde{w}^{(2)}_{\nu\mu}G^{(1)}_{\nu\mu}(t,t^+).\end{aligned} \tag{3.27}$$

Further, for the (irregular) part of the 2B self-energy, we have (cf. Eq. (2.61)),

$$\begin{aligned}\Sigma^{(1)}_{\mu\nu}(t,t') = &\sum_{\bar{\mu}}\sum_{\bar{\nu}}\tilde{w}^{(2)}_{\mu\bar{\mu}}\tilde{w}^{(2)}_{\nu\bar{\nu}}G^{(1)}_{\bar{\mu}\bar{\nu}}(t',t)\\ &\times\left\{\xi G^{(1)}_{\mu\nu}(t,t')G^{(1)}_{\bar{\nu}\bar{\mu}}(t,t')-G^{(1)}_{\mu\bar{\nu}}(t,t')G^{(1)}_{\bar{\nu}\mu}(t,t')\right\},\end{aligned} \tag{3.28}$$

where, consistently with the HF self-energy, only the direct term involves ξ.

Let us compare the numerical effort behind Eqs. (3.27) and (3.28) to that of a general basis representation that offers not as much diagonality, i.e., where all matrix elements of the interaction $w^{(2)}$ have to be taken into account. The determination of the HF self-energy along Eq. (3.27) requires an effort of n_b^3 for the direct term and n_b^2 for the exchange term. In contrast, in the general case, we know that two internal summations are due for both terms leading overall to an effort of n_b^4, compare with Eq. (2.46). Hence, we save a factor of (at least) n_b operations. For the irregular parts of the second Born self-energy, the situation is even more dramatic: Instead of the general scaling[16] like n_b^8 according to formula (2.61), we are left with n_b^4 in FE-DVR representation. Computationally, this means an enormous increase of efficiency as during the integration of the KBEs, the 1pSE has to be computed many times, see Chap. 4.

The generalization of the above scaling behavior to arbitrary 1pSEs is straightforward. If the respective self-energy diagram involves M vertex points (M intermediate integrations or summations), the effort is reduced from n_b^{2M} to $n_\mathrm{b}^* = n_\mathrm{b}^M$ in FE-DVR representation, i.e., instead of a quadratic scaling in n_b^* we are left with a linear one. This is a very promising result and should enable calculations with significantly larger basis dimensions, higher-order MBAs and (or) substantially longer time propagation.

Having obtained an efficient representation of the Hamiltonian and the self-energy, we are now ready to consider the evaluation of the collision integrals and the numerical solution of the KBEs (see Chap. 4).

[16] Restore all orbital indices and insert the full matrix for $w^{(2)}$.

Chapter 4
Computation of Equilibrium States and Time-Propagation

While in the last chapter, we have discussed possible and advantageous representations of the 1pNEGF when dealing with the description of inhomogeneous quantum many-body systems far from equilibrium, the present chapter gives an overview on the computational aspects when numerically solving the KBEs with a generic two-time (i.e., irregular) self-energy beyond the HF level. First, we will cover the initial state preparation on the basis of the Dyson equation in τ-space [68, 129] (cf. Sect. 4.1), and, thereafter, we will discuss the time evolution of the 1pNEGF (cf. Sect. 4.2) along the Keldysh contour [80].

In the second part, in addition to the description of the general algorithm, important issues are the parallelization of the two-time propagation [153] and an efficient implementation of the generalized Kadanoff-Baym ansatz (GKBA) introduced in Sect. 2.4.2.

4.1 Preparing the Initial State: Ground State or Equilibrium

In fact, a code that solves the KBEs (2.32) in real time is fully sufficient to generate also self-consistent (stationary and correlated) initial states. To this end, we adiabatically switch on the interaction [154] and, at time t_0, start from the ideal non-interacting system the 1pNEGF of which is usually known. The generalized two-body interaction $w^{(2)}(t-t')$ of Eq. (2.30) is then replaced by,

$$w^{(2)}\big(t-t'\big) \to \lambda(t)w^{(2)}\big(t-t'\big), \tag{4.1}$$

and the switching function $\lambda(t)$ gradually changes from zero at time t_0 to one at a later time t_s, for an example, see Fig. 4.1. If the switching time $t_s - t_0$ is sufficiently long (at least comparable to $\hbar$ over the typical level spacing), the many-body system passes through a series of intermediate eigenstates, and, finally, the equilibrium (eigen)state of the fully interacting system is reached[1]. Recalling the KBEs of

[1] This approach is originally due to Keldysh [59] and gets along without mixed Green's functions as no initial correlations are present.

K. Balzer, M. Bonitz, *Nonequilibrium Green's Functions Approach to Inhomogeneous Systems*, Lecture Notes in Physics 867,
DOI 10.1007/978-3-642-35082-5_4, © Springer-Verlag Berlin Heidelberg 2013

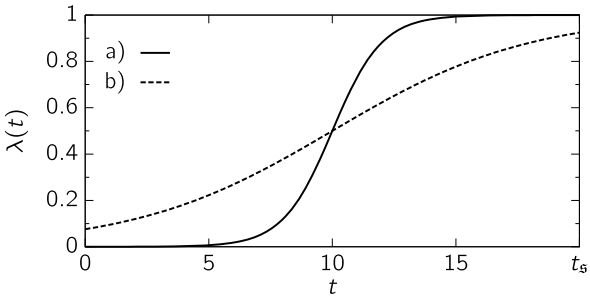

Fig. 4.1 Adiabatic switch-on of the interaction on the time interval $[t_0, t_s] = [0, 20]$ with switching functions of the form $\lambda(t) = 1 - [\exp(\lambda_0(t - 10)) + 1]^{-1}$. While function (a) is suitable for modeling the switch-on, function (b) cannot be used as it is not sufficiently zero (one) at the interval boundaries

Eq. (2.32), we emphasize that the switching function enters in two ways: as function of t in the first equation and as function of t' in the second, adjoint equation[2].

In view of the fact that full two-time solutions of the KBEs are limited in propagation time and that there are only few time steps to waste (see the discussion in Sect. 4.2.1 below), it is basically not an advantage to use adiabatic switching if the initial state is interacting. By contrast, it is more favorable to obtain an initial state directly from the KBEs' equilibrium limit—the Dyson equation—though this requires to include mixed Green's functions in the subsequent real-time propagation. To outline the preparation of initial states by solving the Dyson equation is the issue of the present section. The term "ground state" will refer to the special case of $\beta \to \infty$ (zero-temperature limit), and a "well-defined" initial state means one which is self-consistent and which remains stationary in a subsequent time propagation of the 1pNEGF if no external field is applied and the same approximation level is used for the self-energy.

4.1.1 Time or Frequency Space?

There are two equivalent ways of addressing the Dyson equation. Either we can treat it in the form of Eq. (2.38), or we can look at its (discrete) Fourier transform with respect to the time variable τ. While the former approach is the most natural one dealing with the imaginary track of the Keldysh contour, the latter represents the standard formulation often preferred in equilibrium and ground-state calculations. However, if one is mainly interested in the system's real-time evolution, whereby the collision integrals in the KBEs range over the full time contour and involve integrations over mixed Green's functions, it is useful to stay with time space.

In Sect. 4.1.2, we will discuss the solution of the Dyson equation in the τ-domain. In frequency space, the Dyson equation is given by,

$$\left\{\omega\delta_{ik} - \langle i|h^{(1)}|k\rangle\right\} G_{kj}^{(1),\mathrm{M}}(\omega) = \delta_{ij} + \Sigma_{ik}^{(1),\mathrm{M}}(\omega) G_{kj}^{(1),\mathrm{M}}(\omega), \tag{4.2}$$

[2]Therefore, also in the two-time self-energies, the switching function must carry the correct time argument (not only the physically relevant center of mass time!).

or, in integral form:

$$G_{ij}^{(1),\mathrm{M}}(\omega) = G_0^{(1),\mathrm{M}}(\omega) + G_{0,ik}^{(1),\mathrm{M}}(\omega)\,\Sigma_{kl}^{(1),\mathrm{K}}(\omega)G_{lj}^{(1),\mathrm{M}}(\omega), \tag{4.3}$$

with the (effectively) non-interacting Green's function $G_0^{(1),\mathrm{M}}$ and $\Sigma^{(1),\mathrm{K}}$ defined consistently to Eq. (2.42). In terms of the inverse Green's function, Eq. (4.3) can also be written as,

$$\left[G_{ij}^{(1),\mathrm{M}}\right]^{-1}(\omega) = \left[G_{0,ij}^{(1),\mathrm{M}}\right]^{-1}(\omega) - \Sigma_{ij}^{(1),\mathrm{K}}(\omega). \tag{4.4}$$

An iterative scheme to obtain self-consistent solutions of (4.3) up to second order is described, e.g., in Refs. [155, 156] which focus on calculations for closed- and open-shell atoms (from He up to Kr).

If a diagonal representation exists[3], a formal solution of Eq. (4.3) reads,

$$G_{ij}^{(1),\mathrm{M}}(\omega) = \frac{\delta_{ij}}{\omega - \omega_{0,i} - \Sigma_{\mathrm{irreg},i}^{(1),\mathrm{M}}(\omega)}, \tag{4.5}$$

where $\omega_{0,i}$ are the energies of the (effective) single-particle Hamiltonian. In the ground state ($\beta \to \infty$), we recover the connection of Eq. (4.5) to the spectral or Lehmann representation [55]:

$$\begin{aligned} G_{ij}^{(1),\mathrm{M}}(\omega) = &\sum_k \frac{\langle\Psi_0^{(N)}|\hat{f}_i|\Psi_k^{(N+1)}\rangle\langle\Psi_k^{(N+1)}|\hat{f}_j^\dagger|\Psi_0^{(N)}\rangle}{\omega - \omega_k^{(N+1)} + \omega_0^{(N)} + \mathrm{i}\eta} \\ &+ \sum_k \frac{\langle\Psi_0^{(N)}|\hat{f}_j^\dagger|\Psi_k^{(N-1)}\rangle\langle\Psi_k^{(N-1)}|\hat{f}_i|\Psi_0^{(N)}\rangle}{\omega + \omega_k^{(N-1)} - \omega_0^{(N)} - \mathrm{i}\eta}, \end{aligned} \tag{4.6}$$

where $|\Psi_0^{(N)}\rangle$ denotes the exact ground-state wave function of the system with energy $\omega_0^{(N)}$ and particle number N. Further, $\{|\Psi_k^{(N\pm1)}\rangle\}$ indicates the full set of states of the associated $N \pm 1$-particle system with energies $\omega_k^{(N\pm1)}$, and $\eta \to 0^+$ is an infinitesimal positive parameter that ensures convergence. In the numerator of Eq. (4.6), the matrix elements are the so-called Feynman-Dyson amplitudes. In the denominator, the expressions $\omega_k^{(N\pm1)} - \omega_0^{(N)}$ represent the state-selective addition and removal energies.

We note that the Matsubara Green's function can also be expanded in a Fourier series of the form [55] ($n = 0, \pm1, \pm2, \ldots$),

$$\begin{aligned} G_{ij}^{(1),\mathrm{M}}(\tau) &= \frac{1}{\beta}\sum_n \exp\left(-\mathrm{i}\omega_n\tau\right)G_{ij}^{(1),\mathrm{M}}(\mathrm{i}\omega_n), \\ G_{ij}^{(1),\mathrm{M}}(\mathrm{i}\omega_n) &= \int_0^\beta \mathrm{d}\tau\, \exp\left(\mathrm{i}\omega_n\tau\right)G_{ij}^{(1),\mathrm{M}}(\tau), \end{aligned} \tag{4.7}$$

[3] I.e., if, both, the single-particle Hamiltonian and the irregular part of the 1pSE are diagonal with respect to the same (spin-)orbital basis.

where, in the case of fermions[4], the Matsubara frequencies are given by,

$$\omega_n = (2n+1)\pi(\beta\hbar)^{-1}. \tag{4.8}$$

The discreteness is a direct consequence of the fact that the τ-interval is bounded[5]. Moreover, representation (4.7) must not be confused with the spectral one of Eq. (4.3) or Eq. (4.5), though there exists a unique relation between both as first pointed out by Baym and Mermin, see Ref. [157].

4.1.2 Solution of the Dyson Equation in τ-Space

For the numerical solution of the Dyson equation for inhomogeneous systems in thermodynamic equilibrium, we use the grand canonical ensemble and start from Eq. (2.42) following the idea of Ref. [68]. As a first step, we need to calculate the effectively non-interacting Green's function $G_0^{(1),\mathrm{M}}(\tau)$ which obeys,

$$\left\{\mathrm{i}\hbar\frac{\partial}{\partial\tau} - \langle i|h^{(1)}|k\rangle - \Sigma_{0,ik}^{(1),\mathrm{M}}\right\} G_{0,kj}^{(1),\mathrm{M}}(\tau) = \delta(\tau)\delta_{ij}. \tag{4.9}$$

Note that $\Sigma_0^{(1),\mathrm{M}}$ is defined through Eq. (2.41). In the eigenbasis determined by the effective one-particle Hamiltonian, $h^{(1),\mathrm{eff}} = h^{(1)} + \Sigma_0^{(1),\mathrm{M}}$, the solution is diagonal and can be written in the form,

$$G_{0,ij}^{(1),\mathrm{M}}(\tau) = \delta_{ij} f(\varepsilon_i - \mu;\beta)\exp\big[-\tau(\varepsilon_i - \mu)\big]. \tag{4.10}$$

Here, the energies ε_i are the eigenvalues of the effective Hamiltonian, $f(\varepsilon_i - \mu;\beta)$ denotes the Fermi-Dirac distribution, and μ is the chemical potential. The latter follows implicitly by demanding the normalization $N = \sum_i f(\varepsilon_i - \mu;\beta)$, where N is the given average particle number.

As the energies ε_i generally depend on $\rho_1 = G_0^{(1),\mathrm{M}}(0^-)$ through the self-energy, Eq. (4.10) must be iterated to determine a self-consistent solution. To this end, a symmetric 1pRDM "not too far away" from the intended fixed point may serve as starting point. Finally, the Green's function in the original spin-orbital basis is obtained by inverse transformation using the eigenvectors of $h^{(1),\mathrm{eff}}$. We mention that this goes along with a mixing of different exponential decays of Eq. (4.10).

In the zero-temperature limit ($\beta \to \infty$), the iterative procedure of computing $G_0^{(1)}(\tau)$ is equivalent to the self-consistent field (SCF) method [36] and the chemical potential will be situated within the energy interval of the highest occupied "molecular" orbital and the lowest unoccupied "molecular" orbital (HOMO-LUMO gap).

[4] For bosons, we have even multiples of $(\beta\hbar)^{-1}$.

[5] To define the Fourier transform, however, the time τ is periodically extended beyond the interval $[-\beta, +\beta]$.

As a consequence, methods known from SCF codes which improve convergence[6] are also applicable here, for an overview, see Ref. [35].

Once the effectively non-interacting Green's function is obtained, we can account for irregular parts of the 1pSE by solving Eq. (2.42). This, again, requires one to iterate. However, there are basically two strategies to account for the right hand side. Either one can transform the integral equation (2.42) into a set of multiple linear systems of equations (how this works is shown in Refs. [68, 129]), or one can evaluate the nested convolution integrals directly. The latter approach is generally more stable and reliable. Also, it saves computer memory and remains practical for large basis dimensions. To be comprehensive, we write out Eq. (2.42) in full ($\tau \in [-\beta, +\beta]$):

$$G_{ij}^{(1),\mathrm{M}}(\tau) = G_{0,ij}^{(1),\mathrm{M}}(\tau) + I_{ij}^{(1),\mathrm{M}}(\tau), \tag{4.11}$$

where (we sum over k),

$$\begin{aligned} I_{ij}^{(1),\mathrm{M}}(\tau) &= \int_0^\beta \mathrm{d}\bar{\tau}\, G_{0,ik}^{(1),\mathrm{M}}(\tau-\bar{\tau})\big\{J_{kj}^{(1),\mathrm{M}}(\bar{\tau}) - K_{kj}^{(1),\mathrm{M}}(\bar{\tau})\big\}, \\ J_{ij}^{(1),\mathrm{M}}(\tau) &= \int_0^\beta \mathrm{d}\bar{\tau}\, \Sigma_{ik}^{(1),\mathrm{M}}(\tau-\bar{\tau}) G_{kj}^{(1),\mathrm{M}}(\bar{\tau}), \\ K_{ij}^{(1),\mathrm{M}}(\tau) &= \begin{cases} \Sigma_{0,ik}^{(1),\mathrm{M}} G_{kj}^{(1),\mathrm{M}}(\tau), & 0 \le \tau \le \beta, \\ 0, & \text{otherwise.} \end{cases} \end{aligned} \tag{4.12}$$

While the self-energy $\Sigma^{(1),\mathrm{M}}(\tau)$ in the second line of Eq. (4.12) is a functional of the full Matsubara Green's function and is, therefore, updated in each iteration, in the third line of Eq. (4.12), $\Sigma_0^{(1),\mathrm{M}}$ is constant and a functional of the non-interacting Green's function only. Moreover, the Matsubara Green's function tends[7] to be large around $\tau = 0, \pm\beta$ and decays towards $\pm\frac{\beta}{2}$ (compare with Eq. (4.10)). For this reason, it is highly recommended to use an adapted (non-equidistant) τ-grid such as a uniform power mesh [68, 158]. This allows for a more adequate representation of the Green's function but usually requires interpolation to account for specific time differences $\tau - \bar{\tau}$ in Eq. (4.12).

As outlined in Sect. 2.2.2, it is sufficient to search for a self-consistent solution of the Dyson equation on the interval $[-\beta, 0]$. Along this line, a sensitive control parameter is provided by the particle number $N = \sum_i G_{ii}^{(1),\mathrm{M}}(0^-)$, and good measures for self-consistency are the element-wise convergence of the 1pRDM as well as the convergence of the correlation energy,

$$\langle \hat{H}_{\mathrm{cor}} \rangle = \frac{1}{2} \int_0^\beta \mathrm{d}\tau\, \mathrm{Tr}\left\{ \Sigma^{(1),\mathrm{M,irreg}}(-\tau) G^{(1),\mathrm{M}}(\tau) \right\}. \tag{4.13}$$

[6] E.g., by averaging (damping) or extrapolation schemes.

[7] Depending on the chosen basis.

Finally, regarding the real-time evolution of the Green's function, the specification of the Matsubara Green's function at $\tau = 0^-$ and its τ-dependence represent proper KMS boundary conditions in the sense of Eq. (2.22).

Applications of the iterative procedure along Eqs. (4.11) and (4.12) can be found, e.g., in the computation of quasi-particle band gaps of silicon and germanium, see Ref. [158], or in self-consistent second Born as well as GW calculations for atoms and molecules, see Refs. [68, 131]. Extensions to few-electron quantum dots are presented in Ref. [129].

4.2 Nonequilibrium

In general, a NEGF study of systems far from equilibrium requires to integrate the Kadanoff-Baym equations (2.32) simultaneously with respect to the two contour time variables t and t'. Initial conditions are realized by supplying the lesser Green's function $G^{(1),<}(t_0, t_0)$ and, if the initial state is correlated, either $G^{(1),\lceil}(t_0 - \mathrm{i}\beta, t_0)$ (compare with Sect. 4.1) or an additional self-energy $\Sigma^{(1)}_{\mathrm{in}}$, cf., e.g., Ref. [118]. The third option would be to start from the non-interacting Green's function and, as outlined above, to perform an adiabatic switch-on of the interaction prior to the computation of the actual dynamics of interest.

As the KBEs represent non-Markovian equations of motion when the one-particle self-energy is irregular (i.e., when correlations are included), each infinitesimal time evolution has, in principle, to account for the full past of the system's dynamics. This leads to a two-time propagation with a memory kernel $\mathscr{K}$ as illustrated in Fig. 4.2. Only if the 1pSE is regular, i.e., time diagonal, or further approximations such as the generalized Kadanoff-Baym ansatz (GKBA) are applied, the time propagation can be simplified and organized along the direction of the physically relevant center of mass time.

4.2.1 Two-Time Propagation Method

For the two-time propagation of the 1pNEGF for homogeneous systems[8], a numerical algorithm is outlined in Ref. [114] with reference to optically excited semiconductor electron-hole plasmas and nuclear heavy-ion collisions. The key points are here the use of the momentum representation and the performance of the convolution integrals (cf. $\mathscr{K}$ in Fig. 4.2) by fast Fourier transform.

Applications to finite and inhomogeneous systems follow, for the most part, the generic work of Stan et al. [80] which covers the Hartree-Fock (HF), the second Born (2B) and the GW approximation. Here, the main idea is to set up a matrix

[8] Practically, all the literature considers the case of fermions.

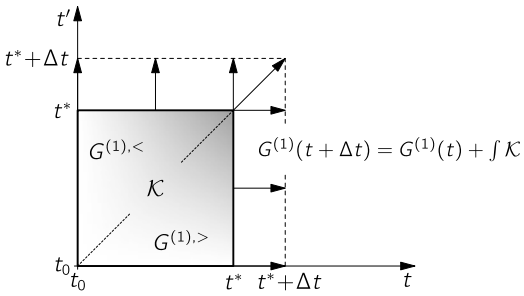

Fig. 4.2 Illustration of the two-time propagation of the 1pNEGF $G^{(1)}(t,t')$ under the presence of the memory kernel $\mathscr{K}$

algebra for the time-stepping procedure which is based on the time-evolution operator constructed from the single-particle plus Hartree-Fock energy. This allows one to eliminate the HF self-energy from the collision integrals (i.e., from the r.h.s. of the KBEs).

To be able to describe later a parallelized version of the propagation method for inhomogeneous systems, we repeat the most important steps of Ref. [80]. First, we discretize[9] the time variables t and t' in units of a constant time step Δt. Further, we make use of the fact that the greater and lesser correlation functions are related by Eq. (2.22), i.e., due to symmetry, we only need to compute, for example, $G^{(1),>}(t,t')$ for $t > t'$ and $G^{(1),<}(t,t')$ for $t \leq t'$. As the two-time HF self-energy is regular and proportional to a contour delta function $\delta_{\mathscr{C}}(t-t')$ (compare with Eqs. (2.45) and (2.46)), the corresponding collision term can be evaluated to,

$$\int_{\mathscr{C}} \mathrm{d}\bar{t}\, \Sigma^{(1),\mathrm{HF}}(t,\bar{t}) G^{(1)}(\bar{t},t') = \Sigma^{(1),\mathrm{HF}}(t) G^{(1)}(t,t'), \tag{4.14}$$

where the quantity $\Sigma^{(1),\mathrm{HF}}(t)$ has just the form of an additional potential which depends on the interaction $w^{(2)}$ and the 1pRDM. In the KBEs, we can easily account for this term by replacing the single-particle energy $h^{(1)}(t)$ by an effective one: $h^{(1)}_{\mathrm{eff}}(t) = h^{(1)}(t) + \Sigma^{(1),\mathrm{HF}}(t)$. Hence, the first KBE reads (dropping spin and orbital degrees of freedom),

$$\begin{aligned} \left\{-\mathrm{i}\hbar\frac{\partial}{\partial t} - h^{(1)}_{\mathrm{eff}}(t)\right\} G^{(1)}(t,t') &= \delta_{\mathscr{C}}(t-t') + I^{(1)}(t,t'), \\ I^{(1)}(t,t') &= \int_{\mathscr{C}} \mathrm{d}\bar{t}\, \Sigma^{(1)}_{\mathrm{irreg}}(t,\bar{t}) G^{(1)}(\bar{t},t'). \end{aligned} \tag{4.15}$$

Using the unitary time-evolution operator[10],

$$U(t;\Delta t) = \exp\left(-\frac{\mathrm{i}}{\hbar} h^{(1)}_{\mathrm{eff}}(t)\Delta t\right), \tag{4.16}$$

[9] For an approach that uses relative and center of mass variables, see, e.g., Ref. [159].

[10] Its matrix elements follow from diagonalizing $h^{(1),\mathrm{eff}}$.

we can derive simple expressions for the time stepping of each NEGF component[11]. For a sufficiently small time step of length Δt, one obtains,

$$\begin{aligned} G^{(1),>}(t^*+\Delta t,\bar{t}) &= U(t^*;\Delta t)G^{(1),>}(t^*,\bar{t}) - V(t^*;\Delta t)I_1^{(1),>}(t^*,\bar{t}),\\ G^{(1),<}(\bar{t},t^*+\Delta t) &= G^{(1),<}(\bar{t},t^*)U^\dagger(t^*;\Delta t) - I_2^{(1),<}(\bar{t},t^*)V^\dagger(t^*;\Delta t), \end{aligned} \tag{4.17}$$

and, along the time diagonal,

$$\begin{aligned} &G^{(1),<}(t^*+\Delta t,t^*+\Delta t)\\ &\quad = U(t^*;\Delta t)\big(G^{(1),<}(t^*,t^*) + W(t^*;\Delta t)\big)U^\dagger(t^*;\Delta t), \end{aligned} \tag{4.18}$$

where (matrix valued),

$$V(t;\Delta t) = \frac{1}{h^{(1),\mathrm{eff}}(t)}\left\{1-\exp\left(-\frac{\mathrm{i}}{\hbar}h^{(1)}_{\mathrm{eff}}(t)\Delta t\right)\right\}, \tag{4.19}$$

and[12],

$$\begin{aligned} W(t;\Delta t) &= \sum_{n=0}^{\infty} w_n(t;\Delta t),\\ w_n(t;\Delta t) &= \frac{\mathrm{i}\hbar\Delta t}{n+1}\big[h^{(1),\mathrm{eff}}(t), w_{n-1}(t;\Delta t)\big]_-,\\ w_0(t;\Delta t) &= -\mathrm{i}\hbar\Delta t\, I_{12}^{(1),<}(t), \end{aligned} \tag{4.20}$$

with $I_{12}^{(1),<}(t) = I_1^{(1),<}(t,t) - I_2^{(1),<}(t,t)$. If needed, the mixed Green's function $G^{(1),\rceil}$ must be propagated according to,

$$\begin{aligned} &G^{(1),\rceil}(t^*+\Delta t, t_0-\mathrm{i}\bar{\tau})\\ &\quad = U(t^*;\Delta t)G^{(1),\rceil}(t^*,t_0-\mathrm{i}\bar{\tau}) - V(t^*;\Delta t)I^{(1),\rceil}(t^*,t_0-\mathrm{i}\bar{\tau}). \end{aligned} \tag{4.21}$$

In Eqs. (4.17) and (4.21), all quantities are known for times $t, t' \le t^*$ (see Fig. 4.2), and the "collision" integrals $I_1^{(1),>}(t,t')$, $I_2^{(1),<}(t,t')$ and $I^{(1),\rceil}(t,t_0-\mathrm{i}\tau)$ are the components of the convolution integral in Eq. (4.15). To obtain their structure in terms of the 1pSE and 1pNEGF components, one applies the Langreth-Wilkins rules. In addition, we note that the following symmetries hold,

$$I_1^{(1),\gtrless}(t,t') = -\big[I_2^{(1),\gtrless}(t',t)\big]^\dagger, \qquad I_{1,2}^{(1),>}(t,t) = I_{1,2}^{(1),<}(t,t). \tag{4.22}$$

Basically, the integration error of the above scheme is of the order Δt^2. However, there exist different ways to improve the time integration [80]. One possibility is to recalculate the HF self-energy and the collision integrals at times t^* using the nonequilibrium Green's functions for $t^*+\Delta t$. A subsequent time stepping with

[11] The derivation is given in Ref. [80]

[12] The n-th term is of the order Δt^{n+1} such that contributions with $n > 3$ can usually be neglected.

averaged values[13] for $\Sigma^{(1),\mathrm{HF}}$ and $I^{(1),x}$ ($x = >, <, \lceil$) then leads to an improved Green's function at time $t^* + \Delta t$. Moreover, during the time evolution, one should check for particle number conservation by verifying that,

$$\mathrm{Tr}\left\{I_{12}^{(1),<}(t,t)\right\} = 0. \tag{4.23}$$

This relation is very sensitive to potential implementation errors and follows from inserting Eq. (4.18) into $N = -\mathrm{i}\hbar\mathrm{Tr}\{G^{(1),<}(t+\Delta t, t+\Delta t)\}$ and using the cyclic invariance of the trace as well as the unitarity of $U(t;\Delta t)$.

From the numerical point of view, it is obvious that the extent of the memory kernel $\mathscr{K}$ in Fig. 4.2 limits the performance of the KBE solver in two aspects:

(i) the final propagation time $t_{\mathfrak{f}}$ is limited by the amount of Green's functions that can be stored in the random access memory (RAM) of the computer,
(ii) the growing region of time integration in the collision integrals quadratically slows down the algorithm with time progression.

4.2.2 Parallelization Strategies

In order to soften or to (partly) overcome the above limitations, a reasonable idea is to use state-of-the-art high-performance computing strategies. In the following, we want to outline a parallel algorithm based on the steps (4.17), (4.18) and (4.21) that allows one to efficiently solve the KBEs on multi-processor machines using practically all available local RAM. This means that we do not require a shared memory environment.

To describe the parallel algorithm, we, in the following, use the terminology of the message passing interface (MPI), e.g., Ref. [160]. This means, we launch multiple copies of one and the same program which are referred to as "processes" or "ranks". Parallelization is then achieved by a cooperative action of these copies synchronized through collective or point-to-point communication. When p processes are started, we label them from 0 to $p-1$, and usually process 0 takes over the function of the master for serial parts of the algorithm that are not (or cannot be) parallelized.

The main idea of the algorithm is a clever distribution of the 1pNEGF over the memory of the individual MPI processes. To motivate such an approach, we examine the collision integrals relevant in Eqs. (4.17) and (4.21) for fixed t^*, $\bar{t}$ and $\bar{\tau}$. After applying the Langreth-Wilkins rules (cf. Table 2.1), we have,

[13] The averaging is performed separately for each matrix component, i.e., for the self-energy for example the average is $\bar{\Sigma}_{ij}^{(1),\mathrm{HF}}(t,t') = \frac{1}{2}\{\Sigma_{ij}^{(1),\mathrm{HF}}(t,t') + \Sigma_{ij}^{(1),\mathrm{HF}}(t,t'+\Delta t)\}$ when propagating in the t'-direction, cf. also Ref. [80].

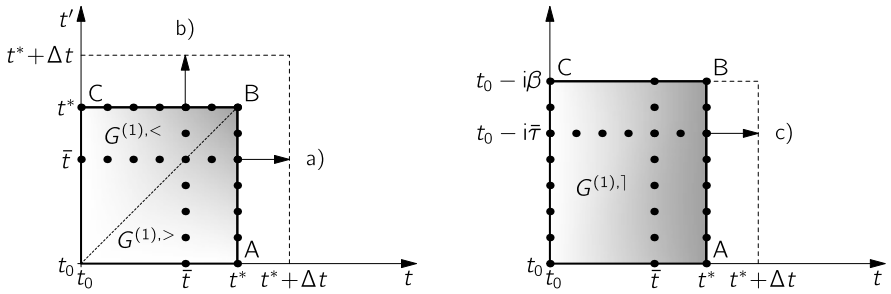

Fig. 4.3 Two-time propagation of the 1pNEGF components. The *solid dots* mark the real-time (*left panel*) and the imaginary-time contributions (*right panel*) to the collision integrals in Eqs. (4.24) to (4.26): (**a**) $I_1^{(1),>}(t^*,\bar{t})$, (**b**) $I_2^{(1),<}(\bar{t},t^*)$, and (**c**) $I^{(1),\rceil}(t^*,t_0-\mathrm{i}\bar{\tau})$. As in Fig. 4.2, the lesser (greater) correlation function is computed for $t \le t'$ ($t > t'$). Note that the irregular part of the one-particle self-energy $\Sigma^{(1)}(t,t')$, with $t,t' \in \mathscr{C}$, functionally depends on, both, $G^{(1)}(t,t')$ and $G^{(1)}(t',t)$

$$
\begin{aligned}
I_1^{(1),>}(t^*,\bar{t}) &= \int_{t_0}^{t^*} \mathrm{d}t'\, \Sigma_{\mathrm{irreg}}^{(1),>-<}(t^*,t') G^{(1),>}(t',\bar{t}) \\
&\quad + \int_0^{\bar{t}} \mathrm{d}t'\, \Sigma_{\mathrm{irreg}}^{(1),>}(t^*,t') G^{(1),<->}(t',\bar{t}) \\
&\quad - \mathrm{i}\hbar \int_0^{\beta} \mathrm{d}\tau'\, \Sigma_{\mathrm{irreg}}^{(1),\rceil}(t^*,t_0-\mathrm{i}\tau') G^{(1),\lceil}(t_0-\mathrm{i}\tau',\bar{t}), \qquad (4.24) \\
I_2^{(1),<}(\bar{t},t^*) &= \int_{t_0}^{\bar{t}} \mathrm{d}t'\, G^{(1),>-<}(\bar{t},t') \Sigma_{\mathrm{irreg}}^{(1),<}(t',t^*), \\
&\quad + \int_0^{t^*} \mathrm{d}t'\, G^{(1),<}(\bar{t},t') \Sigma_{\mathrm{irreg}}^{(1),<->}(t',t^*) \\
&\quad - \mathrm{i}\hbar \int_0^{\beta} \mathrm{d}\tau'\, G^{(1),\rceil}(\bar{t},t_0-\mathrm{i}\tau') \Sigma_{\mathrm{irreg}}^{(1),\lceil}(t_0-\mathrm{i}\tau',t^*), \qquad (4.25) \\
I^{(1),\rceil}(t^*,t_0-\mathrm{i}\bar{\tau}) &= \int_0^{t^*} \mathrm{d}t'\, \Sigma_{\mathrm{irreg}}^{(1),>-<}(t^*,t') G^{(1),\rceil}(t',t_0-\mathrm{i}\bar{\tau}) \\
&\quad - \mathrm{i}\hbar \int_0^{\beta} \mathrm{d}\tau'\, \Sigma_{\mathrm{irreg}}^{(1),\rceil}(t^*,t_0-\mathrm{i}\tau') G^{(1),\lceil}(t_0-\mathrm{i}(\tau'-\bar{\tau}),t_0), \\
&\qquad (4.26)
\end{aligned}
$$

where the notation $\mathscr{X}^{\gtrless-\lessgtr}$ ($\mathscr{X} = G^{(1)}, \Sigma^{(1)}$) indicates the difference $\mathscr{X}^{\gtrless} - \mathscr{X}^{\lessgtr}$, and the mixed Green's function in the second integral of Eq. (4.26) can be replaced by the Matsubara Green's function, cf. Eq. (2.22). In Fig. 4.3, the solid dots mark the Green's functions which contribute in these three integrals. While some Green's functions enter directly, some are hidden in the one-particle self-energy, see also the figure caption. Graphically, the latter are located on the edges of the expanding square (rectangle) in the left (right) panel of Fig. 4.3, cf. the paths $\overline{\mathrm{AB}}$ and $\overline{\mathrm{BC}}$.

Computationally, it is highly advantageous when the Green's functions marked in Fig. 4.3 are contained in the RAM attributed to the process which performs the integration. In that case, no Green's function $G^{(1),\gtrless}(t,t')$ and $G^{(1),\rceil}(t,t_0-\mathrm{i}\tau)$ with past time arguments $t,t'\leq t^*$ needs to be exchanged between the program copies. In addition, working in parallel for different $\bar{t}$ and $\bar{\tau}$, the individual processes then can propagate (one after another) the lesser, the greater and the mixed Green's function, and the resulting components at $t^*+\Delta t$ automatically belong to the correct memory[14], see the arrows labeled (a), (b) and (c) in Fig. 4.3.

The problem remains that the above memory allocation must be realized for each tuple (t,t') and (t,τ) with t and t' ranging from t_0 to the final propagation time t_f and τ ranging from zero to β. So how can this be achieved? In the case of two MPI processes, we start with alternately assigning the correlation functions[15] to the individual processes, i.e., we make $G^{(1),\gtrless}(2n\Delta t,t')$ and $G^{(1),\gtrless}(t,2n\Delta t)$ known to the first process and $G^{(1),\gtrless}((2n+1)\Delta t,t')$ and $G^{(1),\gtrless}(t,(2n+1)\Delta t)$ to the second process ($n=0,1,2,\ldots,(t_\mathrm{f}\Delta t^{-1}-1)/2$). Similarly, we proceed for the mixed Green's function. As the τ-grid is generally not equidistant (compare with Sect. 4.1.2), we first discretize the interval $[0,\beta]$ according to $\tau_0=0,\tau_1,\ldots,\tau_{M-2},\tau_{M-1}=\beta$, where M is the number of mesh points. Then, we assign $G^{(1),\rceil}(2n\Delta t,t_0-\mathrm{i}\tau)$ and $G^{(1),\rceil}(t,t_0-\mathrm{i}\tau_{2m})$ to the first process and $G^{(1),\rceil}((2n+1)\Delta t,t_0-\mathrm{i}\tau)$ as well as $G^{(1),\rceil}(t,t_0-\mathrm{i}\tau_{2m+1})$ to the second ($m=0,1,\ldots,\frac{M}{2}-1$). In addition, both processes need to know the Matsubara Green's function, cf. the last term in Eq. (4.26). Aside from the Green's functions that enter through the self-energies in Eqs. (4.24) to (4.26), we obtain the desired allocation of memory.

Interestingly, the described memory distribution allows for a parallel precomputation of the self-energies as the required Green's functions are always locally known. Doing so, at fixed time t^* and integer n,m with $(2n+1)\Delta t\leq t^*$ and $(2m+1)<M$, the first process calculates $\Sigma^{(1),\gtrless}_\mathrm{irreg}(2n\Delta t,t^*)$ and $\Sigma^{(1),\rceil}_\mathrm{irreg}(t^*,t_0-\mathrm{i}\tau_{2m})$, whereas the second one computes $\Sigma^{(1),\gtrless}_\mathrm{irreg}((2n+1)\Delta t,t^*)$ and $\Sigma^{(1),\rceil}_\mathrm{irreg}(t^*,t_0-\mathrm{i}\tau_{2m+1})$. The following symmetries apply:

$$\begin{aligned}\Sigma^{(1),\gtrless}(t,t')&=-\left[\Sigma^{(1),\gtrless}(t',t)\right]^\dagger,\\ \Sigma^{(1),\lceil}(t_0-\mathrm{i}\tau,t)&=\left[\Sigma^{(1),\rceil}(t,t_0-\mathrm{i}(\beta-\tau))\right]^\dagger.\end{aligned}\tag{4.27}$$

Of course, the obtained values for the 1pSEs must be shared between both processes before calculating the collision integrals. This is most easily implemented by using the MPI broadcast function.

Finally, we remark that the time-diagonal time step of Eq. (4.18) is carried out in sequence with the adjacent time steps in t- and t'-direction (cf. Fig. 4.2) and that all newly computed Green's function components for $t^*+\Delta t$ must be transferred

[14] I.e., they can be stored locally.

[15] Note that, for $t\leq t'$ ($t'<t$), we mean the lesser (greater) function.

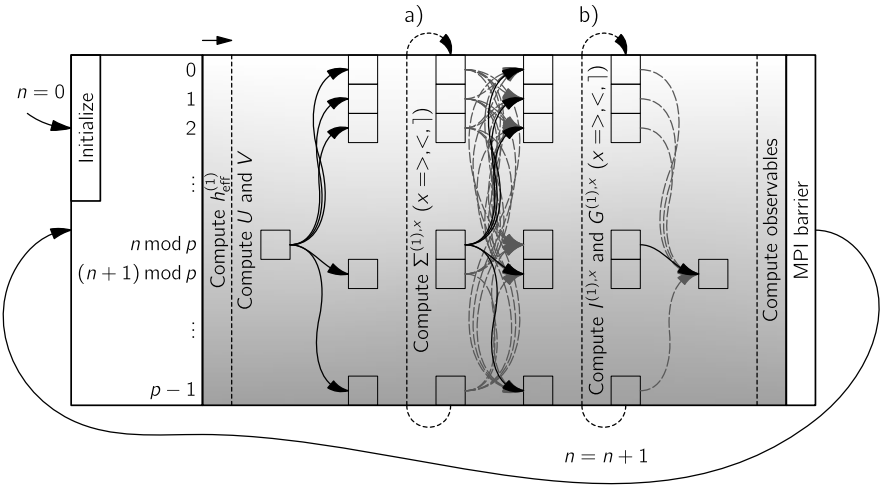

Fig. 4.4 MPI parallelization of the numerical solution of the two-time Kadanoff-Baym equations. *Within the gray-shaded area*, the individual processes are listed from top to bottom and the sequence of execution is from left to right. While communications of process ($n \bmod p$) are highlighted by *solid arrows*, all remaining communications are indicated by *gray dashed arrows*. The loops labeled as (**a**) and (**b**) have to be performed for all $i \leq n$ and all $j \leq M-1$, compare with steps (iv) to (vi) of the algorithm overview. The final MPI barrier ensures synchronization before the next time step is initiated

once to the other process (by a point-to-point communication). The latter is a consequence of the fact that the total 1pNEGF (i.e., the final memory kernel for $t_\mathfrak{f}$) is effectively stored twice which is the only drawback or compromise of this approach. On the other hand, the memory distribution enables a well load-balanced parallelization which gets along with minimum communication overhead.

Furthermore, the generalization to more than two MPI processes is straightforward. In the case of p processes, the correlation function $G^{(1),\gtrless}(t,t')$ must be stored in the memory of process p_1 and p_2 with[16],

$$p_1 = t\,\Delta t^{-1} \bmod p, \qquad p_2 = t'\,\Delta t^{-1} \bmod p, \tag{4.28}$$

whereas, the mixed Green's function $G^{(1),\rceil}(t, t_0 - \mathrm{i}\tau_m)$ with $m = 0, 1, \ldots, M-1$ has to be part of process p_3 and p_4 where,

$$p_3 = t\,\Delta t^{-1} \bmod p, \qquad p_4 = m \bmod p. \tag{4.29}$$

As mentioned before, the Matsubara Green's function $G^{(1),\mathrm{M}}$ must be completely known to all processes.

To be more comprehensive, we give a short summary of the parallel algorithm when p MPI processes are involved (for illustration of the required MPI communications, see Fig. 4.4):

[16] In the implementation, t and t' are multiples of Δt.

(i) All processes get the kinetic energy (matrix) $t^{(1)}$, the binary interaction $w^{(2)}$, and the discretized Matsubara Green's function $G^{(1),\mathrm{M}}(\tau_m)$ as input and initialize a local counter, $n = 0$.

(ii) Process 0 uses the Matsubara Green's function to initialize $G^{(1),<}(t_0, t_0)$, and $G^{(1),\rceil}(t_0, t_0 - \mathrm{i}\tau)$ for all $\tau = \tau_m$ $(m = 0, 1, \ldots, M-1)$, cf. Eq. (2.22).

(iii) Process $(n \bmod p)$ computes and diagonalizes the effective single-particle energy $h^{(1)}_{\mathrm{eff}}(t_0 + n\Delta t)$. Thereafter, it calculates $U(t_0 + n\Delta t; \Delta t)$ and $V(t_0 + n\Delta t; \Delta t)$ of Eqs. (4.16) and (4.19) and sends both quantities to all remaining processes.

(iv) For all non-negative integers $i \leq n$ and $j \leq M-1$, process $(i \bmod p)$ computes the self-energies $\Sigma^{(1),>}(t_0 + n\Delta t, t_0 + i\Delta t)$ and $\Sigma^{(1),<}(t_0 + i\Delta t, t_0 + n\Delta t)$ and process $(j \bmod M)$ computes $\Sigma^{(1),\rceil}(t_0 + n\Delta t, t_0 - \mathrm{i}\tau_j)$. Each self-energy computation is followed by a broadcast to all other processes.

(v) For all $i \leq n$, as in (iv), process $(i \bmod p)$, first, computes the collision integrals $I_1^{(1),>}(t_0 + n\Delta t, t_0 + i\Delta t)$ and $I_2^{(1),<}(t_0 + i\Delta t, t_0 + n\Delta t)$ and, second, propagates the correlation functions according to Eq. (4.17). Process $(n \bmod p)$ additionally undertakes the time-diagonal step of Eq. (4.18). Furthermore, each newly computed correlation function is transferred to process $((n+1) \bmod p)$.

(vi) For $j \leq M-1$, as in (iv), process $(j \bmod M)$ computes the collision integral $I^{(1),\rceil}(t_0 + n\Delta t, t_0 - \mathrm{i}\tau_j)$ and propagates the mixed Green's function by using Eq. (4.21). Similar to v., each newly computed Green's function is transferred to process $((n+1) \bmod p)$.

(vii) As process $(n \bmod p)$ has knowledge of the current time-diagonal Green's function $G^{(1),<}(t_0 + n\Delta t, t_0 + n\Delta t)$ and the corresponding collision integrals, it is clear that it computes all relevant observables. We note that the correlation part of the interaction energy is most simply evaluated as,

$$\langle H_{\mathrm{cor}} \rangle(t) = -\frac{\mathrm{i}}{2} \mathrm{Tr}\left\{ I_1^{(1),>}(t,t) \right\}. \tag{4.30}$$

(viii) After synchronization, all processes increment their counter n by one and return to point (iii).

We mention that a parallel algorithm similar to the one described above has been independently developed by Garny and Müller, see Ref. [161].

In practice, the parallel KBE solver following steps (i) to (viii) reveals good performance. Figure 4.5 shows the efficiency measured in terms of the speed-up ratio for three different MPI calculations with up to 512 processes. The speed-up ratio $S(p) = T_1/T_p$ is a measure of the degree of parallelization and compares the total runtime T_p using p processes to a serial run which requires the duration T_1. The test calculations[17] include about 25 spin orbitals and the second Born approximation for the self-energy of an inhomogeneous quantum system [153]. Overall, the overhead

[17] The calculations have been performed on the *xe* and *ice1* nodes of the North-German Supercomputing Alliance (HLRN) via Grant No. shp0006 (https://www.hlrn.de, retrieved 2011).

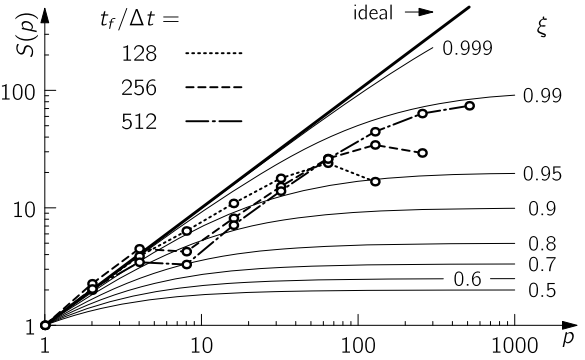

Fig. 4.5 Typical algorithm performance: speed-up ratio $S(p) = T_1/T_p$ (*dots*) as function of the number of MPI processes for two-time NEGF calculations of different length t_f. The *thick solid line* indicates the case $S(p) = p$. The *thin solid lines* refer to the Amdahl's predictor [162] $S(p) = \{(1-\xi) + \xi/p\}^{-1}$ at degree of parallelization ξ. Calculations were performed on the *xe* and *ice1* nodes of the HLRN, see footnote 17

due to communication and synchronization is small leading to a typical degree of parallelization of more than 95 %. We note that the performance drop in Fig. 4.5 between $p = 4$ and 8 is due to architecture differences when using more than 4 central processing units (CPUs). Thus, for large MPI calculations, the performance may be even better than indicated.

4.2.3 Single-Time Propagation using the GKBA

From the numerical point of view, the generalized Kadanoff-Baym ansatz (GKBA) of Eq. (2.70) (Sect. 2.4.2) is very promising. This is because it allows for propagating the 1pNEGF only along the time diagonal (cf. Fig. 4.2) which is computationally faster[18] and requires essentially less memory. Note that the GKBA is formulated in the real-time domain, and a consistent equilibrium version is so far not known. This inhibits us to self-consistently (on the level of the GKBA) define a correlated and equilibrated initial state through an equilibrium Dyson equation according to Eq. (2.38) or (2.42). Alternatively, the time propagation can start from the (effectively) non-interacting system. In order to systematically include initial correlations, we then have to resort to the technique of adiabatic switching as outlined in the introduction of this chapter. In the following, we give details for the NEGF time propagation under the GKBA. For the reasons mentioned above, we do not explicitly treat terms that account for initial correlations since they are included via the adiabatic switching procedure.

[18]Though, it still slows down with time progression due to the memory integral, compare with Eqs. (4.37) and (4.39).

Once the double-time retarded and advanced propagators $G^{(1),\mathrm{R}}$ and $G^{(1),\mathrm{A}}$ are known, the GKBA allows us to use the relation,

$$G^{(1),\gtrless}(t,t') = \mathrm{i}\hbar\left\{G^{(1),\mathrm{R}}(t,t')G^{(1),\gtrless}(t',t') - G^{(1),\gtrless}(t,t)G^{(1),\mathrm{A}}(t,t')\right\}, \quad (4.31)$$

in all expressions that require off-time-diagonal Green's functions. In particular, it is, therefore, sufficient to use Eq. (4.18) for the time stepping. Writing out the associated collision integral $I_{12}^{(1),<}(t)$ yields (see Eqs. (4.20) and (4.22) and neglect initial correlations),

$$\begin{aligned} I_{12}^{(1),<}(t^*) &= I_1^{(1),<}(t^*,t^*) - I_2^{(1),<}(t^*,t^*) \\ &= \int_{t_0}^{t} \mathrm{d}\bar{t}\left\{\Sigma^{(1),>}(t^*,\bar{t})G^{(1),<}(\bar{t},t^*) - \Sigma^{(1),<}(t^*,\bar{t})G^{(1),>}(\bar{t},t^*)\right. \\ &\quad \left. + G^{(1),<}(t^*,\bar{t})\Sigma^{(1),>}(\bar{t},t^*) - G^{(1),>}(t^*,\bar{t})\Sigma^{(1),<}(\bar{t},t^*)\right\}. \end{aligned} \quad (4.32)$$

In the GKBA scheme, this integral depends on all time-diagonal correlation functions and the double-time retarded and advanced functions. It can also be written as,

$$I_{12}^{(1),<}(t^*) = I_1^{(1),<}(t^*,t^*) + \left[I_1^{(1),<}(t^*,t^*)\right]^\dagger. \quad (4.33)$$

For further simplification, we consider the equations of motion for $G^{(1),\mathrm{R/A}}$, which we treat on the HF level[19]:

$$\begin{aligned} &\left\{\mathrm{i}\hbar\frac{\partial}{\partial t} - h_{\mathrm{eff}}^{(1)}(t)\right\}G^{(1),\mathrm{R/A}}(t,t') = \delta_{\mathscr{C}}(t-t'), \\ &\text{and the adjoint Eq. with } t \leftrightarrow t', \end{aligned} \quad (4.34)$$

where $h_{\mathrm{eff}}^{(1)}(t) = h^{(1)}(t) + \Sigma^{(1),\mathrm{HF}}(t)$ is defined as introduced in Sect. 4.2.1. When the time dependence of the effective single-particle energy is determined outside of Eq. (4.34) [in practice, we evaluate it using the 1pRDM $\rho_1(t) = -\mathrm{i}\hbar G^{(1),<}(t,t)$] the solution reads,

$$G^{(1),\mathrm{R/A}} = \mp\mathrm{i}\theta_{\mathscr{C}}\left(\pm\left[t-t'\right]\right)Y^{(1)}(t,t'), \quad (4.35)$$

with,

$$\begin{aligned} Y^{(1)}(t,t') &= \exp\left(-\frac{\mathrm{i}}{\hbar}\int_{t'}^{t}\mathrm{d}\bar{t}\,h_{\mathrm{eff}}^{(1)}(\bar{t})\right), \\ Y^{(1)}(t,t') &= \left[Y^{(1)}(t',t)\right]^\dagger \quad (*), \\ Y_{ij}^{(1)}(t,t) &= \delta_{ij}. \end{aligned} \quad (4.36)$$

Inserting Eqs. (4.31) and (4.35) in Eq. (4.32) leads to,

[19] To consider them in the presence of correlations would lead to equations of motion that are as difficult to solve as the full two-time KBEs.

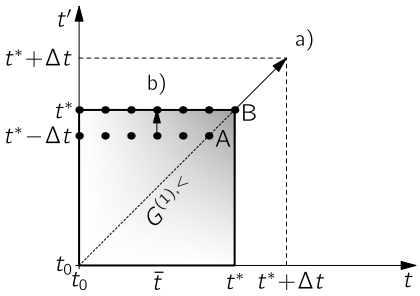

Fig. 4.6 Time propagation of the 1pNEGF using the GKBA. The reconstruction (4.31) allows for a propagation along the time diagonal, see arrow (a). In terms of $Y^{(1)}(\bar{t}, t^*)$ (*dots*), the retarded and advanced Green's function can be obtained recursively, cf. Eq. (4.38) and arrow (b). At points A and B, $Y^{(1)}$ is just the unit matrix, cf. Eq. (4.36)

$$
\begin{aligned}
&I_{12}^{(1),<}(t^*) \\
&\quad = \int_{t_0}^{t} \mathrm{d}\bar{t} \left\{ \left[\Sigma^{(1),>}(t^*, \bar{t}) G^{(1),<}(\bar{t}, \bar{t}) - \Sigma^{(1),<}(t^*, \bar{t}) G^{(1),>}(\bar{t}, \bar{t}) \right] Y^{(1)}(\bar{t}, t^*) \right. \\
&\qquad \left. + Y^{(1)}(t^*, \bar{t}) \left[G^{(1),<}(\bar{t}, \bar{t}) \Sigma^{(1),>}(\bar{t}, t^*) - G^{(1),>}(\bar{t}, \bar{t}) \Sigma^{(1),<}(\bar{t}, t^*) \right] \right\}. \quad (4.37)
\end{aligned}
$$

Of course, in the same line of action, one has to evaluate the two-time self-energies for a given MBA.

In the implementation of the GKBA, we use symmetry (*) of Eq. (4.36) and need to know the quantity $Y^{(1)}(\bar{t}, t^*)$ for all times $\bar{t} \leq t^*$. For progressed time propagation, this means the execution of a rather large number of diagonalizations of the effective single-particle Hamiltonian in a single time step. This would be unfavorable for calculations that require a large spin-orbital basis. To our advantage, $Y^{(1)}$ obeys a simple recurrence relation when the time step Δt is sufficiently small ($\bar{t} \leq t^*$):

$$
\begin{aligned}
Y^{(1)}(\bar{t}, t^*) &= \exp\left(\frac{\mathrm{i}}{\hbar} \int_{\bar{t}}^{t^*-\Delta t} \mathrm{d}t' \, h_{\mathrm{eff}}^{(1)}(t') + \frac{\mathrm{i}}{\hbar} \int_{t^*-\Delta t}^{\bar{t}} \mathrm{d}t' \, h_{\mathrm{eff}}^{(1)}(t') \right) \\
&= \exp\left(-\frac{\mathrm{i}}{\hbar} \int_{t^*-\Delta t}^{\bar{t}} \mathrm{d}t' \, h_{\mathrm{eff}}^{(1)}(t') + \frac{\mathrm{i}}{\hbar} h_{\mathrm{eff}}^{(1)}(t^* - \Delta t) \Delta t \right) \\
&= Y(\bar{t}, t^* - \Delta t) U^{\dagger}(t^* - \Delta t; \Delta t). \quad (4.38)
\end{aligned}
$$

To arrive at the last equality, we have used the Baker-Campbell-Hausdorff formula ($\exp(a+b) = \mathrm{e}^{a}\mathrm{e}^{b}\mathrm{e}^{-\frac{1}{2}[a,b]_-}$, in which the commutator vanishes) and have identified the time-evolution operator of Eq. (4.16).

With Eq. (4.38), we avoid many successive diagonalizations of the effective single-particle Hamiltonian and can straightforwardly construct the new retarded or advanced Green's function which enter the collision integral (4.37), see Fig. 4.6. As a result, the GKBA scheme requires the propagation of the lesser correlation function along the time diagonal according to Eq. (4.18) and the simultaneous time

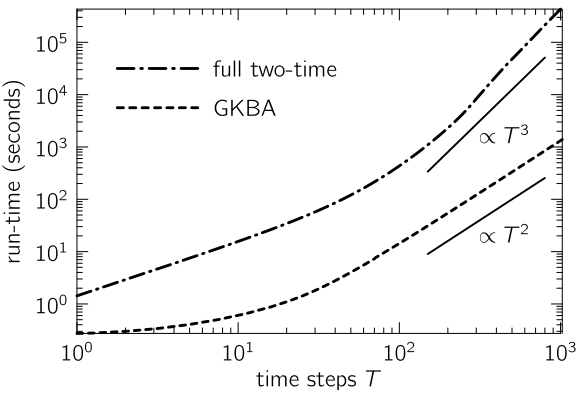

Fig. 4.7 Typical performance of a GKBA calculation compared to the full two-time scheme of Sect. 4.2.1. Whereas for two-time calculations, the runtime scales as T^3 with T being the number of time steps, it is reduced to a quadratic scaling when using the GKBA. The data represent serial 2B calculations with identical parameters. Figure after Ref. [113]

stepping of the quantity $Y^{(1)}$. For the latter, we have to evaluate (compare with Eqs. (4.36) and (4.38)),

$$Y^{(1)}\big(\bar{t}, t^* + \Delta t\big) = Y\big(\bar{t}, t^*\big)U^\dagger\big(t^*; \Delta t\big), \tag{4.39}$$

for $\bar{t} \leq t^*$, whereas, along the time diagonal, it is,

$$Y^{(1)}_{ij}\big(t^* + \Delta t, t^* + \Delta t\big) = \delta_{ij}. \tag{4.40}$$

Compared to full two-time calculations, the GKBA propagation is not only memory friendly, but also will be essentially faster. This is because one propagates the 1pNEGF exclusively in the direction of the time diagonal and, with Eqs. (4.39) and (4.40), an efficient treatment of the memory kernel is possible. Figure 4.7 shows a comparison between a typical GKBA and the corresponding full two-time calculation as function of the number of time steps T propagated, cf. Ref. [113]. As expected, the runtime of the full calculation (dash-dotted line) scales like T^3 in the long-time limit. On the contrary, the use of the GKBA allows for a much faster time evolution and leads overall to a runtime which saturates at a beneficial T^2-behavior; see the dashed line, which indicates an about two orders of magnitude smaller total runtime below $T = 10^3$ and an even larger speedup for $T > 10^3$.

Part IV
Applications for Inhomogeneous Systems

Chapter 5
Lattice Systems

This chapter aims at giving a brief overview on the current status of Kadanoff-Baym approaches to lattice systems. To this end, we address the most relevant literature[1] and, as a basic example, show NEGF results for a Hubbard-type dimer.

As "lattice" systems, we generally denote quantum many-body systems where the particle motion is restricted to a finite or infinite set of localized sites in coordinate space. Prominent examples can be found in condensed matter systems and include, for example, the electron dynamics between the 3d (and/or 4f) orbitals in transition metal oxides—for respective LDA + U calculations[2] see, e.g., Ref. [163]. However, the "lattice" sites need not necessarily be arranged in form of a well defined grid (i.e., on a real lattice described by a specific unit cell). Instead, also other nanoscale systems can directly be described by lattice-type Hamiltonians. Among these systems are, e.g., molecular junctions, small carbon nanotubes and wires, or atomic size point contacts.

Theoretically as well as computationally, lattice systems can usually be described by a small set of parameters. This is due to the fact that the interaction between the charge carriers is typically short-ranged such that one can confine oneself to a purely local and (or) nearest-neighbor interaction. Furthermore, a specific hopping amplitude[3] (resembling the kinetic energy) is often sufficient to describe the movement of the particles from one lattice site to another.

[1] We mainly focus on papers, that apply specific many-body approximations to the KBEs and, for example, do not cover dynamical mean-field theory-based works. For an overview in this direction, see Refs. [42, 164] and references therein.

[2] While LDA means "local-density approximation", the parameter U indicates a purely local Hubbard-type interaction, cf. Sect. 5.2.

[3] The hopping amplitude is related to the overlap between the one-particle orbitals on different lattice sites.

K. Balzer, M. Bonitz, *Nonequilibrium Green's Functions Approach to Inhomogeneous Systems*, Lecture Notes in Physics 867,
DOI 10.1007/978-3-642-35082-5_5, © Springer-Verlag Berlin Heidelberg 2013

5.1 Overview

The application of the Keldysh-Kadanoff-Baym formalism to the description of lattice systems in nonequilibrium to date mainly concerns the zero-temperature limit and small systems with a low number of single-particle states.

To give a chronological overview, we first mention Ref. [165], where the Kondo effect and the zero-temperature transport properties of the Anderson impurity model have been studied on the level of the GW approximation by Thygesen and Rubio. Thereafter, the current-voltage (IV) characteristics of a generic two-level system coupled to wide-band leads has been investigated in detail in Ref. [166]. Here, beyond the HF level, the inclusion of correlations in the 2B and GW approximation has led to an essential shift of the conductance peaks and an additional asymmetry in the peak profiles. As the responsible mechanism one has exposed the broadening of the spectral function and the closure of the energy gap between the occupied and unoccupied states.

In order to study the quantum transport through double quantum dots and to address the influence of initial correlation and memory effects on the transient dynamics, the KBEs have then been solved by Myöhänen et al. in Ref. [167]. Extensions to larger system sizes and other quantities such as transient currents, dipole moments, spectral functions and charging times have been presented by the same authors in Ref. [168]. Furthermore, applications including AC and DC fields are subject to Ref. [169], and generalizations to superconducting leads can be found in the work of Stefanucci et al. [76].

In parallel with the study of quantum transport phenomena, there have appeared works by Puig von Friesen et al. on small 1D Hubbard nanoclusters [85, 170], where non-linear effects have been studied including the HF, 2B, GW and TM approximation. There, the main focus has been on the spectral functions, the density response to an external perturbation and the appearance of damping and (multiple) steady states. Throughout, many effects were found to be best described within the TM approximation. Further, in Ref. [171], Verdozzi et al. have performed real-time 2B, GW and TM calculations on a small 3D cubic cluster to benchmark time-dependent density functional theory (TDDFT) results based on the non-perturbative adiabatic local-density approximation (ALDA). Particularly for fast perturbations, the authors have noted that NEGF results are clearly superior to the ALDA due to the inclusion of non-local and non-adiabatic effects.

Thereafter, a thorough comparison of many-body perturbation theory, time-dependent density-matrix renormalization group (TDDMRG) and TDDFT has been presented in Ref. [172] for the Anderson model under nonequilibrium conditions. Moreover, an interesting direction has been the description of double excitations in the Kadanoff-Baym framework, cf. also Sect. 6.2.2. Respective work in the context of a Hubbard-Hamiltonian and its extensions is subject to Ref. [173] and includes the response function and addition and removal energies analyzed within different conserving MBAs. Furthermore, NEGFs have been applied also to investigate the image charge dynamics in quantum transport. In Ref. [174], surface polarization effects such as the dynamical formation of image charges at the dot-lead interface

have been studied in detail. Also, it has been concluded that correlations prevent plateaus in the IV-curves and correct the absence of relaxation processes observed in HF-type solutions. Very recently, in Ref. [175], it has been shown for interacting nanoscale junctions that dynamical correlations suppress the presence of multistability in observables such as the density or the current.

In many of the above-mentioned works, more or less serious limitations of the Kadanoff-Baym approach and unphysical effects have been detected. These include self-interaction errors, the presence of infinite number of poles in the spectral function[4], spurious dynamical excitations and artificial correlation-induced damping leading to steady states. Basically, all these effects can be attributed to the approximate treatment of the one-particle self-energy. Along these lines, it has in particular been shown that also correlation functions (as, e.g., the double occupancy in Hubbard-type systems) can violate important properties such as positiveness. In Ref. [176], it is demonstrated that this is the case for 2B and GW but not for the T-matrix approximation.

5.2 A Basic Example

As an elementary example of a lattice model, we consider an isolated two-site Hubbard cluster at half-filling[5] obeying the dimensionless Hamiltonian,

$$\hat{H} = \sum_{\sigma=\uparrow,\downarrow} \left(-t\left\{\hat{f}^\dagger_{1,\sigma}\hat{f}_{2,\sigma} + \hat{f}^\dagger_{2,\sigma}\hat{f}_{1,\sigma}\right\} + v(t)\,\hat{n}_{1,\sigma}\right) + U\sum_{i=1,2}\hat{n}_{i,\uparrow}\hat{n}_{i,\downarrow}, \quad (5.1)$$

with the spin-density operator $\hat{n}_{i,\sigma} = \hat{f}^\dagger_{i,\sigma}\hat{f}_{i,\sigma}$ and the on-site interaction U (Hubbard U) which penalizes double occupancy of the same site. The first two terms describe the hopping of electrons from the first to the second site and vice versa. On site $i = 1$, we will later apply a spin-independent but time-dependent perturbation of the form $v(t)\,\hat{n}_{1,\sigma}$.

The ground and excited states of the system (5.1) are known analytically, e.g., Ref. [177]. For the hopping amplitude $t = 1$, they are shown in Fig. 5.1 as function of the Hubbard U. Here, the ground-state energy is well described in the 2B approximation, see the dots. On the contrary, the HF approximation indicates a wrong linear U-dependence. In the limit $U \to \infty$, the eigenstates E_- and E_0 as well as E_U and E_+ are degenerate. Moreover, the energy gap (see the arrow) increases linearly with the Hubbard U such that the system becomes insulating at large coupling.

[4] Although the exact finite lattice system has a finite number of poles.

[5] There is one up- and one down-spin electron in the system ($N = N_\uparrow + N_\downarrow = 2$).

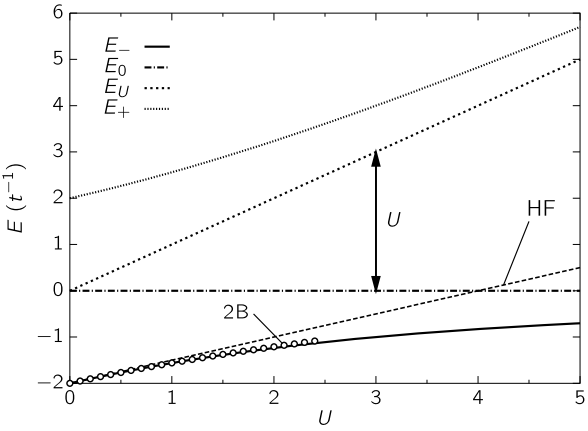

Fig. 5.1 Ground-state ($E_- = \frac{U}{2} - \sqrt{U^2/4 + 4t^2}$) and excited-state energies ($E_0 = 0$, $E_U = U$ and $E_+ = \frac{U}{2} + \sqrt{U^2/4 + 4t^2}$) of the two-site Hubbard model at half-filling and $t = 1$ for different parameters U, cf. [177]. Whereas the HF approximation (*dashed line*) leads to a linear dependence of the ground-state energy on U, the 2B approximation (*dots*) well approaches the exact result. The indicated main energy gap is equal to the Hubbard U. In the limit $U \to \infty$, E_- and E_0 as well as E_U and E_+ become degenerate

5.2.1 Dynamics Following a Non-Perturbative Excitation

In this Section, we examine the dynamics of the two-site Hubbard model (5.1) following a non-linear perturbation. To this end, we consider $v(t)$ being proportional to a step function, i.e.,

$$v(t) = v_0 \theta(t - t_0), \tag{5.2}$$

with a variable amplitude v_0. We note that this case has also been investigated by Puig von Friesen et al. in Ref. [170].

In Fig. 5.2(a) to (c), we show the local density response of the system,

$$\langle \hat{n}_1 \rangle(t) = -2\mathrm{i}\hbar G_{11}^{(1),<}(t, t), \tag{5.3}$$

for different many-body approximations and amplitudes ranging from $v_0 = 0$ to 5. The total density $\langle \hat{n}_1 \rangle + \langle \hat{n}_2 \rangle$ is constant, being normalized to $N = 2$, and we have used the spin degeneracy factor $\xi = 2$ as introduced in Sect. 3.3.4. In the case of weak perturbations, $v_0 < 1$, all three panels show the same behavior: The local density starts to oscillate and indicates a temporal depopulation of the first site (the stronger the perturbation, the larger the depopulation). In addition, with increasing v_0, the characteristic time period of this oscillation decreases. However, in the regime of moderate to strong excitations, $v_0 > 1$, the three calculations yield completely different results. While the HF solution in panel (a) indicates a permanent oscillation of $\langle \hat{n}_1 \rangle(t)$, the inclusion of correlations in the 2B approximation in panel (b) leads—for sufficiently large amplitudes $v_0 \gtrsim 2.5$—to damped solutions

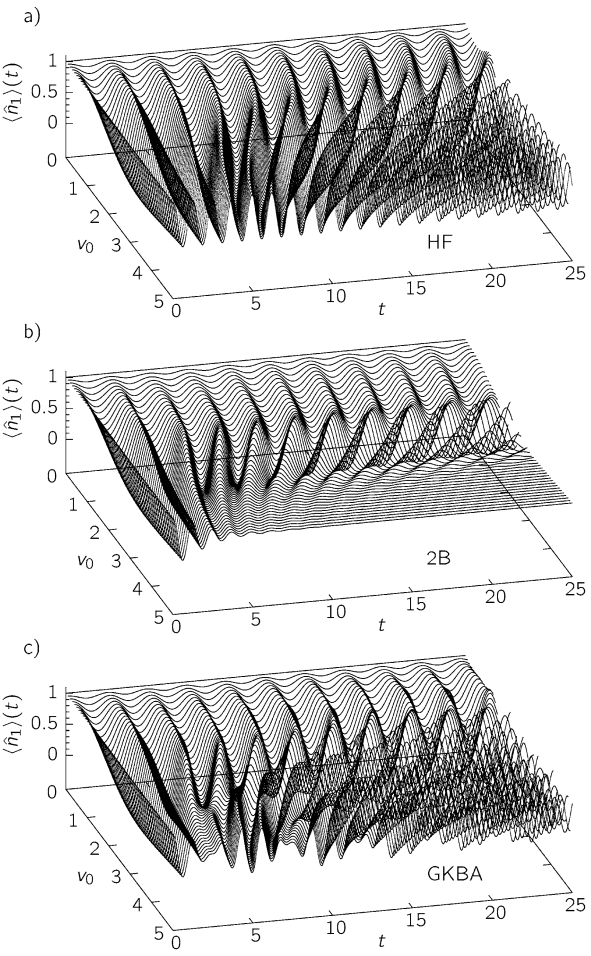

Fig. 5.2 Density response of the two-site Hubbard cluster of Eq. (5.1) at $U = 1$ following a perturbation acting only on the first site for $t \geq t_0 = 0$. (**a**) Hartree-Fock (HF) approximation, (**b**) second Born (2B) approximation and (**c**) GKBA with 2B kernel. While, in (**a**) and (**c**), the density performs an undamped oscillation, in panel (**b**), the density is strongly damped for $v_0 \gtrsim 2.5$ leading to an unphysical steady state, compare with Ref. [170]

where finally a steady state is reached which is characterized by a low electron density on site $i = 1$. As such a behavior is not observed when the model is solved exactly, see Ref. [170], it is clearly an artifact of the many-body approximation (MBA) used[6]. On the other hand, in Fig. 5.2(c), we observe that damped solutions are not obtained when one applies the generalized Kadanoff-Baym ansatz[7] (GKBA), cf. Sect. 2.4.2. Here, the use of HF propagators in the retarded and advanced Green's functions apparently prevents steady states though correlations are included on the 2B level.

Figure 5.3 compares approximate and exact results for $\langle \hat{n}_1 \rangle(t)$ in the limit of large v_0. As seen before, in contrast to HF (dashed line), the 2B result (solid line) is

[6] We emphasize that energy and particle number conservation is fulfilled at all times.

[7] The GKBA data are provided by S. Hermanns (University Kiel) [178].

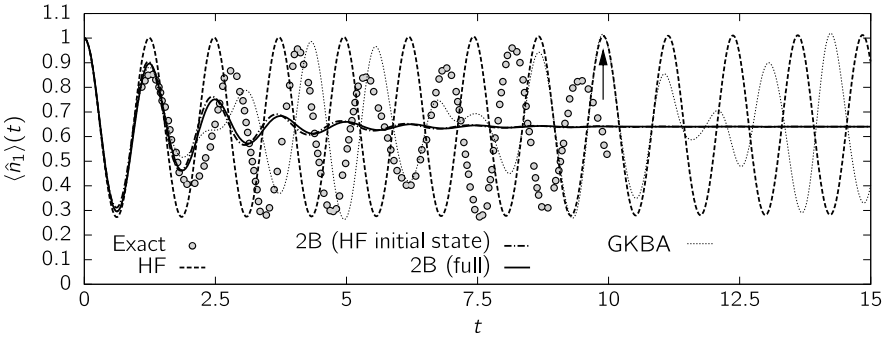

Fig. 5.3 Density response of the two-site Hubbard cluster at $U = 1$ and $v_0 = 5$ for HF, 2B and GKBA. Note that the damping in 2B approximation does not depend on the initial state, compare the dash-dotted and the solid line. The exact data (*dots*) is adapted from Ref. [170]

strongly damped and reaches a steady state after about six oscillations. Neither the damping constant nor the final site occupation however depend on the approximate treatment of the initial state, compare the solid and dash-dotted curves which refer to the self-consistent and HF initial state, respectively, and which practically lie on top of each other. Hence, the damping in 2B is clearly a dynamical phenomenon. Moreover, it is found that the GKBA result (see the thin dotted line) is overall reasonably close to the exact one and does not reveal damping. However at specific points in time, it seems to mimic the HF result, see the arrow.

Formally, the correlation-induced damping observed in Figs. 5.2(b) and 5.3 can be attributed to the fact that a MBA is usually based on partial summations of MBPT diagrams which include terms of all orders. This means, there may exist terms which only compensate each other in an exact description of the problem. The non-compensating terms can then simulate effective bath states although the system is actually finite and isolated [85]. In other words, the MBA can artificially increase the phase space and, hence, facilitates artificial damping.

Finally, what remains an interesting point is the relatively sharp transition between the undamped and damped parameter regime in panel (b). A simple explanation of this fact is still missing.

5.2.2 Absorption Spectrum in Second Born Approximation

In the previous section, we have analyzed the two-site Hubbard cluster beyond the linear regime and have identified the emergence of artificial steady states. However, also in the linear regime, care must be taken when using a Kadanoff-Baym approach. To demonstrate this, we now compute the excitation spectrum of the same Hubbard cluster by propagating the NEGF in real time. As a small perturbation we consider,

$$v(t) = v_0 \delta(t - t_0), \tag{5.4}$$

in Eq. (5.1) and set $v_0 \ll 1$; typically $v_0 = 0.01$.

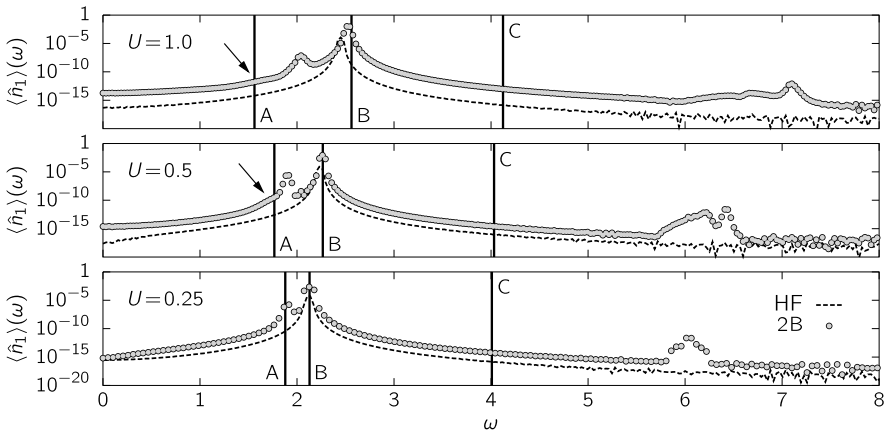

Fig. 5.4 Approximate linear-response excitation spectrum $\langle \hat{n}_1 \rangle(\omega)$ of the two-site Hubbard cluster for different U. The *thick vertical lines* indicate the exact excitation energies of transition A, B and C, respectively. Note that only transition B exists for the perturbation introduced by Eqs. (5.1) and (5.4). In 2B approximation, the energy of the single excitation B is generally superior to HF, see the *upper-most panel* ($U = 1.0$). However for small and large U, there appear additional, unphysical excited states not observed in the exact solution of the problem, compare also with Ref. [178]. We emphasize that the width of the HF and 2B peaks is determined by the limited length of the time propagation

From the exact diagonalization data (recall Fig. 5.1), we know that there exist three excited states in the system with energy E_0, E_U and E_+. This means, we may expect three ground-state transitions:

$$\begin{aligned} E_- &\to E_0 \quad \text{(below called A)}, \\ E_- &\to E_U \quad \text{(called B)}, \\ E_- &\to E_+ \quad \text{(called C)}. \end{aligned} \tag{5.5}$$

However, it is easily shown that only transition B with excitation frequency $\omega = E_U - E_-$ ($\hbar = 1$) has a non-vanishing transition moment for the perturbation introduced in Eq. (5.1), i.e., for a linear coupling of the time-dependent field $v(t)$ to the electron density on the first site. Furthermore, transition B represents a single electron excitation and therefore—in contrast to a double excitation[8]—does not require a correlated treatment of the system. As a consequence, it should appear *already* in a mean-field description of the spectrum[9].

Figure 5.4 shows the linear response spectrum,

$$\langle \hat{n}_1 \rangle(\omega) = \int \mathrm{d}t \, \mathrm{e}^{-\mathrm{i}\omega t} \, \langle \hat{n}_1 \rangle(t)|_{v_0 \ll 1}, \tag{5.6}$$

for the case of $U = 0.25$, 0.5 and 1.0 in HF and 2B approximation.

[8] A double excitation is a correlation-induced process where two electrons are excited simultaneously.

[9] For a more detailed discussion on single and double excitations, see Sects. 6.2.1 and 6.2.2.

First, we notice that, as expected, the single excitation B is well resolved in both results. Particularly for larger U, the 2B approximation accounts for most of the correlation-induced shift towards a larger excitation energy, cf. the vertical line B in the upper-most panel of Fig. 5.4. On the other hand, for $U = 0.25$, we observe that the second Born approximation seems to reproduce also the transition A which promotes the system into the first excited state of energy E_0. If we consider the cases $U = 0.5$ and $U = 1.0$, however, the identification of this transition becomes subtle. Here, the relevant peak shifts to a larger frequency which is opposite to what is expected from exact diagonalization, cf. the vertical line labeled A. In addition, there is a second peak forming which is located about the expected position but has a rather small spectral weight (see the arrows).

As there is—independently of the value of the Hubbard U—no evidence for transitions other than B in the exact excitation spectrum, we clearly have to identify the additional peaks obtained in the 2B approximation as unphysical artifacts. With the same argument, we also have to rule out the series of high-energy states, see $5.5 < \omega < 7.5$ in all panels of Fig. 5.4.

The origin of these artifacts is most probably the same as for the damping found in the previous Section, i.e., the non-cancellation of terms in the applied many-body approximation. A more detailed analysis of the artificial states in Fig. 5.4 including their U-dependence and oscillator strength is subject of ongoing work.

Chapter 6
Non-Lattice Systems

As "non-lattice" systems we refer to all finite, inhomogeneous quantum many-body systems that cannot be described *a priori* by a lattice-Hamiltonian with strongly localized (one-particle) states. This means, we deal with systems the particle density of which is predominantly a continuous function in space[1]. Usually, the general form of this density crucially depends on two parameters: the external confinement potential and the interaction between the particles. As outlined in Sect. 3.2, an adequate basis representation of the NEGF is required to accurately resolve changes in the continuous particle density.

As representative examples of non-lattice systems we, in this chapter, consider small (model) atoms and molecules and electrons in quantum dots or wells. We present Green's function calculations for the correlated ground states and analyze the nonequilibrium dynamics induced by weak and strong time-dependent external perturbations. In Sect. 6.2.2, we, in particular, address a NEGF approach to the description of excitations which are of multi-particle character. Precisely, we will focus on double excitations in few-electron quantum wells.

6.1 Small Atoms and Molecules. Ground State Properties and Response to External Fields

In atomic and molecular physics [179], it is convenient to use *atomic units* (a.u.). Here, the characteristic length scale is the electron Bohr radius,

$$a_0 = \frac{4\pi\varepsilon_0\hbar^2}{me^2} = \frac{\hbar}{\alpha mc}, \tag{6.1}$$

with $\varepsilon_0 = 8.854 \cdot 10^{-12}$ F/m being the dielectric constant, $m = 9.109 \cdot 10^{-31}$ kg ($e = 1.602 \cdot 10^{-19}$ C) the electron mass (charge), $\alpha^{-1} = 4\pi\varepsilon_0/e^2 \approx 137$ the inverse

[1] We note that there also may exist discontinuities which are induced by boundary conditions or other constraints.

K. Balzer, M. Bonitz, *Nonequilibrium Green's Functions Approach to Inhomogeneous Systems*, Lecture Notes in Physics 867,
DOI 10.1007/978-3-642-35082-5_6, © Springer-Verlag Berlin Heidelberg 2013

fine structure constant, and $c = 2.998 \cdot 10^8$ m/s the vacuum speed of light. One Bohr radius is equivalent to approximately 0.529 Å. Energies are measured in units of Hartree,

$$E_\mathrm{h} = \frac{e^2}{4\pi\varepsilon_0 a_0} = \alpha^2 c^2 m, \tag{6.2}$$

where $1E_\mathrm{h}$ corresponds to about 27.2 eV which is twice the Rydberg energy, $E_\mathrm{r} \approx 13.6$ eV—the binding energy of the 1s-electron in the hydrogen atom. Using definition (6.2), the time is consequently measured in multiples of $\hbar E_\mathrm{h}^{-1}$, i.e.,

$$\tau_0 = \frac{\hbar}{\alpha^2 c^2 m} = \frac{16\pi^2 \varepsilon_0^2 \hbar^3}{m e^4}, \tag{6.3}$$

and the velocity in αc. One atomic unit of time hence equals 24.2 attoseconds.

In general, all definitions and equations given in the international system of units[2] are transferred into atomic units by setting $\hbar = m = e = (4\pi\varepsilon_0)^{-1} = 1$. Consequently, the mass of the proton ($1.673 \cdot 10^{-27}$ kg) is 1836 a.u.

6.1.1 Model-Like Treatment

In this section, we will adopt the restriction that the electrons inside an atom or a molecule move only along one axis [180]. In principle, this means a drastic abstraction neglecting, e.g., the system's angular momentum or ro-vibrational degrees of freedom. As a consequence, applications and theory-experiment comparisons are limited. However, the simplicity of such a one-dimensional approach has allowed for a large number of numerical and ab-initio investigations of one- and two-electron problems in atomic physics. To name only a few, we refer to the study of photoelectron spectra of the hydrogen atom [181–183], extensive work on the one-dimensional helium atom, e.g., Refs. [180, 184–187], including electron rescattering and nonsequential ionization in strong laser fields [188] as well as ion-recoil spectra [189], and the modeling of pump-probe scenarios with enhanced double ionization following a shake-up state population, see Ref. [41]. The theoretical tools used vary from semi-classical approaches [190], via time-dependent extended HF [191], density functional theory (DFT) [192, 193], and multiconfiguration expansions [194] to the full numerical solution of the two-electron time-dependent Schrödinger equation (TDSE).

The success of 1D model atoms has also stimulated the description of molecules in reduced dimensionality. A number of publications, e.g., Refs. [195–197], deal with the hydrogenic molecules H_2 and H_3 and their positive ions exposed to intense fields. In addition, there also exist semi-classical studies [198–200]. On the other hand, the coupling of the electron dynamics in hydrogen to quantized photon fields

[2] SI units, SI: Système International d'unités.

is subject to Ref. [201]. More complex molecules are treated with time-dependent multiconfiguration HF, e.g., [16, 202, 203], and DFT [204].

Computationally, a one-dimensional description of atoms (molecules) is problematic due to the Coulomb singularity. To avoid divergences in 1D, we, in the following, use the method of regularization (we emphasize, that different approaches exist, see, e.g., Refs. [205, 206]). To this end, a harmonic cutoff is assigned to the Coulomb potential between electrons (+) or an electron and a proton (−) at small distances $x_{ij} = x_i - x_j$. Mathematically, this is achieved by replacing,

$$\pm\frac{1}{|x_{ij}|} \to \pm\frac{1}{\{x_{ij}^2+\kappa\}^{1/2}} \approx \pm\frac{1}{\kappa^{1/2}} \mp \frac{1}{2\kappa^{3/2}}x_{ij}^2 + \mathcal{O}\big(x_{ij}^4\big) \quad (\text{for } |x_{ij}| \ll 1), \tag{6.4}$$

with the softening (or regularization) parameter κ. At large differences, the long-range x_{ij}^{-1}-behavior is retained.

In 1D, an atomic or molecular system can then be described by the following electronic Hamiltonian (a.u.),

$$\hat{H}(t) = \sum_{i=1}^{N}\left(-\frac{1}{2}\frac{\partial^2}{\partial x_i^2} + E(t)\,x_i - \sum_{j=1}^{M}\frac{Z_j}{\{(x_i-s_j)^2+\kappa_j\}^{1/2}}\right) + \sum_{i<j}^{N}\frac{1}{\{(x_i-x_j)^2+\kappa\}^{1/2}}, \tag{6.5}$$

which includes an external, time-dependent (laser) field $E(t) = -\frac{\partial A_x(t)}{\partial t}$ which is linearly polarized in x-direction and treated classically in dipole approximation[3]. The integer N counts the number of electrons with coordinates x_i ($i = 1, 2, \ldots, N$), and the integer M refers to the number of nuclei which are assumed as point-like particles located at positions s_j ($j = 1, 2, \ldots, M$) and have the atomic number (positive charges) Z_j. As outlined above, the parameter κ (κ_j) regularizes the electron-electron (electron-nucleus) interaction. For a single neutral N-electron atom, it is $M = 1$ and $Z_1 = N$. On the other hand, if $M > 1$ and $N = M$, the Hamiltonian describes a neutral molecule. Moreover, if we set $N < M$ or $N > M$, we can model the corresponding (molecular) ions.

While for atoms the relevant energy is the electronic part $E_\mathrm{e} = \langle\hat{H}(t)\rangle$, for molecules, it is the binding energy E_b, i.e., the sum of E_e and the total Coulomb repulsion energy of the nuclei:

$$E_\mathrm{b} = E_\mathrm{e} + \sum_{i<j}^{M}\frac{Z_i\,Z_j}{d_{\mathrm{b},ij}}, \tag{6.6}$$

[3] $A_x(t)$ denotes the x-component of the vector potential.

where $d_{\mathrm{b},ij} = |s_i - s_j|$ are the bond lengths between the individual atoms. Of course, any molecular ground state is characterized by the global minimum of Eq. (6.6) including variation of the nuclear geometry.

In terms of the 1pNEGF, the regular HF self-energy[4] $\Sigma^{(1),\mathrm{HF}}(t)$ and the respective collision term $I_1^{(1),>}$ of Sect. 4.2.2 (which includes the irregular parts), the electronic energy is given by,

$$E_\mathrm{e} = E_0 + E_\mathrm{HF} + E_\mathrm{cor}, \tag{6.7}$$

where,

$$\begin{aligned} E_0 &= -\mathrm{i}\hbar\,\mathrm{Tr}\left\{h^{(1)}(t)G^{(1),<}(t,t)\right\}, \\ E_\mathrm{HF} &= -\frac{\mathrm{i}\hbar}{2}\,\mathrm{Tr}\left\{\Sigma^{(1),\mathrm{HF}}(t)G^{(1),<}(t,t)\right\}, \\ E_\mathrm{cor} &= -\frac{\mathrm{i}\hbar}{2}\,\mathrm{Tr}\left\{I_1^{(1),>}(t,t)\right\}, \end{aligned} \tag{6.8}$$

and, in the one-electron energy $h^{(1)}(t) = t^{(1)} + v^{(1)}(t)$, the potential energy has the form $v^{(1)}(t) = E(t)\,x - \sum_{j=1}^{M} Z_j\{(x-s_j)^2 + \kappa_j\}^{-1/2}$.

The degree of electron-electron correlation in the model atom or molecule can be expressed by means of the correlation energy, which is the difference of the exact and the HF total energy, i.e., $E_\mathrm{exact} - E^*_\mathrm{HF}$, where $E^*_\mathrm{HF} = E_0 + E_\mathrm{HF}$ indicates the result of a pure mean-field calculation. In a nonequilibrium Green's function approach beyond the HF level, this value must be compared to the approximate correlation energy E_cor of Eq. (6.7).

Other important observables are, e.g., the (field-induced) time-dependent dipole moment,

$$d(t) = -\mathrm{i}\hbar\int_{-\infty}^{+\infty}\mathrm{d}x\,\left\{(x-s_0)\,G^{(1),<}(x\,t,x\,t)\right\}, \tag{6.9}$$

with $s_0 = \frac{1}{M}\sum_{j=1}^{M} s_j$ as point of reference, and the one-electron density,

$$\rho_1(x,t) = -\mathrm{i}\hbar\,G^{(1),<}(x\,t,x\,t). \tag{6.10}$$

In equilibrium, we replace the lesser correlation function in Eqs. (6.9) and (6.10) by the Matsubara Green's function[5], i.e., $G^{(1),<}(x\,t_0,x'\,t_0) = \frac{\mathrm{i}}{\hbar}G^{(1),\mathrm{M}}(x,x';0^-)$.

In the form of Eq. (6.5), the model Hamiltonian involves a rather large number of parameters. In principle, the numerical values of κ_j and κ should be chosen such that roughly the ground-state binding energies, bond lengths and ionization potentials of the corresponding 3D system are recovered. However, in the examples to be discussed below, we consider the uniform case $\kappa_j = \kappa = 1$ for all $j = 1,\ldots,M$. This choice is well motivated for the one-dimensional helium atom, cf. [180], leading to a first (second) ionization potential of $0.755E_\mathrm{h}$ ($2.238E_\mathrm{h}$) compared to $0.904E_\mathrm{h}$

[4] Without the contour delta function.

[5] Recall definition (2.39).

Table 6.1 1D helium model: typical convergence of the ground-state energy E_e as function of the number of τ-grid points (n_τ) used in the NEGF calculation. Energies are in units of E_h, cf. Eq. (6.2)

	$n_\tau = 101$	$n_\tau = 301$	$n_\tau = 601$	$n_\tau = 1001$
2B[a]	−2.23	−2.2334	−2.23341	−2.233419

[a]Values from Ref. [207]

($2.903 E_h$) of the real atom [37]. Moreover, this choice is also commonly used for other atoms and molecules, see, e.g., Ref. [196].

To start with, we report on the ground-state properties of some representative model atoms and molecules. All NEGF calculations have been carried out using the finite element-discrete variable representation (FE-DVR) introduced in Sect. 3.3. This means, the 1pNEGF and the 1pSE are expanded as ($\mathscr{X} = G, \Sigma$),

$$\mathscr{X}^{(1)}(x\,t, x'\,t') = \sum_{\mu\nu} \chi_\mu(x)\,\chi_\nu(x)\,\mathscr{X}^{(1)}_{\mu\nu}(t, t'), \tag{6.11}$$

with multi-indices $\mu = (i, m)$, $\nu = (i', m')$ and the one-dimensional FE-DVR functions $\chi_\mu(x) = \chi^i_m(x)$, cf. Eq. (3.16). Computationally highly advantageous is the FE-DVR, because it leads to a simple and analytical structure of the self-energy $\Sigma^{(1)}_{\mu\nu}$ as summarized in Sect. 3.3.4 for the HF and 2B approximation. For self-consistently solving the Dyson equation, cf. Eqs. (4.11) and (4.12), about $n_b = 150$ FE-DVR basis functions and up to about 1000 non-equidistant τ-grid points have been used, compare with Sect. 4.1.2. To describe the ground state, we set $\beta = 100\,E_h^{-1}$. Exact reference data is computed from the time-dependent Schrödinger equation (TDSE) using the method of imaginary time-propagation [209].

First, let us concentrate on the most elementary closed-shell, two-electron atom: helium (He), which is modeled by Eq. (6.5) with $N = 2$, $M = 1$ and $Z_1 = 2$. In a HF approach, the singlet ground state is described by a single doubly-occupied orbital (of energy $-0.750 E_h$) and has a total energy of $E_{e,HF} = -2.224210 E_h$. By contrast, in the 2B approximation, we obtain a lower ground-state energy of $E_{e,2B} = -2.233419 E_h$ [207] which complies with the Rayleigh-Ritz minimum principle. When comparing these values to the exact TDSE result of $E_e = -2.238258 E_h$, we find that 2B accounts for more than 60 % of the correlation energy.

Whereas, in HF approximation, an accurate ground state is simple to generate, it is more difficult in the case of 2B. This is due to the non-analytic τ-dependence of the Matsubara Green's function $G^{(1),M}_{\mu\nu}(\tau)$ when the self-energy has an irregular part, compare Eq. (4.11) to the HF-type solution outlined in Eq. (4.10). Table 6.1 shows the 2B convergence of the helium ground-state energy for a typical uniform-power mesh with n_τ grid points (for the mesh's definition and specific parameters, the reader is referred to Ref. [207]). Moreover, the typical convergence with the number of finite elements and Gauss-Lobatto points in the FE-DVR description is illustrated in Ref. [210].

Beyond helium, the next complicated closed-shell atom is beryllium (Be) involving four electrons ($N = 4$) and a four-fold charged nucleus ($M = 1$, $Z_1 = 4$). The

Table 6.2 Ground-state (binding) energies of the one-dimensional model atoms (molecules) in units of E_h. For the molecules, the value in brackets indicates the interatomic bond length d_b measured in multiples of the associated Bohr radius a_0, cf. Eq. (6.1)

	He	Be	H_2	H_3^+	LiH
HF	−2.2242	−6.7394	−1.3531 (1.9925)	−1.4710 (2.1827)	−4.8534 (3.3860)
2B	−2.2334	−6.7714	−1.3740 (2.0561)	−1.5035 (2.2790)	−4.8886 (3.5053)
Exact	−2.2383[a]	−6.7852[b]	−1.391 (2.151)	−1.5324 (2.385)	−4.91 (3.6)

[a]See, e.g., Ref. [180]

[b]From Ref. [208]

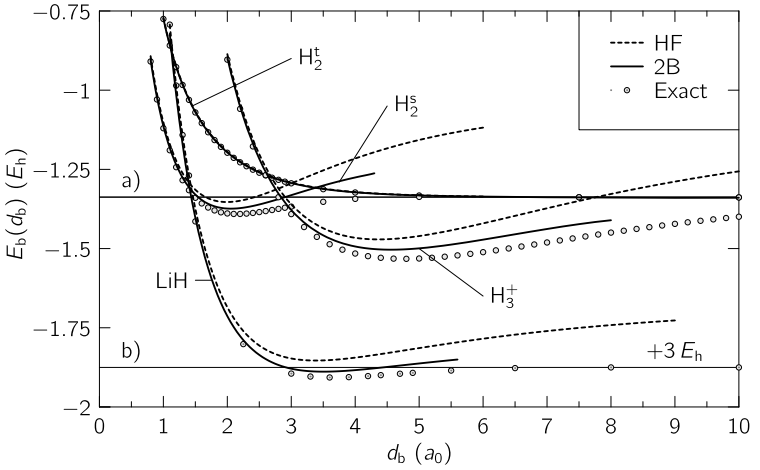

Fig. 6.1 Exact and approximate binding energy curves, i.e., E_b as function of interatomic distance d_b, for the models of hydrogen (H_2^s: singlet, H_2^t: triplet), the molecular ion H_3^+ and lithium hydride (LiH). Note that, for H_3^+, d_b measures the distance between both outermost hydrogen atoms (we assume equal H-H spacings), and that, for LiH, the curve is shifted upwards by $3\,E_h$. The thresholds for complete fragmentation—the dissociation thresholds—are given by the *thin horizontal lines* labeled (a) and (b)

corresponding HF, 2B and exact ground-state energy are listed in Table 6.2 together with results for molecular hydrogen (H_2: $N = M = 2$, $Z_{1,2} = 1$), the heteronuclear molecule lithium hydride (LiH: $N = 4$, $M = 2$, $Z_1 = 3$, $Z_2 = 1$) and the linear version of the molecular ion H_3^+ ($N = 2$, $M = 3$, $Z_{1,2,3} = 1$).

For the beryllium atom, the improvement of the HF result, due to correlations in 2B approximation, is similar to that of the helium atom—however, the correlation energy is more than three times as large. Concerning the molecules, whether or not the individual atoms combine into molecules depends on the binding energy E_b, cf. Eq. (6.6). Figure 6.1 shows the respective binding energy curves as calculated from the repeated solution the Dyson equation (and the TDSE) varying the

interatomic distance(s). In fact, independently of the used MBA, all considered 1D molecules are electronically stable, i.e., the binding energy has a clear minimum which defines the equilibrium bond length d_b (for numerical values, see the numbers in brackets in Table 6.2). In addition, the 2B result is systematically lower than HF and correctly leads to larger bond lengths. However, there is a problem regarding dissociation: While the TDSE predicts reasonable dissociation thresholds (see the thin horizontal lines in Fig. 6.1), which coincide with ground-state calculations on the fragments, the dissociation process is poorly resolved in HF and 2B. This is due to the fact that all considered molecules have a (singlet) closed-shell configuration in their ground states but dissociate into open-shell fragments, i.e., individual neutral or charged atoms. Such a transition cannot be captured in a semilocal (spin-restricted) ansatz for the Green's function[6]. For an early discussion on this topic, see, e.g., Löwdin [211]. Furthermore, this problem does not occur for spin-polarized systems, compare with the Hydrogen in the triplet state (H_2^t) in Fig. 6.1. There, the binding energy behaves correctly in the limit $d_\mathrm{b} \to \infty$ but, as expected, no bond is formed.

The approximate and exact one-electron ground-state densities of the model atoms and molecules of Table 6.2 are shown in Fig. 6.2(a) and (b). In regions of high density, we observe that the electron densities for H_2, H_3^+ and LiH as obtained in different MBAs differ essentially more than that of the atoms—for He and Be, the deviation from the exact density is relatively small. However, throughout, the 2B approximation (solid lines) leads to a systematic improvement of the HF result (dashed lines). For lithium hydride, the agreement with the exact density (dots) is even very good.

Furthermore, Fig. 6.2(c) illustrates the regularized ionic potentials as created by the nuclei. For the molecules, these depend on the used MBA which is a result of the self-consistent determination of the bond lengths, cf. Fig. 6.1. Nevertheless, this dependence is small such that the following conclusion can be drawn: The density differences are mainly correlation-induced and are not a consequence of an inaccurate (too small) bond-length. Hence, we also find that an N-electron molecule in 1D is, in general, more strongly correlated than the corresponding atom with the same number of electrons. For a more detailed analysis of the molecular ground states in terms of natural orbitals and their HF (2B) occupations, we refer to Ref. [207].

In order to give an idea of a typical Green's function calculation in nonequilibrium, we now focus on the electron dynamics in the 1D helium atom. First, we will see how the neglect of self-consistency regarding initial correlations affects the time evolution. Second, we will trace the electron dynamics following an instantaneous switch-on of a laser field. In Eq. (6.5), this is modeled by an electric field of the form,

$$E(t) = E_0 \theta(t - t_0)\, \cos\big(\omega_\mathrm{ph}(t - t_0)\big), \tag{6.12}$$

[6]Note, that we treat different spin degrees of freedom only by a degeneracy factor as outlined in Sect. 3.3.4.

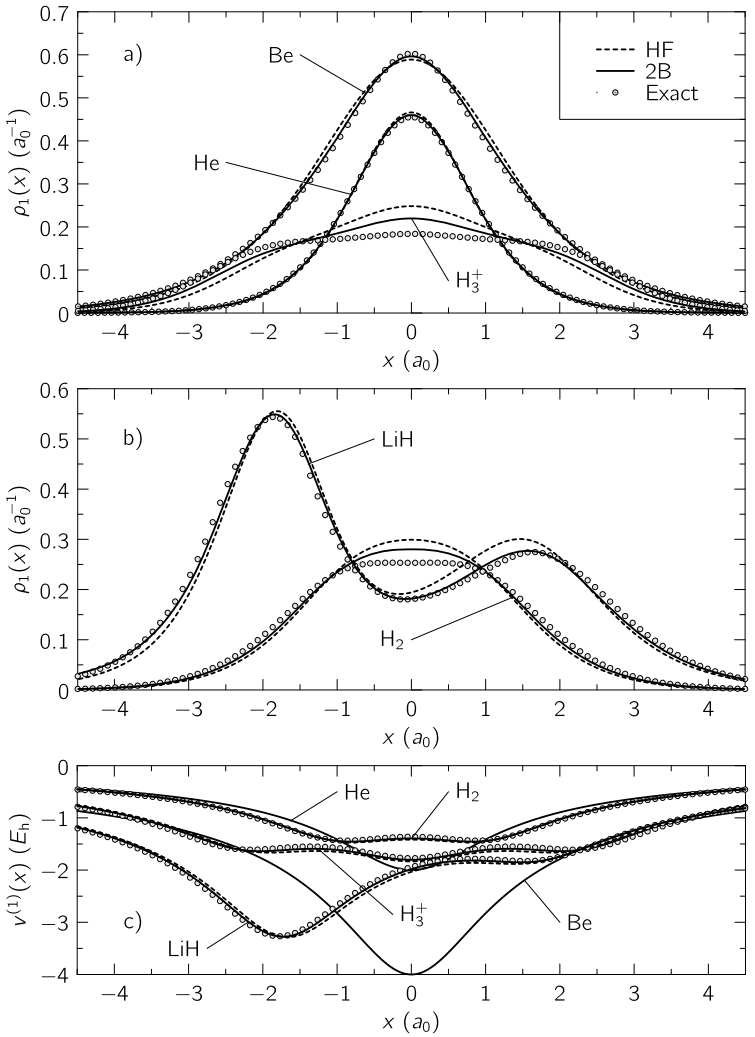

Fig. 6.2 (**a**) Self-consistent one-electron ground-state density $\rho_1(x)$ for the following one-dimensional model atoms: helium (He), beryllium (Be) and the molecular ion H_3^+. While the HF (2B) approximation is indicated by *dashed* (*solid*) *lines*, the exact ground-state density as obtained from propagating the Schrödinger equation in imaginary time is shown by the *dots*. (**b**) The same for the molecules hydrogen (H_2) and lithium hydride (LiH). In both panels, the density is normalized to $N\xi^{-1}$, where $\xi = 2$ accounts for the spin degeneracy. Panel (**c**) shows the regularized Coulomb potential induced by the nuclei which are located at the origin or, respectively, at a distance d_b apart

where E_0 is the field strength, ω_{ph} the photon energy and t_0 the time when the field is turned on. Below, we consider the case of a strong field of intensity $3.5 \cdot 10^{14}$ W/cm^2 ($E_0 = 0.1$ a.u.) and use a photon energy of $\omega_{ph} = 0.54\, E_h$ (84 nm or 14.7 eV ultra-

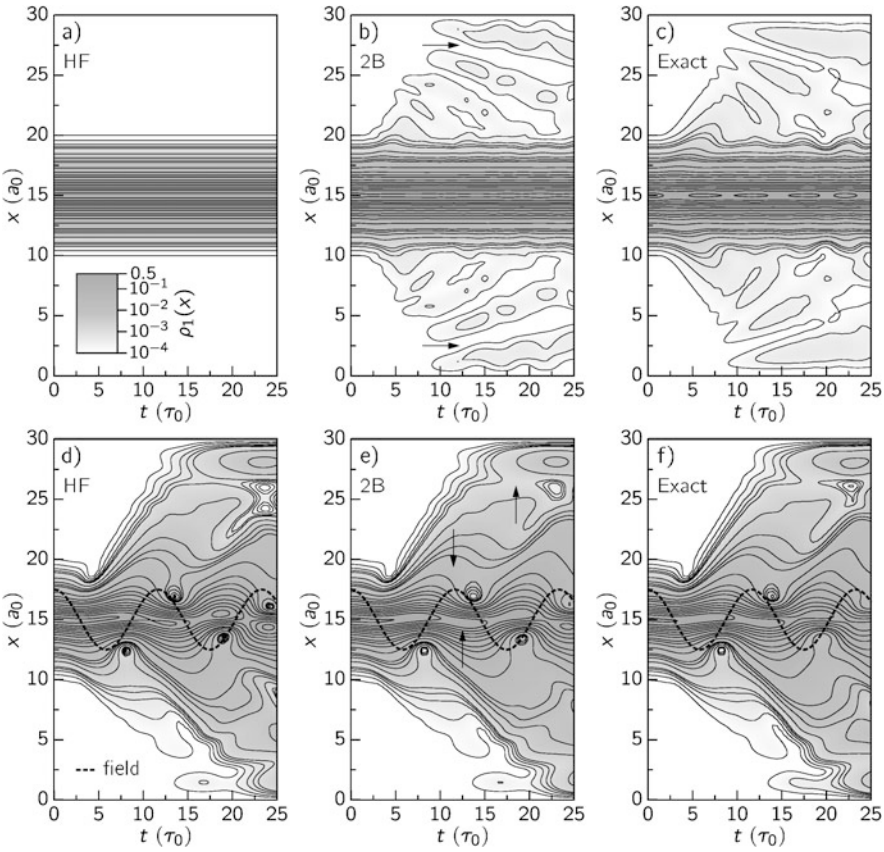

Fig. 6.3 Time evolution of the one-electron density $\rho_1(x)$ in the 1D helium atom; all values in the logarithmic contour-density plot are given in atomic units. (**a**)–(**c**): Time evolution without laser field in (**a**) HF and (**b**) 2B approximation. Panel (**c**) shows the exact result. Initially, at $t_0 = 0$, the system is prepared in the HF ground state. (**d**)–(**f**): Response of the atom to an instantaneously turned on laser field, cf. Eq. (6.12), with $E_0 = 0.1$ ($3.5 \cdot 10^{14}$ W/cm^2) and $\omega_{\rm ph} = 0.54 E_{\rm h}$ (84 nm ultra-violet radiation). In contrast to (**a**)–(**c**), here, the initial states are the self-consistent ground states. In all panels, the helium atom is centered at $x = 15a_0$, and the contour lines cover a density range from 10^{-4} to $0.5a_0^{-1}$ with four contour lines in each decimal power between 10^{-4} and 0.1, and contours between 0.1 and 0.5 each 0.05 a.u. Figure after Ref. [153]

violet (uv) radiation) which is about the transition energy to the first excited singlet state in the helium model; again, we choose $\kappa = \kappa_1 = 1$.

Without the laser field, the system's time evolution depends on, both, the initial state and the MBA used in the time propagation of the 1pNEGF. If the initial state is the ground state, it should remain stationary and so should all observables. However, whether or not this is true in an approximate calculation depends on the following: If different MBAs are used in the (equilibrium) Dyson equation and in the subsequent time propagation (the solution of the two-time KBEs), the initial state is usually not stationary. Figures 6.3(a) to (c) show this effect in terms of the time-dependent

electron density in the He atom when the ground state is approximated on the HF level, i.e., does not incorporate electron-electron correlations. In HF approximation, panel a), the initial ground state remains an eigenstate of the HF Hamiltonian. Therefore, the density profile does not change in time, $\rho_1(x,t) = \rho_1(x,t_0)$. However, if the ground state evolves under the influence of correlations, e.g., approximated on the 2B-level (see panel (b)), the electrons start to perform a collective, "breathing"-like oscillation in the Coulomb potential of the doubly-charged ion. Note that the appearance of an interference pattern (see the arrows) is enhanced due to the finite simulation box of width $30a_0$ leading to hard (elastic) electron reflection. Moreover, we observe that the oscillatory behavior is well resolved in 2B, compare Fig. 6.3(b) to the exact TDSE result shown in panel (c).

Now, let us turn on the laser field of Eq. (6.12) and include self-consistent initial states[7] to avoid the oscillations of Figs. 6.3(b) and (c). While Figs. 6.3(d) and (e) show the density response again in HF and 2B approximation, panel (f) indicates the exact result involving the fully correlated ground state. As we can see, the non-perturbative laser field drives the electrons out of the ground state leading to a strongly time-dependent density $\rho_1(x)$ at high and low density, i.e., the electrons now oscillate in the net field of the ion and the uv laser (note that ionization is suppressed due to the finite simulation box). Again, as in panels (b) and (c), the 2B approximation captures many details in the time dependence which are absent in the HF solution, see, e.g., the arrows.

The results along Figs. 6.3(a) to (f) can be seen as proof of principle calculations and validate the quality of the 2B approximation for the description of time-dependent processes in atomic model systems. Taking advantage of the FE-DVR basis, the results can straightforwardly be extended to molecules, see Ref. [153] for an example on lithium hydride. In the remaining part of this Section, we outline how to compute (ground-state) excitation spectra from the two-time NEGF.

The excitation spectrum of the 3D helium atom is complex and shows an infinite number of Rydberg-like series, compare with Tanner et al. [37]. The first series is energetically below (and converges to) the first ionization threshold I_1 and involves all singly-excited states. Above I_1, but below the second ionization threshold I_2, we find the series of autoionizing resonances (doubly-excited states) each of which converges to an excited-state energy of the singly-charged ion. In one dimension, the spectrum is qualitatively the same even if soft-Coulomb potentials are used, see, e.g., Ref. [194]. Thus, how do we access the excited states of the model atom?

For the dipole spectrum, the procedure is the following: First, starting from the ground state, we calculate the time-dependent dipole moment $d(t)$ in linear response, i.e., for a small perturbation which is proportional to a delta function in time (δ-kick). The Fourier transform, $d(\omega) = \int \mathrm{d}t\, \mathrm{e}^{-\mathrm{i}\omega t}\, d(t)$, is then peaked at the excitation energies of basically all dipole-allowed transitions and the peak heights correspond to the transition moments (oscillator strengths). Further, $d(\omega)$ contains

[7] In 2B approximation, this means we, in addition to the correlation functions, have also to propagate the mixed Green's functions, which are obsolete in a mean-field (HF) description.

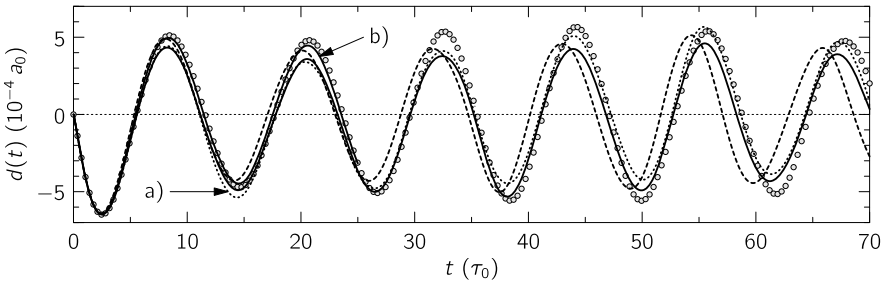

Fig. 6.4 Time-dependent dipole moment $d(t)$ of the 1D helium atom following a perturbative dipole δ-kick. HF: *dashed line*, 2B: *solid lines* up to $t = 25\,\tau_0$ and $t = 70\,\tau_0$, respectively, and TDSE result: *dots*. The GKBA result is shown by the *dotted line*, cf. label (**a**). Except for the TDSE calculation and the 2B result (**b**) (these use self-consistent initial states), the atom is prepared in the HF ground state at $t_0 = 0$

Table 6.3 Selected approximate and exact excitation energies $\hbar\omega_{N,n}$ (in units of E_h) of the 1D helium atom; $\kappa = \kappa_1 = 1$. While transitions with $N = 1$ indicate single excitations, all transitions with $N > 2$ are double excitations. The exact first (second) ionization threshold is $I_1 = 0.755\,E_\mathrm{h}$ ($I_2 = 2.238\,E_\mathrm{h}$)

	$\omega_{1,1}$	$\omega_{1,2}$	$\omega_{1,3}$	$\omega_{2,1}$	$\omega_{2,2}$	$\omega_{3,1}$
HF	0.549	0.670	0.709	–[b]	–[c]	–[d]
2B	0.537	n.a.[a]	n.a.	n.a.	n.a.	n.a.
Exact	0.533	0.677	0.712	1.356	1.415	1.701

[a] not accessible (n.a.) from a short calculation of less than 100 a.u. length

[b–d] not included in HF

information on singly- as well as multiply-excited states. Doubly- and multiply-excited states are however *a priori* not included in an effective single-particle (HF) approach, cf. [173] and also Sect. 6.2.1. Therefore, a correlated treatment is indispensable.

Figure 6.4 shows the time-dependent dipole moment for the 1D helium atom following a δ-kick with $E(t) = E_0\delta(t - t_0)$ and $E_0 = 0.01$ in Eq. (6.5). In 2B approximation, with the GKBA (dotted line) and without (solid lines), the time-dependent dipole moment reasonably well approaches the exact result. In comparison to HF (dashed line), we observe a shift towards a larger main oscillation period. Spectroscopically, this main oscillation indicates the dominant excitation process, i.e., the transition to the first excited singlet state which is the energetically lowest single excitation. All other excitations are rather hidden in the time series and only a thorough analysis allows for their determination [153]. Table 6.3 gives the result for some characteristic excitation energies $\hbar\omega_{N,n}$, where N and n are the principal hydrogenic quantum numbers as defined, e.g., in Ref. [37]. Unfortunately, the NEGF calculations are limited to relatively short propagation times such that ac-

cessing doubly-excited states is very difficult[8]. Beyond the HF-level, no sufficiently long calculations could have been performed so far—neither using the full two-time scheme nor using the GKBA.

6.1.2 3D Atoms and Molecules

In the previous Section, we have neglected the three-dimensional nature of the atoms and molecules. To treat these systems in their full dimensionality, however, all definitions along Eqs. (6.5) to (6.10) remain valid except for the fact that, in the Hamiltonian, we have to replace all x_{ij} (s_j) by vectors $\mathbf{r}_{ij} = |\mathbf{r}_i - \mathbf{r}_j|$ ($\mathbf{s}_j$) in $\mathbb{R}^3$ and have to consider a pure Coulomb interaction between the charge carriers, i.e., $\kappa = \kappa_j = 0$.

Numerical calculations on real atoms and molecules based on the nonequilibrium Green's function have been presented by Dahlen, Stan and van Leeuwen. While, in Refs. [68], the authors concentrate on the ground-state properties obtained in different MBAs and test various levels of self-consistency in the GW approximation, they, in Refs. [92, 130, 132], extend the Kadanoff-Baym approach to nonequilibrium situations and propagate the 1pNEGF in real time for the beryllium atom and the hydrogen molecule in the 2B approximation.

Concerning the ground states, the total energy of the elementary atoms and diatomic molecules He, Be, Ne, Mg, H_2 and LiH has been computed from the Dyson equation in Ref. [68] together with the ionization potential which is accessible from the extended Koopmans' theorem. There, the inclusion of correlations on the level of the self-consistent 2B approximation has led to an essential improvement of the HF results. As an illustration we, in Fig. 6.5, show results (adapted from Ref. [131]) for the binding energy of the charge-neutral hydrogen molecule as function of the interatomic distance. Just as in the case of the 1D models (compare with Fig. 6.1), one observes that the 2B approximation is capable to well approach the exact binding energy curve. In addition, as outlined before in Sect. 6.1.1, the HF and 2B approximation both fail in the limit $d_\mathrm{b} \to \infty$, where the molecule dissociates.

Moreover, in Ref. [212], Stan et al. have demonstrated—on the basis of the GW approximation—that partially self-consistent calculations may lead to equally accurate results for the ground state as fully self-consistent calculations. A great advantage of such partly self-consistent schemes is that they are computationally less demanding and, hence, allow for the treatment of larger systems.

Regarding nonequilibrium applications, it has been possible to include up to 30 molecular orbitals (HF basis functions) which are constructed as linear combinations of atomic Slater functions, see, e.g., Ref. [130]. Starting from the self-consistent ground state, in Refs. [92, 130, 132], Dahlen et al. have computed the time-dependent correlations functions $G^{(1),\gtrless}(t,t')$ for the hydrogen molecule in

[8] At least for the helium atom, where single and double excitations are energetically well separated from one another.

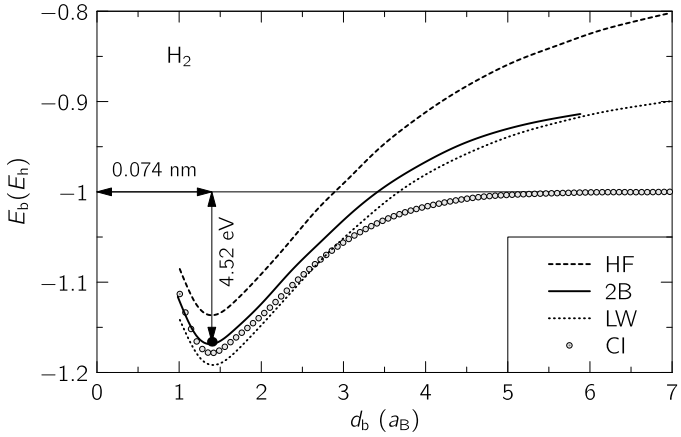

Fig. 6.5 Binding energy E_b of the 3D hydrogen molecule as function of the internuclear distance d_b. While the *dashed* (*solid*) *line* indicates the self-consistent HF (2B) approximation, the *dotted line*, denoted LW, refers to the energy obtained from the GW-type Luttinger-Ward functional [90] evaluated with the HF Green's function, for details see [92]. Further, the *dots* indicate the exact binding energy curve obtained by configuration interaction (CI) calculations. Figure after Ref. [131]

the presence of an electric field applied along the molecular axis. From this information, they also obtain the time-dependent spectral function and compare it to the respective spectral function in equilibrium[9].

As an example for a NEGF calculation for a real 3D atom, we, in Fig. 6.6, display the result for the polarizability of beryllium[10] as obtained from the time-dependent dipole moment in the linear response regime. From this quantity, one can estimate the excitation energy of the $^1S \rightarrow {}^1P$ transition. In the Hartree-Fock approximation, one obtains the maximum of $\alpha(\omega)$ at the position of the dashed vertical line which refers to $\omega = 0.178 E_h$. On the other hand, the exact maximum is located at $\omega = 0.194 E_h$, see the dash-dotted line. The dots in Fig. 6.6 show the frequency-dependent polarizability as obtained in the 2B approximation. In addition, the horizontal bars indicate the FWHM and the peak position for various shorter propagation times $t < 51$ a.u. From these values we can extract the 2B result: Taking the average of all frequencies leads to an excitation energy of $\omega = 0.189 E_h$ which is closer to the exact excitation energy than to the HF result, see the solid vertical line.

In summary, we emphasize that the determination of other, energetically higher excitations along the above lines is very difficult as the correlated calculations are limited in the final propagation time. Moreover, NEGF calculations on three-dimensional atomic (molecular) systems larger than the ones mentioned have not yet been performed due to the computational complexity involved. Straightforward extensions may only be possible by the use of pseudopotentials.

[9] Both spectral functions are obtained by the real-time propagation method.

[10] Adapted from Ref. [132].

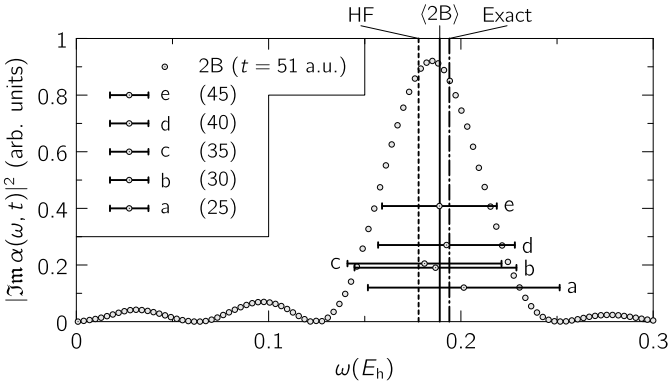

Fig. 6.6 Polarizability of the beryllium atom (*dots*) computed from the real-time evolution of the Green's function in 2B approximation: $\alpha(\omega,t) = -1/E_0 \int_0^t \mathrm{d}\bar{t}\, \exp(\mathrm{i}\omega\bar{t})\, d(\bar{t})$, where $E_0 \ll 1$ is the electric field strength of a perturbative dipole δ-kick applied to the system, and $d(t)$ is the time-dependent dipole moment. Whereas the energy of the $^1\mathrm{S} \rightarrow {}^1\mathrm{P}$ transition in HF approximation is given by the *dashed line*, the exact transition energy is indicated by *dash-dotted line*. Further, the *horizontal bars* show the full width at half maximum of $\alpha(\omega,t)$ for times t smaller that 51 a.u. (see the values in parentheses). The average position of the peak is indicated by the *solid line*, cf. $\langle 2\mathrm{B}\rangle$. Figure after Ref. [132]

6.2 Few-Electron Quantum Dots and Wells

Quantum dots are nanoscale semiconductor structures in solids that are capable to confine the quantum motion of electrons (or excitons) in practically all three spatial dimensions. The resulting system has quasi zero-dimensionality and can contain a single, a few or several thousand electrons. The presence of the confinement leads to discrete single- and multi-particle eigenstates as they are present in atoms. This is why QDs are likewise referred to as "artificial atoms" [213]. For an overview on the rich electronic structure of QDs, see Reimann and Manninen [214] and references therein.

In the above terminology, pairs or clusters of QDs are the equivalent to molecules in which the electrons can, e.g., tunnel quantum-mechanically from one dot to another. For a compilation of the resulting collective, optical and transport properties, see, e.g., Ref. [215]. Many experimental aspects of the electron transport through double quantum dots are reviewed in Ref. [216]. Moreover, the charge carriers in the QD can also couple to the lattice vibrations of the surrounding solid—the phonons. This interaction can have a large influence on the dot's optical absorption spectrum [108]. In addition, when being contacted to external electron reservoirs (leads), QDs can operate as switching devices. Along these lines, a QD can even work as a single-electron transistor due to the Coulomb blockade effect, see [217]. Finally, in the research area of quantum computation, QD systems have been proposed for quantum gates, e.g., Ref. [218].

In comparison to QDs, quantum well (QW) structures [219] are very similar in many aspects though, here, the electrons experience a confinement only in certain

directions. Typically, the charge carriers are trapped in the growth direction of the substrate, whereby the structure consists of layers of at least two different semiconductor materials, i.e., it forms a heterostructure. The crossover from one material to the other induces a potential barrier and is thus responsible for the confinement. In many situations, the electrons can move almost freely in the lateral direction but are strongly confined in the perpendicular plane (vertical direction). In this case, the confinement dominates the QW properties.

A very important feature of, both, quantum dots and wells is the fact that the interaction strength between the charge carriers and the energy states can be externally controlled by fabrication and/or by applying an external electric field (a voltage) or a magnetic field. This paves the way for interesting nanotechnology applications [220] and, from the theoretical point of view, allows for the investigation of different parameter regimes including the transition from a weakly interacting quantum system to a strongly coupled, quasi-classical system, e.g., [221]. Furthermore, whereas in QDs the confinement is often well described by a harmonic potential, the vertical confinement in QWs typically consists of hard-wall potentials at the interface boundaries and is nearly constant within the carrier material. Moreover, the mobility of electrons in QDs and QWs is altered by the material embedding. This fact is usually taken into account by an effective (typically smaller) electron mass m^* and a modified dielectric constant $\varepsilon^*\varepsilon_0$ with typically $\varepsilon^* > 1$. The characteristic length scale is then the effective Bohr radius (see below).

To name a few NEGF applications, e.g., Kwong et al. [103] have studied the dynamics of an optically excited electron-hole plasma in QWs. Using the Matsubara Green's function, the ground states of few-electron QDs with harmonic confinement have been investigated at zero and finite temperatures in Ref. [129]. Extensions of this work to nonequilibrium situations can be found in Ref. [222]. In the following, we want to focus on a quantum well with an adjustable width L containing only a few N electrons.

In units of the characteristic confinement energy $E_0^* = \hbar^2/(m^* L^2)$, the Hamiltonian in vertical direction reads ($\mathbf{r}_i = (0, 0, z_i L)$):

$$\begin{aligned} \hat{H}(t) &= \sum_{i=1}^{N}\left(-\frac{1}{2}\frac{\partial^2}{\partial z_i^2} + v(z_i)\right) + \lambda^* \sum_{i<j}^{N} \frac{1}{\{(z_i - z_j)^2 + \kappa\}^{1/2}}, \\ v(z) &= \begin{cases} 0, & 0 < z < 1, \\ +\infty, & \text{otherwise.} \end{cases} \end{aligned} \tag{6.13}$$

Here, the dimensionless coupling parameter λ^* is defined by (a_0^* is the effective Bohr radius),

$$\lambda^* = \frac{L}{a_0^*} = \frac{e^2 m^* L}{4\pi\varepsilon^*\varepsilon_0\hbar^2}, \tag{6.14}$$

and measures the relative interaction strength between the electrons. While the limit $\lambda^* \to 0$ represents the ideal quantum case, where the electrons do not interact, the limit $\lambda \to \infty$ leads to a quasi-classical, Wigner-crystal behavior, e.g., Ref. [223].

Moreover, a soft-Coulomb interaction with $\kappa = 1$ can be motivated along Ref. [224] though it exhibits no cusp[11] [225] at small distances. Nevertheless, it has Coulomb asymptotics. In realistic sub-100 nm semiconductor heterostructures, the coupling parameter can be as large as $\lambda^* = 10$. If we assume a GaAs-based host material, such a value corresponds to a confinement energy of about 0.1 meV, while a 50 nm-QW means $\lambda^* = 5$ ($E_0^* = 0.438$ meV). Note that even a QW width as small as 10 nm corresponds to $\lambda^* = 1$ ($E_0^* = 10.9$ meV) and hence refers to the case of relatively strong electron-electron coupling.

In the following, we investigate the excitation spectrum of a four-electron QW at different coupling strengths. In particular, we focus on double excitations (DEs), which require a correlated treatment and are usually poorly described within time-dependent density functional theory [18]. To distinguish between single and double excitations, we trace the system behavior to the zero-coupling limit and analyze the functional dependence of the oscillator strengths [110]. In addition, we neglect the electron motion in the lateral direction and compute the (dipole) excitation spectrum with respect to the z-confinement only. As in Sect. 6.1.1, we use an FE-DVR ansatz for the spatial degrees of freedom in the 1pNEGF.

6.2.1 Correlation Effects in the Optical Absorption Spectra

In an interacting, finite, multi-electron system, the discrete energetic structure of excited states and their properties can be highly complex. In Sect. 6.1.1, we have seen that this applies already to the most elementary two-electron system—the helium atom. Usually, more and more excitation channels open when electrons are added to the system, and a thorough bookkeeping of states as well as an adequate characterization becomes indispensable to understand the excitation properties.

In many situations, the most basic features of an excitation spectrum can be understood on a single-particle level, i.e., by assuming a set of one-particle orbitals which can be occupied by a maximum of two electrons with opposite spin. In a frozen-orbital (FO) or Koopman's approximation [36], we can take the occupied and unoccupied (virtual) Hartree-Fock or Kohn-Sham orbitals of the ground state to construct excited states. To this end, one or more electrons are promoted into virtual orbitals forming single singly- or multiply-excited Slater determinants for each spin species, cf. Appendix A.1. The excited-state energies are then given by,

$$E = \sum_i{}' \varepsilon_i^{(1)} + \sum_{ij}{}' J_{ij}^{(2)} - \sum_{ij}{}' K_{ij}^{(2)}, \tag{6.15}$$

where $\varepsilon_i^{(1)}$ denotes the energy of orbital i, and all sums run over only those orbitals that contribute in the determinant[12]. Further, $J_{ij}^{(2)}$ and $K_{ij}^{(2)}$ represent the Coulomb and exchange integrals defined as (with HF or Kohn-Sham orbitals $\phi_i^{(1)}(\mathbf{r})$),

[11] A non-zero slope of the interaction potential at $|z_i - z_j| = 0$.

[12] This is indicated by the primes in Eq. (6.15).

$$J_{ij}^{(2)} = \int \mathrm{d}^3 r \int \mathrm{d}^3 r' \left|\phi_i^{(1)}(\mathbf{r})\right|^2 w^{(2)}\left(\mathbf{r}-\mathbf{r}'\right)\left|\phi_j^{(1)}\left(\mathbf{r}'\right)\right|^2,$$
$$K_{ij}^{(2)} = \int \mathrm{d}^3 r \int \mathrm{d}^3 r' \, \phi_i^{(1)}(\mathbf{r})\phi_j^{(1)}(\mathbf{r})\, w^{(2)}\left(\mathbf{r}-\mathbf{r}'\right)\phi_i^{(1)}\left(\mathbf{r}'\right)\phi_j^{(1)}\left(\mathbf{r}'\right). \tag{6.16}$$

Of course, the ground- and excited-state energies obtained from Eq. (6.15) are only approximate due to the neglect of orbital relaxations and correlations. The energy of singly-excited states is however often reasonably well described. On the other hand, the FO approximation can fail to reproduce the excitation energy of doubly-excited states[13]. The reason for this is that doubly-excited states are not necessarily well described by a single doubly-excited Slater determinant. In addition, the transition moments from the ground state to multiply-excited states are all zero *a priori* which limits the applicability of the FO approach.

Finite transition moments are usually obtained only when correlations are included. A correlated treatment of the many-body problem however renders the single-particle picture problematic as the excited states are described by superpositions of many Slater determinants. Consequently, a straightforward and direct characterization of excited states as in the mean-field picture does no longer apply. Nevertheless, according to Stanton and Bartlett [226], we still can count the number of electrons that are simultaneously excited. The corresponding measure is the so-called approximate excitation level (AEL),

$$A_{0\to n} = \frac{1}{2}\mathrm{Tr}\,|\rho_{1,n} - \rho_{1,0}|. \tag{6.17}$$

Here $\rho_{1,n}$ denotes the exact 1pRDM (the prime indicates a second set of coordinates),

$$\rho_{1,n} = \mathrm{Tr}_{2\ldots N}\left|\Psi_n^{(N)}\right\rangle\left\langle\Psi_n^{(N)}\right|', \tag{6.18}$$

which is expressed in the natural orbital basis that diagonalizes the ground-state density matrix $\rho_{1,0}$. Transitions with an AEL close to unity are referred to as single excitations (SEs). On the other hand, an AEL of about 2.0, 3.0 or 4.0 indicates states of essential double-, triple- or quadruple-excitation character, respectively. We note that an integer AEL is obtained only when the system is non-correlated and an effective single-particle approach (such as the FO approximation) is used.

Now, let us come back to the excitation spectrum of a QW structure. In the lower panel of Fig. 6.7, we show all ground-state excitation energies of a four-electron QW at a coupling parameter of $\lambda^* = 5$ which is typical for sub-100 nm heterostructures, cf. Eq. (6.14). The dots indicate the excitation energies $\hbar\omega_{0\to n}$ as they are obtained from exact diagonalization (ED) of the many-body Hamiltonian in terms of the ideal QW states. For a table with exact numbers, see Ref. [110]. Generally, we distinguish between dipole (open dots) and non-dipole transitions (closed dots). Further, the squares refer to the FO result, and the vertical position of the points give the AEL according to Eq. (6.17).

[13] This applies also to other multiply-excited states.

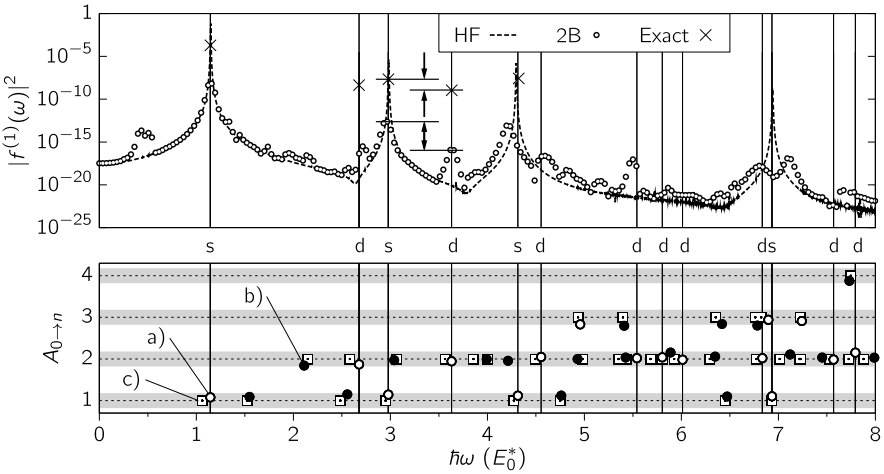

Fig. 6.7 Ground-state excitation spectrum of the four-electron QW at $\lambda^* = 5$. *In the lower panel*, the approximate excitation level $A_{0\to n}$ is shown for all excited states below $\hbar\omega = 8E_0^*$, cf. Eq. (6.17): (**a**) exact dipole transitions (*open dots*), (**b**) exact non-dipole transitions (*full dots*), and (**c**) frozen-orbital approximation (*squares*). *Upper panel*: dipole excitation spectrum in arbitrary units as obtained from the Kadanoff-Baym equations in HF (*dashed*) and 2B approximation (*dots*). The *crosses* indicate the transition dipole moments as obtained from exact diagonalization. Single and double excitations are, respectively, marked with the label "s" and "d"

Indeed, we observe that the AEL allows us to uniquely identify the alternating dipole- and non-dipole transitions in the quantum well as single, double, triple and quadruple excitations. Note that the deviation of the AEL from an integer value is overall less than 0.25, cf. the dots. Moreover, we observe that the FO approximation (with integer AEL) also performs quite well in the case of $\lambda^* = 5$ although there appear some discrepancies for larger excitation energies, compare the location of the squares relatively to the dots.

6.2.2 Electronic Double Excitations from the Kadanoff-Baym Equations

With ED and FO data as reference[14], we now investigate the QW spectrum on the basis of the Kadanoff-Baym equations. Principally, we expect that the time-dependent treatment and the inclusion of correlations should lead to an essential improvement of the FO result.

To obtain the excitation spectrum in a dynamical way, we, in Eq. (6.13), make $v(z)$ time dependent, i.e., set $v(z,t) = v_0\delta(t - t_0)z$ and record the time-dependent

[14] See the lower panel of Fig. 6.7 and the last paragraph in Sect. 6.2.1.

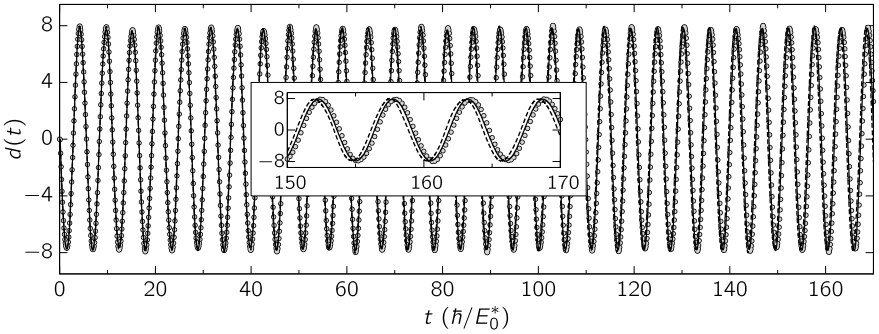

Fig. 6.8 Four-electron quantum well at $\lambda^* = 5$: Linear response of the time-dependent dipole moment $d(t)$ in HF (*dashed line*) and 2B approximation (*solid line*). The *dots* indicate the exact TDSE result. The *inset* shows that differences between HF, 2B and TDSE are small and that accurate results are required to resolve more excitations than just the transition to the first singly-excited state, cf. Figs. 6.7 and 6.9

dipole moment $d(t)$ for the linear response case $v_0 \ll 1$. Figure 6.8 shows $d(t)$ in HF (dashed line) and 2B approximation (solid line) and compares to the exact solution of the time-dependent Schrödinger equation (TDSE), cf. the dots. Basically, there are only small differences between the three curves such that correlation effects are rather hidden in the time series, see also the inset. Essential differences become not visible until performing the Fourier transform of the time-dependent dipole moment, see the upper panel of Fig. 6.7 which shows the absolute square, $|f^{(1)}(\omega)|^2$, of the transformation to the energy (frequency) space.

First of all, we notice that the Hartree-Fock approximation (dashed curve)—as already mentioned in the last section—is unable to describe transitions to doubly-excited states. Apart from this, all single excitations below $8E_0^*$ are well resolved and are in better agreement with the exact result than with the FO approximation, compare with the squares in the lower panel of Fig. 6.7. The latter is a direct consequence of the dynamical treatment. In the 2B approximation, which includes correlation effects up to second order in the interaction, we expect to see also transitions to doubly-excited states. Looking at the figure, we generally observe much more structure in the spectrum, and, indeed, there exist additional peaks that are located at energies for which we have double excitations (DEs) in the system, cf. in particular the three energetically lowest DEs.

Now, it is tempting to identify the additional peaks in the second Born approximation as the correct double excitations. However, in comparison to the exact TDSE solution, we cannot ignore the following deficiencies: (i) the relatively low excitation strength of the approximate DEs (see the arrows in the upper panel of Fig. 6.7), (ii) the occurrence of large energy shifts and splittings for SEs which are well described in HF approximation, and (iii) the presence of additional transitions at low and high energies that cannot be attributed to any excitations in the exact system.

As these drawbacks require detailed explanation, we, in Fig. 6.9, investigate the single and double excitations of the four-electron QW as function of the cou-

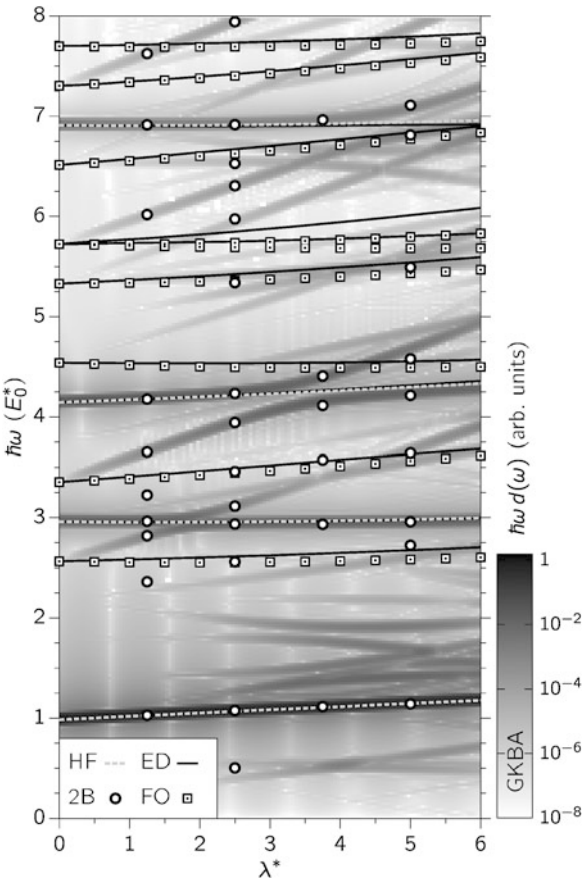

Fig. 6.9 Ground-state dipole excitation spectrum of the four-electron QW as function of the coupling strength λ^*, cf. Eq. (6.14). While the HF result, covering only single excitations, is shown by the four *gray dashed lines*, the exact excitation energies of single and double excitations are given by the *black solid lines*. The double excitations in FO approximation are shown by the *squares*. Correlated treatment in 2B approximation: GKBA (*density plot*) and full two-time solution of the KBEs (*dots*)

pling strength and, particularly, analyze the limit when the system becomes non-interacting, i.e., $\lambda^* \to 0$. The non-interacting limit is crucial as here all DEs vanish[15]. Focusing first on the HF approximation, Fig. 6.9 indicates that it correctly describes all SEs over the whole range of considered coupling parameters, cf. the gray dashed lines versus the FO data (squares). Correlated results are obtained in two ways: using full two-time 2B calculations (dots) for specific λ^*-values on the one hand and applying the GKBA on the other (density plot). Principally, the SEs are also well covered by the GKBA and 2B calculations for small λ^*. However, this does not apply for double excitations. Comparing GKBA to the exact diagonalization data (solid lines) as well as to the FO result, we observe that, admittedly, the correct λ^*-limit is reached, but the DE energy varies throughout too strongly with the coupling parameter (note the different slope). This λ^*-dependence is even such

[15]More precisely, they have zero transition dipole moment for $\lambda^* = 0$, cf. Sect. 6.2.1.

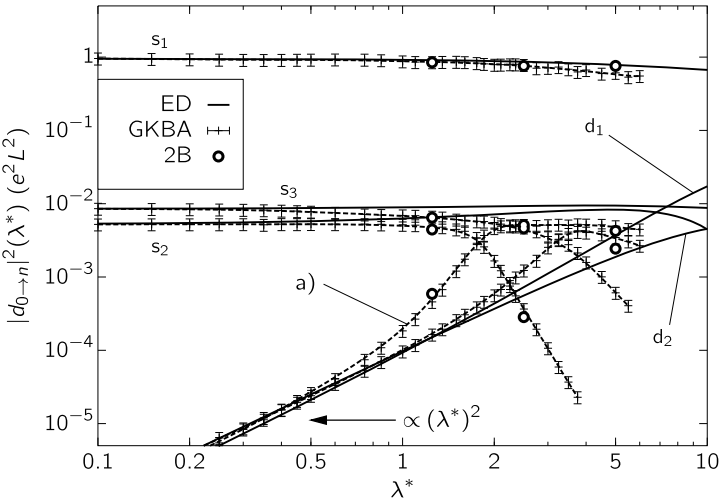

Fig. 6.10 Four-electron QW as in Figs. 6.7 and 6.9. Absolute square of the transition dipole moment for the five energetically lowest excited states (dipole transitions): There are three singly-excited states (s_1, s_2 and s_3) and two doubly-excited states (d_1 and d_1). ED: *solid lines*, GKBA: *dashed lines with errorbars*, and 2B: *dots*. Label (a): Energetically lowest double excitation as obtained by GKBA and 2B, respectively

that "avoided" crossings of the N-particle energy levels occur[16] at, e.g., $\lambda^* \approx 1.75$, 3.5 and 5.0. We emphasize that, in the whole range of considered coupling strengths, such crossings do not appear in the exact system.

By means of the transition dipole moments (TDMs), Fig. 6.10 proves that the relevant non-singly-excited states obtained by GKBA are really of DE character as they show the correct λ^*-dependence of the TDM whose absolute square is proportional to $(\lambda^*)^2$ and, in contrast to SEs[17], thus vanishes for $\lambda^* \to 0$. Following the energetically lowest DE (see the curve labeled (a) in Fig. 6.10), we however observe that the GKBA (2B) result starts to deviate considerably from the exact one for $\lambda^* \approx 1$. This is attributed to the avoided crossing found in Fig. 6.9. In particular, the curve indicates that the DE takes over the role of the second single excitation for larger coupling parameters as, here, the TDM changes only slowly with λ^*. The same happens to the second DE at $\lambda^* \approx 4$. For the moderate-to-strong coupling case $\lambda^* = 5$, this explains the detected energy shifts and splitting effects, compare with the upper panel of Fig. 6.7.

In conclusion, we note the following: On the one hand—on the basis of the λ^*-dependence of the TDMs of the excited states in the QW and by tracing the system behavior to the zero-coupling limit—we can clearly distinguish between states of

[16]Notice, that this behavior is not a specialty of the GKBA as full 2B calculations do confirm this behavior, cf. the dots.

[17]Here, the TDM is nearly constant for $\lambda^* < 1$. Note that both behaviors can be understood by standard perturbation theory.

different excitation character in a NEGF approach. Reasonable results for doubly-excited states have been obtained beyond the HF level for small coupling. On the other hand, however, the 2B calculations are rather poor in approximating the energy of DEs though the respective TDMs have been found to be quite accurate in parameter regimes where there appear no avoided crossings. Furthermore, we have identified additional transitions in the approximate spectrum that do not correspond to excitations in the exact system. It will be interesting to see, how these limitations of a 2B approach can be overcome by considering more advanced many-body approximations.

Chapter 7
Conclusion and Outlook

This monograph was devoted to quantum systems consisting of a finite number of identical particles in equilibrium and nonequilibrium. Examples were electrons in small atoms and molecules as well as electrons in quantum dots. We were interested in the treatment of correlation effects and their dynamics during and after an external excitation—problems of high current interest in many fields. Our approach was based on second quantization and has used the nonequilibrium Green's functions as the central quantities. The main advantages of this method are its internal consistency, the fulfillment of conservation laws and the existence of systematic approximation schemes that can be derived from Feynman diagrams.

While most previous numerical works using NEGFs focused on spatially homogeneous systems, here we concentrated on the numerical analysis of spatially inhomogeneous systems. This situation is more challenging because the one-particle NEGF, in general, depends on two coordinates and two times. Below we summarize the main results and outline future developments.

7.1 Summary

- It has been shown that direct numerical solutions of the two-time Kadanoff-Baym equations are feasible for various spatially inhomogeneous quantum many-body systems with Coulomb interaction, including electrons in atoms and molecules. Another example were electrons in "artificial atoms", i.e., in quantum dots. Compared to Coulomb interaction, systems with short range interaction should be even simpler to treat.
- It has been demonstrated that reasonable results that include two-particle correlations can already be obtained on the level of the second Born approximation, which is among the most simple conserving approximations for the one-particle self-energy beyond the mean-field level. When including direct and exchange terms, the results are also quantitatively reliable in the case of weak to moderate coupling.

K. Balzer, M. Bonitz, *Nonequilibrium Green's Functions Approach to Inhomogeneous Systems*, Lecture Notes in Physics 867,
DOI 10.1007/978-3-642-35082-5_7,

- For inhomogeneous systems, the finite element-discrete variable representation (FE-DVR), as introduced in Chap. 3, has allowed for a drastic simplification of the self-energy computation. The main advantage is that the matrix elements of the binary interaction become highly diagonal and that, hence, the integration or summation over the vertex points in the perturbation diagrams can, at least partly, be performed analytically.
- With the efficient MPI parallelization of the two-time propagation, longer propagation times and (or) calculations on larger systems become feasible.
- A further possibility to reduce computer storage requirements is to reconstruct the two-time NEGFs from their values on the time diagonal. To this end, we have employed the generalized Kadanoff-Baym ansatz with Hartree-Fock propagators for the second Born approximation which retains the conservation laws. It shows, in most cases, very good agreement with full second Born results but allows for orders of magnitude longer propagation times.

7.2 Prospects for Future Applications

The present results are a clear demonstration that inhomogeneous quantum systems are now accessible for a full NEGF analysis. The examples presented in this work are just illustrative examples that can be immediately extended to more complex systems in the near future.

- While the generalized Kadanoff-Baym ansatz (GKBA) has allowed us to access the long-time behavior of correlated quantum systems, its application, so far, was limited to the second Born approximation. This restricts the analysis to weakly or moderately coupled systems. One way to proceed toward strong coupling would be to use the one-particle self-energy in T-matrix approximation and to apply the GKBA to it.
- A few-site Hubbard model and its extensions, are good test systems to understand in more detail the spurious effects that have been observed in the 2B approximation (artificial damping of the dynamics, artificial peaks in the spectrum etc.). In addition, their simplicity allows to implement and test other conserving approximations such as the GW or T-matrix approximation more easily than for spatially continuous systems.
- A topic that requires a more profound analysis is the description of doubly-excited and multiply-excited states within a conserving many-body approximation and the impact of these states on the temporal dynamics.
- To work out the difference between the full two-time propagation and the GKBA, it would be interesting to perform benchmark calculations with an “exact” test self-energy. These calculations should allow one also to extend the adiabatic switching to finite temperatures.
- In many cases of multi-electron systems such as in atoms or condensed matter, not all electrons are actively participating in the system’s dynamics. In that case the problem may often be simplified by performing a projection on an active

sub-system (restricted active space concepts). Such methods exist in quantum chemistry and in atomic physics [230] and may be useful for NEGFs as well.

- When electrons are coupled to a (quasi-)continuum of degrees of freedom such as phonons or photons a self-consistent propagation of all degrees of freedom is often prohibited and not needed. In such cases an efficient way to proceed is to trace over the additional degrees of freedom ("environment") that give rise to additional self-energy contributions.

Despite the progress achieved in recent years and, in particular, the here-presented advances in the treatment of inhomogeneous systems, the NEGF scheme remains—due to the non-Markovian structure of the collision integrals—computationally costly. Therefore, to achieve long propagation times or to treat larger systems, ultimately, one solution is to develop multiscale methods. For a temporal multiscale approach, it should be possible to treat the shortest time scales on a fully non-Markovian two-time level whereas for longer times one switches to the GKBA and, eventually, to the Markov limit (Fermi's golden rule). Another idea, in particular to access larger systems, is to develop hybrid approaches, i.e., efficient combinations with conceptually simpler approaches. For example, for condensed matter applications, one should establish links to density functional theory (DFT). Another promising route for further developments is to establish connections with nonequilibrium versions of dynamical mean-field theory (DMFT).

The above list is by no means complete but contains just a few immediate extensions of the present work. More problems of long-term interest have been mentioned at the beginning of Chap. 1. We expect that the computational strategies developed in the present work to solve the (Keldysh-)Kadanoff-Baym equations for the NEGF for spatially inhomogeneous systems will be very efficient and successful in making the analysis of these questions accessible in the near future.

Appendix A
Second Quantization

The method of second quantization is deeply rooted in relativistic quantum field theory (QFT) which gives a physical meaning of particle indistinguishability and allows for a unification of fields and particles including the effect of interaction [72, 227, 228]. However even for non-relativistic systems, second quantization is very helpful for describing assemblies of identical particles. In particular, it provides mathematical tools that directly account for important symmetries and the (non-)conservation of the system's particle number.

A.1 Symmetry of Many-Body States

The quantum dynamics of N identical non-relativistic particles are described by the time-dependent Schrödinger equation (TDSE),

$$\left(\mathrm{i}\hbar\frac{\partial}{\partial t} - \hat{H}^{(N)}(t)\right)\Psi^{(N)} = 0, \tag{A.1}$$

with the Hamiltonian $\hat{H}^{(N)}$ being invariant under particle exchange. In the simplest case (neglecting spin degrees of freedom etc.), the wave function is an element of the N-particle Hilbert space $\mathscr{H}^{(N)}$ and has the form $\Psi^{(N)} = \Psi(\mathbf{r}_1, \ldots, \mathbf{r}_N, t)$, where the state of each particle i is determined by its position $\mathbf{r}_i$ relative to some reference. As also the probability density $\rho(\mathbf{r}_1, \ldots, \mathbf{r}_N, t) = |\Psi(\mathbf{r}_1, \ldots, \mathbf{r}_N, t)|^2$ is invariant under the exchange of any pair of labels (ensuring indistinguishability), the wave function $\Psi^{(N)}$ must obey the symmetry,

$$\mathscr{P}_{ij}\Psi(\mathbf{r}_1, \ldots, \mathbf{r}_i, \ldots, \mathbf{r}_j, \ldots, \mathbf{r}_N, t) = \mathrm{e}^{-\mathrm{i}\phi}\Psi(\mathbf{r}_1, \ldots, \mathbf{r}_j, \ldots, \mathbf{r}_i, \ldots, \mathbf{r}_N, t). \tag{A.2}$$

Here, $\mathscr{P}_{ij}$ indicates the pairwise permutation operator. In principle, the phase factor $\mathrm{e}^{-\mathrm{i}\phi}$ could be arbitrary. However, we know from experience that at the most only $\phi = 0$ and π are realized[1]. Thus, we deal with even (odd) permutations,

[1] Of course, the operator $\mathscr{P}_{ij}$ is Hermitian (and unitary) and thus has real eigenvalues.

K. Balzer, M. Bonitz, *Nonequilibrium Green's Functions Approach to Inhomogeneous Systems*, Lecture Notes in Physics 867,
DOI 10.1007/978-3-642-35082-5, © Springer-Verlag Berlin Heidelberg 2013

$\mathscr{P}\Psi^{(N)} = +\Psi^{(N)}$ ($\mathscr{P}\Psi^{(N)} = -\Psi^{(N)}$). The corresponding particles are called bosons (fermions). A stringent proof of this phase restriction essentially appears in relativistic quantum mechanics and leads to the spin-statistics theorem and, for fermions, to the Pauli exclusion principle.

If the total wave function is constructed from a complete set of one-particle states $\phi_i(\mathbf{r})$ according to $\Psi^{(N)} = \sum_{i_1 \ldots i_N} a_{i_1 \ldots i_N}(t)\phi_{i_1}(\mathbf{r}_1) \cdot \cdots \cdot \phi_{i_N}(\mathbf{r}_N)$, the symmetry conditions of Eq. (A.2) directly transfer to the coefficients $a_{i_1 \ldots i_N}(t) \in \mathbb{C}$. Moreover, we can introduce properly (anti-)symmetrized N-particle basis states as tensor products. For bosons, the inner product is then a permanent of the matrix $\{\phi_i(\mathbf{r}_j)\}$. For fermions, we obtain Slater determinants,

$$\Phi_{i_1,\ldots,i_N}(\mathbf{r}_1,\ldots,\mathbf{r}_N) = \begin{vmatrix} \phi_{i_1}(\mathbf{r}_1) & \phi_{i_1}(\mathbf{r}_2) & \ldots & \phi_{i_1}(\mathbf{r}_N) \\ \phi_{i_2}(\mathbf{r}_1) & \phi_{i_2}(\mathbf{r}_2) & \ldots & \phi_{i_2}(\mathbf{r}_N) \\ \vdots & \vdots & & \vdots \\ \phi_{i_N}(\mathbf{r}_1) & \phi_{i_N}(\mathbf{r}_2) & \ldots & \phi_{i_N}(\mathbf{r}_N) \end{vmatrix}. \tag{A.3}$$

In this basis, any fermionic wave function can be written as,

$$\Psi^{(N)} = \sum_{i_1 \ldots i_N} b_{i_1 \ldots i_N}(t)\Phi_{i_1,\ldots,i_N}(\mathbf{r}_1,\ldots,\mathbf{r}_N), \tag{A.4}$$

in which the coefficients $b_{i_1,\ldots,i_N}(t) \in \mathbb{C}$ do not need to obey a certain permutation symmetry regarding their indices. With the sum running over all possible Slater determinants, Eq. (A.4) is usually referred to as the configuration interaction (CI) representation of a many-body wave function [36]. On the other hand, if we include only a few determinants, the ansatz is generally called multi-configuration Hartree-Fock (MCHF), e.g., [17]. In the limiting case of only a single Slater determinant, we are back to Eq. (A.3) and the standard (mean-field) Hartree-Fock approach [35].

The central point of the second quantization formalism to be introduced below is that it will automatically keep track of the correct permutation symmetry of the many-body state according to Eq. (A.4).

A.2 Occupation Number Representation

In the following, we assume that the set of one-particle states $\{|i\rangle = \phi_i(\mathbf{r})\}$ with $i = 1, 2, 3, \ldots$ is complete and orthonormal, i.e.,

$$\langle i\,|\,j\rangle = \delta_{ij}, \qquad \sum_i \langle i\,|\,i\rangle = 1. \tag{A.5}$$

One possibility of labeling the fermionic basis states introduced in Eq. (A.3) is to write $\Phi_{i_1,\ldots,i_N}(\mathbf{r}_1,\ldots,\mathbf{r}_N) = \sqrt{N!}|i_1,\ldots,i_N\rangle$, where the indices on the r.h.s. form a sequence with $i_1 < i_2 < \cdots < i_N$, and the prefactor $\sqrt{N!}$ accounts for normalization of $|i_1,\ldots,i_N\rangle$. As the Slater determinant vanishes when two indices are equal, it is clear that the sequence must be strictly monotonic. For bosons, $|i_1,\ldots,i_N\rangle$ means the respective permanent, and it is $i_1 \le i_2 \le \cdots \le i_N$. The correct normalization is

governed by a factor of $\sqrt{n_1!n_2!\ldots n_\infty!}$, where the integers n_i denote the number of particles that occupy the state $|i\rangle$. In both cases, the set of states $|i_1,\ldots,i_N\rangle$ is complete and orthonormal.

Another possibility of labeling is to directly resort to occupation numbers (occupation number representation). Here, any state $|i_1,\ldots,i_N\rangle$ is equally described by the ket vector $|n_1,n_2,\ldots\rangle = |\{n\}\rangle$ with $\sum_i n_i = N$, where, for bosons, n_i can take any positive integer including zero, and, for fermions, one either has $n_i = 0$ or $n_i = 1$. For the inner product of two states, $|\{n\}\rangle$ and $|\{n'\}\rangle$, one then obtains

$$\langle\{n\}|\{n'\}\rangle = \prod_i \delta_{n_i,n_i'}. \tag{A.6}$$

A.3 Particle Creation and Annihilation in Fock Space

In the above sections, the particle number N was constant, and we dealt with a wave function involving strictly N coordinates. However, in many physical situations the number of particles can fluctuate, e.g., through induced particle currents or thermal effects. Theoretically, this becomes most natural in the grand canonical ensemble of statistical physics.

In quantum statistics, the Fock space $\mathscr{H}$ allows for variations in the number of particles [229]. It is defined as the direct sum of all Hilbert spaces with distinct but fixed particle number,

$$\mathscr{H} = \bigoplus_{i=0}^{\infty} \mathscr{H}^{(i)} = \mathscr{H}^{(0)} \oplus \mathscr{H}^{(1)} \oplus \mathscr{H}^{(2)} \oplus \cdots \oplus \mathscr{H}^{(N)} \oplus \cdots. \tag{A.7}$$

An arbitrary state in Fock space then reads,

$$\Psi = \Psi^{(0)} + \Psi^{(1)} + \Psi^{(2)} + \cdots + \Psi^{(N)} + \cdots, \tag{A.8}$$

i.e., it is composed of elements of $\mathscr{H}^{(0)}$, $\mathscr{H}^{(1)}$, $\mathscr{H}^{(2)}$ and so on. $\mathscr{H}^{(0)}$ is one-dimensional and consists of the vacuum state $|0\rangle$. Different subspaces of the Fock space with fixed particle number are orthogonal.

All bosonic and fermionic states $|n_1,n_2,\ldots\rangle = |\{n\}\rangle$ with arbitrary particle number belong to the Fock space. For this reason, it is useful to define operators which can increase or decrease the number of particles in $|\{n\}\rangle$ by one (producing a different state in $\mathscr{H}$) but let the symmetry of the many-body state unaffected. For fermions, we define such creation ($\hat{f}^\dagger$) and annihilation operators ($\hat{f}$) by,

$$\begin{aligned} \hat{f}_i^\dagger |n_1,n_2,\ldots,n_i,\ldots\rangle &= (-1)^s(1-n_i)|n_1,n_2,\ldots,n_i+1,\ldots\rangle, \\ \hat{f}_i |n_1,n_2,\ldots,n_i,\ldots\rangle &= (-1)^s n_i |n_1,n_2,\ldots,n_i-1,\ldots\rangle, \end{aligned} \tag{A.9}$$

where $s = \sum_{j=1}^{i-1} n_j$, and $\hat{f}_i|0\rangle = 0$ is just a special case of the annihilator action. If the initial state has particle number N, the result of Eq. (A.9) is a properly antisym-

metrized $(N \pm 1)$-particle state[2]. The built-in antisymmetrization manifests itself in the (equal-time) canonical anticommutation relations[3],

$$\begin{aligned} \left[\hat{f}_i, \hat{f}_j^\dagger\right]_+ &= \delta_{ij}, \\ \left[\hat{f}_i, \hat{f}_j\right]_+ = \left[\hat{f}_i^\dagger, \hat{f}_j^\dagger\right]_+ &= 0, \end{aligned} \tag{A.10}$$

where $[\hat{a}, \hat{b}]_+ = \hat{a}\hat{b} + \hat{b}\hat{a}$. For bosons, the only difference is that, instead of the anticommutator, we have to take the commutator, $[\cdot, \cdot]_-$.

Some useful relations hold:

$$\begin{aligned} |i_1, i_2, \ldots, i_N\rangle &= \prod_{n=1}^{N} \hat{f}_{i_n}^\dagger |0\rangle, \qquad \langle i_1, i_2, \ldots, i_N| = \langle 0| \prod_{n=1}^{N} \hat{f}_{i_n}, \\ \left[\hat{f}_i, \left(\hat{f}_j^\dagger \hat{f}_k\right)\right]_- &= \delta_{ij} \hat{f}_k, \qquad \left[\hat{f}_i^\dagger, \left(\hat{f}_j^\dagger \hat{f}_k\right)\right]_- = -\delta_{ik} \hat{f}_j^\dagger, \\ \left[\hat{f}_i, \left(\hat{f}_j^\dagger \hat{f}_k^\dagger \hat{f}_m \hat{f}_l\right)\right]_- &= \delta_{ij} \hat{f}_k^\dagger \hat{f}_m \hat{f}_l + \delta_{ik} \hat{f}_j^\dagger \hat{f}_l \hat{f}_m, \\ \left[\hat{f}_i^\dagger, \left(\hat{f}_j^\dagger \hat{f}_k^\dagger \hat{f}_m \hat{f}_l\right)\right]_- &= -\delta_{il} \hat{f}_j^\dagger \hat{f}_k^\dagger \hat{f}_m - \delta_{im} \hat{f}_k^\dagger \hat{f}_j^\dagger \hat{f}_l. \end{aligned} \tag{A.11}$$

Finally, we mention that, if the one-particle states $|i\rangle$ change under a unitary transformation, $\{|i\rangle\} \to \{|i'\rangle\}$, the creation and annihilation operators transform according to,

$$\hat{f}_{i'}^\dagger = \sum_i \langle i|i'\rangle \hat{f}_i^\dagger, \qquad \hat{f}_{i'} = \sum_i \langle i'|i\rangle \hat{f}_i. \tag{A.12}$$

A.4 General Form of Operators

The creation and annihilation operators defined in Eq. (A.9) are the basic quantities of the second quantization method. With them, we can reformulate arbitrary operators in quantum mechanics and can redefine how to compute observables and expectation values of Hermitian operators.

First, it is easily verified that,

$$\hat{\rho}_{1,ij} = \hat{f}_i^\dagger \hat{f}_j, \tag{A.13}$$

is the one-particle reduced density matrix (1pRDM) operator. Second, the particle number operator (the identity operator in the Fock subspace $\mathscr{H}^{(1)}$) takes the form $\hat{N} = \sum_i \hat{f}_i^\dagger \hat{f}_i$.

In general, an N-particle operator $\hat{A}^{(N)}$ can be of S-particle type, i.e.,

[2] Analogous expressions exist for bosons: $\hat{b}_i^\dagger |n_1, \ldots, n_i, \ldots\rangle = \sqrt{n_i + 1} |n_1, \ldots, n_i + 1, \ldots\rangle$ and $\hat{b}_i |n_1, \ldots, n_i, \ldots\rangle = \sqrt{n_i} |n_1, \ldots, n_i - 1, \ldots\rangle$.

[3] This is a direct consequence of the definitions in (A.9).

$$\hat{A}^{(N)} = \sum_{i_1,\ldots,i_S=1}^{N} \hat{a}^{(S)}_{i_1\ldots i_S}, \quad S \leq N. \tag{A.14}$$

In the second-quantized form, it is rewritten as,

$$\hat{A} = \frac{1}{S!} \sum_{i_1\ldots i_S, i'_1\ldots i'_S} \langle i_1,\ldots,i_S|\hat{a}^{(S)}\big|i'_S,\ldots,i'_1\rangle \hat{f}^\dagger_{i_1}\ldots\hat{f}^\dagger_{i_S}\hat{f}_{i'_S}\ldots\hat{f}_{i'_1}. \tag{A.15}$$

Note that, in contrast to Eq. (A.14) where the sum ranges over the particles, the indices i_1 to i'_S in Eq. (A.15) label the one-particle states $|i_1\rangle$ to $|i'_S\rangle$ and that the ordering of the second set of $\hat{f}$-operators is inverted. Moreover, the term "second quantization" is motivated by the fact that the form of Eq. (A.15) looks similar to an expectation value taken between wave functions[4]. In this language, the one-particle TDSE can be seen as a classical field equation, and the operators $\hat{f}_i$ and $\mathrm{i}\hat{f}^\dagger_i$ become canonically paired variables ($\hbar \equiv 1$), see Ref. [84].

The most relevant operators are of one- and two-body type:

(i) For the operator of the kinetic energy $\hat{T}^{(N)} = \sum_{i=1}^{N} \hat{t}^{(1)}_i = \sum_{i=1}^{N} \frac{-\hbar^2}{2m}\nabla^2_{\mathbf{r}_i}$ of a system of N particles (mass m), we obtain,

$$\hat{T} = \sum_{i,j} \langle i|\hat{t}^{(1)}|j\rangle \hat{f}^\dagger_i \hat{f}_j. \tag{A.16}$$

Other operators of one-body type, such as the single-particle potential energy $\hat{V}^{(N)}$, have an analogous form where $\hat{t}^{(1)}_i$ has to be replaced by the proper operator.

(ii) The interaction energy operator $\hat{W}^{(N)} = \sum_{i<j}^{N} \hat{w}^{(2)}_{ij}$ becomes,

$$\hat{W} = \frac{1}{2}\sum_{ij,kl} \langle ij|\hat{w}^{(2)}|kl\rangle \hat{f}^\dagger_i \hat{f}^\dagger_j \hat{f}_l \hat{f}_k. \tag{A.17}$$

The matrix elements $\langle i|\hat{t}^{(1)}|j\rangle$ and $\langle ij|\hat{w}^{(2)}|kl\rangle$ in (i) and (ii) are often called one-particle and two-particle integrals, respectively. Following the physicist's notation[5], we have in coordinate space,

$$\begin{aligned} \langle i|\hat{t}^{(1)}|j\rangle &= -\frac{\hbar^2}{2m}\int \mathrm{d}^3r\, \phi^*_i(\mathbf{r})\nabla^2\phi_j(\mathbf{r}), \\ \langle ij|\hat{w}^{(2)}|kl\rangle &= \int \mathrm{d}^3r \int \mathrm{d}^3r'\, \phi^*_i(\mathbf{r})\phi^*_k(\mathbf{r}')w^{(2)}(\mathbf{r}-\mathbf{r}')\phi_j(\mathbf{r})\phi_l(\mathbf{r}'). \end{aligned} \tag{A.18}$$

If the binary interaction $w^{(2)}$ is symmetric and the states $|i\rangle$ are real, the two-electron integrals are fully symmetric with respect to interchange of $i \leftrightarrow j$, $k \leftrightarrow l$ and pairs $ij \leftrightarrow kl$.

[4] The analogy becomes even more obvious when one transforms into coordinate space. Here, $\hat{f}^\dagger_i$ and $\hat{f}_i$ become continuous and are usually called "field operators" with notation $\hat{\psi}^\dagger(\mathbf{r})$ and $\hat{\psi}(\mathbf{r})$.

[5] In contrast to the chemists notation, see Ref. [36].

The evaluation of observables becomes straightforward using Eq. (A.15). For the mean kinetic energy

$$\langle \hat{T} \rangle = \sum_{i,j} \langle i|\hat{t}^{(1)}|j\rangle \langle \hat{f}_i^\dagger \hat{f}_j \rangle$$

and other observables of one-body type, the task is to compute the expectation values $\langle \hat{f}_i^\dagger \hat{f}_j \rangle$ which are the elements of the 1pRDM $\langle \hat{\rho}_1 \rangle$. For the interaction energy $\langle \hat{W} \rangle$, we correspondingly need the elements of the two-particle density matrix $\langle \hat{\rho}_2 \rangle$.

In the case of mixed states[6], $\langle \hat{\rho}_1 \rangle$ and $\langle \hat{\rho}_2 \rangle$ are given by,

$$\langle \hat{\rho}_1 \rangle = \mathrm{Tr}\{\hat{\rho}\hat{\rho}_1\}, \qquad \langle \hat{\rho}_2 \rangle = \mathrm{Tr}\{\hat{\rho}\hat{\rho}_2\}, \tag{A.19}$$

where $\mathrm{Tr}\{\hat{\rho}\ldots\} = \sum_r p_r \langle r|\ldots|r\rangle$ and $\hat{\rho} = \sum_r p_r |r\rangle\langle r|$ denotes the full density operator of the system (the sum ranges over all system realizations $|r\rangle$ of which each has a real probability p_r and $\sum_r p_r = 1$). For pure states, we have a single realization only, i.e., $\hat{\rho} = |r\rangle\langle r|$, where $|r\rangle$ is expanded, e.g., in terms of Slater determinants or permanents (in occupation number representation): $|r\rangle = \sum_{\{n\}} c_{\{n\}} |\{n\}\rangle$.

[6] E.g., for a particle ensemble at finite temperatures.

Appendix B
Perturbation Expansion. Supplements

"*The problem that intrigued me in Copenhagen was how to delineate the structure of approximations to multi-particle Green's functions that would include conservation laws.*"
(Gordon Baym, in Ref. [1])

This part of the appendix does not aim at giving a detailed introduction to the perturbation expansion of the one-particle nonequilibrium Green's function (1pNEGF) or the one-particle self-energy (1pSE). For a comprehensive discussion on this topic—including the explanation of the diagram technique for the 1pSE and the Luttinger-Ward functional Φ—the reader is referred to Ref. [91] or the textbooks [55, 56]. Instead, we here give a derivation of two relations used in Sect. 2.3.2. First, we show how to evaluate functional derivatives of a contour-ordered product, and, second, we give details on how to arrive at Eqs. (2.57) and (2.58).

B.1 Derivative of a Contour-Ordered Product

For a contour-ordered product of two operators $\hat{a}$ and $\hat{b}$ in the Heisenberg picture, we want to calculate the derivative of its average with respect to a time-dependent scalar function $c_{ij}^{(1)}(\bar{t})$, i.e., with t and t' located on the Keldysh contour,

$$\frac{\delta}{\delta c_{ij}^{(1)}(\bar{t})}\left\langle \hat{T}_{\mathscr{C}}\hat{a}(t)\hat{b}\left(t'\right)\right\rangle. \tag{B.1}$$

In order to evaluate expression (B.1), we first consider the change of the time-evolution operator $\hat{U}(t,t') \to \hat{U}(t,t') + \delta\hat{U}(t,t')$ when the system's Hamiltonian is perturbed according to $\hat{H}(t) \to \hat{H}(t) + \delta\hat{H}(t)$. It is straightforward to show[1], that $\delta\hat{U}(t,t')$ is generally given by,

$$\delta\hat{U}\left(t,t'\right) = -\frac{\mathrm{i}}{\hbar}\int_{t}^{t'} \mathrm{d}\bar{t}\,\hat{U}(t,\bar{t})\delta\hat{H}(\bar{t})\hat{U}\left(\bar{t},t'\right). \tag{B.2}$$

[1] Using the equation(s) of motion of the time-evolution operator, cf. Eq. (2.4).

K. Balzer, M. Bonitz, *Nonequilibrium Green's Functions Approach to Inhomogeneous Systems*, Lecture Notes in Physics 867,
DOI 10.1007/978-3-642-35082-5, © Springer-Verlag Berlin Heidelberg 2013

In the following, we choose the perturbation to be $\delta\hat{H}(t) = \sum_{ij} \delta c_{ij}^{(1)}(t)\hat{\rho}_{1,ij}$, where $\hat{\rho}_{1,ij} = \hat{f}_i^\dagger \hat{f}_j$ is the 1pRDM. If we assume $t \le \bar{t} \le t'$, we can write,

$$\begin{aligned}\frac{\delta\hat{U}(t,t')}{\delta c_{ij}^{(1)}(\bar{t})} &= -\frac{\mathrm{i}}{\hbar}\sum_{kl}\int_t^{t'} \mathrm{d}\bar{\bar{t}}\; \hat{U}(t,\bar{\bar{t}})\frac{\delta c_{kl}^{(1)}(\bar{\bar{t}})}{\delta c_{ij}^{(1)}(\bar{t})}\rho_{1,kl}\hat{U}\big(\bar{\bar{t}},t'\big) \\ &= -\frac{\mathrm{i}}{\hbar}\hat{U}\big(t',\bar{t}\big)\rho_{1,ij}\hat{U}\big(\bar{t},t'\big), \end{aligned} \tag{B.3}$$

where we have used,

$$\frac{\delta c_{kl}^{(1)}(t)}{\delta c_{ij}^{(1)}(t')} = \delta_{ki}\delta_{lj}\delta\big(t-t'\big). \tag{B.4}$$

Now, relation (B.3) helps us to rewrite Eq. (B.1). To this end, we use the definition of the average $\langle\ldots\rangle$ in terms of successive time evolutions (compare with Eq. (2.9)). For $t > t'$, we obtain,

$$\frac{\delta\langle\hat{T}_{\mathscr{C}}\hat{a}(t)\hat{b}(t')\rangle}{\delta c_{ij}^{(1)}(\bar{t})} = \frac{\delta}{\delta c_{ij}^{(1)}(\bar{t})}\frac{\mathrm{Tr}\{\hat{U}(t_0-\mathrm{i}\beta,t)\hat{a}\hat{U}(t,t')\hat{b}\hat{U}(t',t_0)\}}{\mathrm{Tr}\{\hat{U}(t_0-\mathrm{i}\beta,t_0)\}}, \tag{B.5}$$

which, by applying the chain rule, evaluates to ($Z_0 = \mathrm{Tr}\{\hat{U}(t_0-\mathrm{i}\beta,t_0)\}$),

$$\begin{aligned}&\frac{\delta\langle\hat{T}_{\mathscr{C}}\hat{a}(t)\hat{b}(t')\rangle}{\delta c_{ij}^{(1)}(\bar{t})} \\ &= -\frac{\mathrm{i}\theta_{\mathscr{C}}(t'-\bar{t})}{\hbar Z_0}\mathrm{Tr}\big\{\hat{U}(t_0-\mathrm{i}\beta,t)\hat{a}\hat{U}\big(t,t'\big)\hat{b}\hat{U}\big(t',\bar{t}\big)\rho_{1,ij}\hat{U}(\bar{t},t_0)\big\} \\ &\quad -\frac{\mathrm{i}\theta_{\mathscr{C}}(\bar{t}-t')\theta_{\mathscr{C}}(t-\bar{t})}{\hbar Z_0}\mathrm{Tr}\big\{\hat{U}(t_0-\mathrm{i}\beta,t)\hat{a}\hat{U}(t,\bar{t})\rho_{1,ij}\hat{U}\big(\bar{t},t'\big)\hat{b}\hat{U}\big(t',t_0\big)\big\} \\ &\quad -\frac{\mathrm{i}\theta_{\mathscr{C}}(\bar{t}-t)}{\hbar Z_0}\mathrm{Tr}\big\{\hat{U}(t_0-\mathrm{i}\beta,\bar{t})\rho_{1,ij}\hat{U}(\bar{t},t)\hat{a}\hat{U}\big(t,t'\big)\hat{b}\hat{U}\big(t',t_0\big)\big\} \\ &\quad +\frac{\mathrm{i}}{\hbar Z_0^2}\mathrm{Tr}\big\{\hat{U}(t_0-\mathrm{i}\beta,t)\hat{a}\hat{U}\big(t,t'\big)\hat{b}\hat{U}\big(t',t_0\big)\big\}\mathrm{Tr}\big\{\hat{U}(t_0-\mathrm{i}\beta,\bar{t})\rho_{1,ij}\hat{U}(\bar{t},t_0)\big\}, \\ &= -\frac{\mathrm{i}}{\hbar}\big\langle\hat{T}_{\mathscr{C}}\hat{a}(t)\hat{b}\big(t'\big)\rho_{1,ij}(\bar{t})\big\rangle + \frac{\mathrm{i}}{\hbar}\big\langle\hat{T}_{\mathscr{C}}\hat{a}(t)\hat{b}\big(t'\big)\big\rangle\big\langle\rho_{1,ij}(\bar{t})\big\rangle. \end{aligned} \tag{B.6}$$

Note, that the last equality also holds for $t < t'$, i.e., it represents the final result for the functional derivative:

$$\frac{\delta\langle\hat{T}_{\mathscr{C}}\hat{a}(t)\hat{b}(t')\rangle}{\delta c_{ij}^{(1)}(\bar{t})} = \frac{\mathrm{i}}{\hbar}\big\langle\hat{T}_{\mathscr{C}}\hat{a}(t)\hat{b}\big(t'\big)\big\rangle\big\langle\rho_{1,ij}(\bar{t})\big\rangle - \frac{\mathrm{i}}{\hbar}\big\langle\hat{T}_{\mathscr{C}}\hat{a}(t)\hat{b}\big(t'\big)\rho_{1,ij}(\bar{t})\big\rangle. \tag{B.7}$$

We note that the r.h.s. of Eq. (B.7) contains two contributions each of which includes four operators. The first term is Hartree-like (i.e., it contains a product of two two-operator expectation values) and the second term includes a four-operator expectation value.

B.2 Equations for $\Sigma^{(1)}$ and $\delta G^{(1)}/\delta v^{(1)}$ in Terms of $\delta\Sigma^{(1)}/\delta v^{(1)}$

In the second part of Sect. 2.3.2, we have discussed on how one can gradually generate higher-order approximations of the one-particle self-energy. To this end, one iterates Eq. (2.57) under the knowledge of Eq. (2.58). For the sake of completeness, we want to give a brief derivation of these two important equations.

We start with the second one, i.e., with Eq. (2.58) and review the KBEs in the closed form (space and spin indices are omitted; $h^{(1)}(t) = t^{(1)} + v^{(1)}(t)$),

$$\begin{aligned}\left\{\mathrm{i}\hbar\frac{\partial}{\partial t} - h^{(1)}(t)\right\}G^{(1)}(t,t') &= \delta_{\mathscr{C}}(t-t') + \int_{\mathscr{C}}\mathrm{d}\bar{\bar{t}}\;\Sigma^{(1)}(t,\bar{\bar{t}})G^{(1)}(\bar{\bar{t}},t'),\\ G^{(1)}(t,t')\left\{-\mathrm{i}\hbar\frac{\partial}{\partial t'} - h^{(1)}(t')\right\} &= \delta_{\mathscr{C}}(t-t') + \int_{\mathscr{C}}\mathrm{d}\bar{\bar{t}}\;G^{(1)}(t,\bar{\bar{t}})\Sigma^{(1)}(\bar{\bar{t}},t').\end{aligned} \tag{B.8}$$

Differentiation of the KBEs with respect to $v^{(1)}(\bar{t})$ leads to,

$$\begin{aligned}&\left\{\mathrm{i}\hbar\frac{\partial}{\partial t} - h^{(1)}(t)\right\}\frac{\delta G^{(1)}(t,t')}{\delta v^{(1)}(\bar{t})} - \delta_{\mathscr{C}}(t-t')G^{(1)}(t,t')\\ &\quad= \int_{\mathscr{C}}\mathrm{d}\bar{\bar{t}}\left\{\frac{\delta\Sigma^{(1)}(t,\bar{\bar{t}})}{\delta v^{(1)}(\bar{t})}G^{(1)}(\bar{\bar{t}},t') + \Sigma^{(1)}(t,\bar{\bar{t}})\frac{\delta G^{(1)}(\bar{\bar{t}},t')}{\delta v^{(1)}(\bar{t})}\right\},\end{aligned} \tag{B.9}$$

and a corresponding adjoint equation where t and t' are exchanged. A general solution of these equations for $\delta G^{(1)}/\delta v^{(1)}$ is of the form [88],

$$\begin{aligned}\frac{\delta G^{(1)}(t,t')}{\delta v^{(1)}(\bar{t})} &= G^{(1)}(t,\bar{t})G^{(1)}(\bar{t},t')\\ &\quad+\int_{\mathscr{C}}\mathrm{d}t_1\int_{\mathscr{C}}\mathrm{d}t_2\,G^{(1)}(t,t_1)\frac{\delta\Sigma^{(1)}(t_1,t_2)}{\delta v^{(1)}(\bar{t})}G^{(1)}(t_2,t')\\ &\quad+Y(t,t',\bar{t}),\end{aligned} \tag{B.10}$$

if the three-point auxiliary function $Y(t,t',\bar{t})$ obeys,

$$\left\{\mathrm{i}\hbar\frac{\partial}{\partial t} - h^{(1)}(t)\right\}Y(t,t',\bar{t}) = \int_{\mathscr{C}}\mathrm{d}\bar{\bar{t}}\;\Sigma^{(1)}(t,\bar{\bar{t}})Y(\bar{\bar{t}},t',\bar{t}), \tag{B.11}$$

and its adjoint with $t \leftrightarrow t'$. One easily proves this result by insertion and use of (B.8). Next, all terms in Eq. (B.10) must be consistent with the KMS boundary conditions, cf. Eq. (2.22)(a) and (b), i.e., in particular, $Y(t_0 - \mathrm{i}\beta, t', \bar{t}) = -Y(t_0, t', \bar{t})$ and $Y(t, t_0 - \mathrm{i}\beta, \bar{t}) = -Y(t, t_0, \bar{t})$. As this must be fulfilled for all times $\bar{t}$, it follows that Y is either independent of $\bar{t}$ and equals the 1pNEGF or is zero. The former case is contradictory in the physical units. Therefore, it is $Y = 0$, and we obtain Eq. (2.58) which can be written also as,

$$\frac{\delta G^{(1)}(t,t')}{\delta v^{(1)}(t_1)} = \int_{\mathscr{C}}\mathrm{d}\bar{t}\int_{\mathscr{C}}\mathrm{d}\bar{\bar{t}}\;G^{(1)}(t,\bar{t})G^{(1)}(\bar{\bar{t}},t')\Gamma(\bar{t}\bar{\bar{t}},t_1), \tag{B.12}$$

with the "vertex" function,

$$\Gamma\left(tt',\bar{t}\right)=\delta_{\mathscr{C}}\left(t-t'\right)\delta_{\mathscr{C}}\left(t'-\bar{t}\right)+\frac{\Sigma^{(1)}(t,t')}{\delta v^{(1)}(\bar{t})}. \tag{B.13}$$

In order to derive Eq. (2.57), we insert Eq. (B.12) into Eq. (2.51) and obtain,

$$\begin{aligned}&\left\{\mathrm{i}\hbar\frac{\partial}{\partial t}-h^{(1)}(t)\right\}G^{(1)}\left(t,t'\right)-\delta_{\mathscr{C}}\left(t-t'\right)\\&\quad=-\mathrm{i}\hbar\int_{\mathscr{C}}\mathrm{d}t_1\,w^{(2)}(t-t_1)G^{(1)}\left(t_1,t_1^+\right)G^{(1)}\left(t,t'\right)\\&\qquad+\mathrm{i}\hbar\int_{\mathscr{C}}\mathrm{d}t_1\int_{\mathscr{C}}\mathrm{d}\bar{t}\int_{\mathscr{C}}\mathrm{d}\bar{\bar{t}}\,w^{(2)}\left(t^+-t_1\right)G^{(1)}(t,\bar{t})G^{(1)}\left(\bar{\bar{t}},t'\right)\Gamma(\bar{t}\bar{\bar{t}},t_1).\end{aligned} \tag{B.14}$$

The r.h.s. must be equal to the collision integral $\int_{\mathscr{C}}\mathrm{d}\bar{t}\,\Sigma^{(1)}(t,\bar{t})G^{(1)}(\bar{t},t')$ in the Kadanoff-Baym equations. Therefore, we can extract the self-energy to be of the form,

$$\begin{aligned}\Sigma^{(1)}\left(t,t'\right)&=-\mathrm{i}\hbar\delta_{\mathscr{C}}\left(t-t'\right)\int_{\mathscr{C}}\mathrm{d}\bar{t}\,w^{(2)}(t-\bar{t})G^{(1)}\left(\bar{t},\bar{t}^+\right)\\&\quad+\mathrm{i}\hbar\int_{\mathscr{C}}\mathrm{d}\bar{t}\int_{\mathscr{C}}\mathrm{d}\bar{\bar{t}}\,G^{(1)}(t,\bar{t})w^{(2)}\left(t^+-\bar{\bar{t}}\right)\Gamma\left(\bar{t}t',\bar{\bar{t}}\right).\end{aligned} \tag{B.15}$$

Reinserting the definition of the vertex function yields,

$$\begin{aligned}\Sigma^{(1)}\left(t,t'\right)&=-\mathrm{i}\hbar\delta_{\mathscr{C}}\left(t-t'\right)\int_{\mathscr{C}}\mathrm{d}\bar{t}\,w^{(2)}(t-\bar{t})G^{(1)}\left(\bar{t},\bar{t}^+\right)\\&\quad+\mathrm{i}\hbar w^{(2)}\left(t^+-t'\right)G^{(1)}\left(t,t'\right)\\&\quad+\mathrm{i}\hbar\int_{\mathscr{C}}\mathrm{d}\bar{t}\int_{\mathscr{C}}\mathrm{d}\bar{\bar{t}}\,G^{(1)}(t,\bar{t})w^{(2)}\left(t^+-\bar{\bar{t}}\right)\frac{\Sigma(\bar{t}t')}{\delta v^{(1)}(\bar{\bar{t}})}.\end{aligned} \tag{B.16}$$

This is Eq. (2.57).

References

1. M. Bonitz (ed.), *Progress in Nonequilibrium Green's Functions* (World Scientific, Singapore, 2000)
2. M. Bonitz, D. Semkat (eds.), *Progress in Nonequilibrium Green's Functions II* (World Scientific, Singapore, 2003)
3. M. Bonitz, A. Filinov (eds.), *Progress in Nonequilibrium Green's Functions III*. J. Phys. Conf. Ser., vol. 35 (2006), 001-042
4. M. Bonitz, K. Balzer (eds.), *Progress in Nonequilibrium Green's Functions IV*. J. Phys. Conf. Ser., vol. 220 (2010), 011001-012023
5. S. Konabe, S. Okada, Multiple exciton generation by a single photon in single-walled carbon nanotubes. Phys. Rev. Lett. **108**, 227401 (2012)
6. K. Burke, Perspective on density functional theory. J. Chem. Phys. **136**, 150901 (2012)
7. P. Hohenberg, W. Kohn, Inhomogeneous electron gas. Phys. Rev. B **136**, 864 (1964)
8. E. Runge, E.K.U. Gross, Density-functional theory for time-dependent systems. Phys. Rev. Lett. **52**, 997 (1984)
9. V.M. Axt, S. Mukamel, Real-space density-matrix description of dynamic correlations in the optical response of many-electron systems, in *Nonlinear Optical Materials*, vol. 101, ed. by J.V. Maloney (Springer, Berlin, 1998), p. 33
10. R.C. Iotti, E. Ciancio, F. Rossi, Quantum transport theory for semiconductor nanostructures: a density-matrix formulation. Phys. Rev. B **72**, 125347 (2005)
11. M. Bonitz, *Quantum Kinetic Theory* (Teubner, Stuttgart, 1998)
12. S.R. White, Density matrix formulation for quantum renormalization groups. Phys. Rev. Lett. **69**, 2863 (1992)
13. U. Schollwöck, The density-matrix renormalization group. Rev. Mod. Phys. **77**, 259 (2005)
14. U. Schollwöck, The density-matrix renormalization group in the age of matrix product states. Ann. Phys. **326**, 96 (2011)
15. E. Gull, A.J. Millis, A.I. Lichtenstein, A.N. Rubtsov, M. Troyer, Ph. Werner, Continuous-time Monte Carlo methods for quantum impurity models. Rev. Mod. Phys. **83**, 349 (2011)
16. J. Caillat, J. Zanghellini, M. Kitzler, O. Koch, W. Kreuzer, A. Scrinzi, Correlated multi-electron systems in strong laser fields: a multiconfiguration time-dependent Hartree-Fock approach. Phys. Rev. A **71**, 012712 (2005)
17. D. Hochstuhl, M. Bonitz, Two-photon ionization of helium studied with the multiconfigurational time-dependent Hartree-Fock method. J. Chem. Phys. **134**, 084106 (2011)
18. M. Thiele, S. Kümmel, Photoabsorption spectra from adiabatically exact time-dependent density-functional theory in real time. Phys. Chem. Chem. Phys. **11**, 4631 (2009)
19. M. Petersilka, U.J. Gossmann, E.K.U. Gross, Excitation energies from time-dependent density-functional theory. Phys. Rev. Lett. **76**, 1212 (1996)
20. N.N. Matsuzawa, A. Ishitani, D.A. Dixon, T. Uda, Time-dependent density functional theory

DOI 10.1007/978-3-642-35082-5, © Springer-Verlag Berlin Heidelberg 2013

calculations of photoabsorption spectra in the vacuum ultraviolet region. J. Phys. Chem. A **105**, 4953 (2001)
21. E.M. Stoudenmire, S.R. White, Studying two-dimensional systems with the density matrix renormalization group. Annu. Rev. Condens. Matter Phys. **3**, 111 (2012)
22. S. Hermanns, K. Balzer, M. Bonitz, Few-particle quantum dynamics—comparing Nonequilibrium Green's functions with the generalized Kadanoff-Baym ansatz to density operator theory, arXiv:1211.6959 (2012)
23. P. Lipavský, V. Špička, B. Velický, Generalized Kadanoff-Baym ansatz for deriving quantum transport equations. Phys. Rev. B **34**, 6933 (1986)
24. V. Špička, B. Velický, A. Kalvová, Long and short time quantum dynamics: I. Between Green's functions and transport equations. Physica E, Low-Dimens. Syst. Nanostruct. **29**, 154 (2005)
25. V. Špička, B. Velický, A. Kalvová, Long and short time quantum dynamics: II. Kinetic regime. Physica E, Low-Dimens. Syst. Nanostruct. **29**, 175 (2005)
26. V. Špička, B. Velický, A. Kalvová, Long and short time quantum dynamics: III. Transients. Physica E, Low-Dimens. Syst. Nanostruct. **29**, 196 (2005)
27. E. Wigner, On the quantum correction for thermodynamic equilibrium. Phys. Rev. **40**, 749 (1932)
28. L.P. Kadanoff, G. Baym, *Quantum Statistical Mechanics* (Benjamin, New York, 1962)
29. N.D. Mermin, Thermal properties of the inhomogeneous electron gas. Phys. Rev. A **137**, 1441 (1965)
30. M. Eschrig, $T > 0$ ensemble-state density functional theory via Legendre transform. Phys. Rev. B **82**, 205120 (2010)
31. T. Schoof, M. Bonitz, A. Filinov, D. Hochstuhl, J.W. Dufty, Configuration path integral Monte Carlo. Contrib. Plasma Phys. **51**, 687–697 (2011)
32. M. Bonitz, P. Ludwig, H. Baumgartner, C. Henning, A. Filinov, D. Block, O. Arp, A. Piel, S. Käding, Y. Ivanov, A. Melzer, H. Fehske, V. Filinov, Classical and quantum Coulomb crystals. Phys. Plasmas **15**, 055704 (2008)
33. J.W. Abraham, K. Balzer, D. Hochstuhl, M. Bonitz, Quantum breathing mode of interacting particles in a one-dimensional harmonic trap. Phys. Rev. B **86**, 125112 (2012)
34. P. Ludwig, H. Thomsen, K. Balzer, A. Filinov, M. Bonitz, Tuning correlations in multicomponent plasmas. Plasma Phys. Control. Fusion **52**, 124013 (2010)
35. F. Jensen, *Introduction to Computational Chemistry* (Wiley, Chichester, 1999)
36. A. Szabo, N.S. Ostlund, *Modern Quantum Chemistry* (Dover Publications, New York, 1996)
37. G. Tanner, K. Richter, J.-M. Rost, The theory of two-electron atoms: between ground state and complete fragmentation. Rev. Mod. Phys. **72**, 497 (2000)
38. D.R. Yarkony, Diabolical conical intersections. Rev. Mod. Phys. **68**, 985 (1996)
39. B. Walker, B. Sheehy, L.F. DiMauro, P. Agostini, K.J. Schafer, K.C. Kulander, Precision measurement of strong field double ionization of helium. Phys. Rev. Lett. **73**, 1227 (1994)
40. W. Becker, X.J. Liu, P.J. Ho, J.H. Eberly, Theories of photoelectron correlation in laser-driven multiple atomic ionization. Rev. Mod. Phys. **84**, 1011 (2012)
41. S. Bauch, K. Balzer, M. Bonitz, Electronic correlations in double ionization of atoms in pump-probe experiments. Europhys. Lett. **91**, 53001 (2010)
42. E. Pavarini, E. Koch, D. Vollhardt, A. Lichtenstein (eds.), *The LDA+DMFT Approach to Strongly Correlated Materials* (Forschungszentrum Jülich GmbH, Zentralbibliothek, Verlag, Jülich, 2011)
43. D.S. Chemla, J. Shah, Many-body and correlation effects in semiconductors. Nature **411**, 549 (2001)
44. Z. Huang, H. Wang, S. Kais, Entanglement and electron correlation in quantum chemistry calculations. J. Mod. Opt. **53**, 2543 (2006)
45. M.A. Nielsen, I.L. Chuang, *Quantum Computation and Quantum Information* (Cambridge University Press, Cambridge, 2000)
46. M. Uiberacker, Th. Uphues, M. Schultze, A.J. Verhoef, V. Yakovlev, M.F. Kling, J. Rauschenberger, N.M. Kabachnik, H. Schröder, M. Lezius, K.L. Kompa, H.-G. Muller,

M.J.J. Vrakking, S. Hendel, U. Kleineberg, U. Heinzmann, M. Drescher, F. Krausz, Attosecond real-time observation of electron tunnelling in atoms. Nature **446**, 627 (2007)
47. J. Feist, R. Pazourek, S. Nagele, E. Persson, B.I. Schneider, L.A. Collins, J. Burgdörfer, Ab initio calculations of two-electron emission by attosecond pulses. J. Phys. Conf. Ser. **194**, 012010 (2009)
48. A. Rudenko, L. Foucar, M. Kurka, Th. Ergler, K.U. Kühnel, Y.H. Jiang, A. Voitkiv, B. Najjari, A. Kheifets, S. Lüdemann, T. Havermeier, M. Smolarski, S. Schössler, K. Cole, M. Schöffler, R. Dörner, S. Düsterer, W. Li, B. Keitel, R. Treusch, M. Gensch, C.D. Schröter, R. Moshammer, J. Ullrich, Recoil-ion and electron momentum spectroscopy: reaction-microscopes. Phys. Rev. Lett. **101**, 073003 (2008)
49. S. Sukiasyan, Ch. McDonald, C. Destefani, Yu.M. Ivanov, Th. Brabec, Multielectron correlation in high-harmonic generation: a 2D model analysis. Phys. Rev. Lett. **102**, 223002 (2009)
50. J. Itatani, F. Quere, G.L. Yudin, M.Y. Ivanov, F. Krausz, P.B. Corkum, Attosecond streak camera. Phys. Rev. Lett. **88**, 173903 (2002)
51. U. Frühling, M. Wieland, M. Gensch, Th. Gebert, B. Schütte, M. Krikunova, R. Kalms, F. Budzyn, O. Grimm, J. Rossbach, E. Plönjes, M. Drescher, Single-shot terahertz-field-driven X-ray streak camera. Nat. Photonics **3**, 523 (2009)
52. B. Schütte, S. Bauch, U. Früling, M. Wieland, M. Gensch, E. Plönjes, T. Gaumnitz, A. Azima, M. Bonitz, M. Drescher, Evidence for chirped Auger-electron emission. Phys. Rev. Lett. **108**, 253003 (2012)
53. S. Bauch, M. Bonitz, Theoretical description of field-assisted post-collision interaction in Auger decay of atoms. Phys. Rev. A **85**, 053416 (2012)
54. J. Ullrich, R. Moshammer, A. Dorn, R. Dörner, L.Ph.H. Schmidt, H. Schmidt-Böcking, Recoil-ion and electron momentum spectroscopy: reaction-microscopes. Rep. Prog. Phys. **66**, 1463 (2003)
55. A.L. Fetter, J.D. Walecka, *Quantum Theory of Many-Particle Systems* (McGraw-Hill, San Francisco, 1971)
56. G.D. Mahan, *Many-Particle Physics* (Kluwer Academic/Plenum Publishers, New York, 2000)
57. P.C. Martin, J. Schwinger, Theory of many-particle systems I. Phys. Rev. **115**, 1342 (1959)
58. J. Schwinger, Brownian motion of a quantum oscillator. J. Math. Phys. **2**, 407 (1961)
59. L.V. Keldysh, Diagram technique for nonequilibrium processes. Zh. Eksp. Teor. Fiz. **47**, 1515 (1964) [Sov. Phys. JETP **20**, 1018 (1965)]
60. S. Datta, *Electronic Transport in Mesoscopic Systems* (Cambridge University Press, New York, 1995)
61. H. Haug, A.-P. Jauho, *Quantum Kinetics in Transport and Optics of Semiconductors* (Springer, Heidelberg, 1996)
62. A.-P. Jauho, J.W. Wilkins, Theory of high-electric-field quantum transport for electron-resonant impurity systems. Phys. Rev. B **29**, 1919 (1984)
63. H. Haug, C. Ell, Coulomb quantum kinetics in a dense electron gas. Phys. Rev. B **46**, 2126 (1992)
64. D. Semkat, D. Kremp, M. Bonitz, Kadanoff-Baym equations and non-Markovian Boltzmann equation in generalized T-matrix approximation. J. Math. Phys. **41**, 7458 (2000)
65. S. Fujita, Thermodynamic evolution equation for a quantum statistical gas. J. Math. Phys. **6**, 1877 (1965)
66. A.G. Hall, Non-equilibrium Green functions: generalized Wick's theorem and diagrammatic perturbation with initial correlations. J. Phys. A, Math. Gen. **8**, 214 (1975)
67. P. Danielewicz, Quantum theory of nonequilibrium processes I. Ann. Phys. **152**, 239 (1984)
68. N.E. Dahlen, R. van Leeuwen, Self-consistent solution of the Dyson equation for atoms and molecules within a conserving approximation. J. Chem. Phys. **122**, 164102 (2005)
69. M. Bonitz, D. Semkat, H. Haug, Non-Lorentzian spectral functions for Coulomb quantum kinetics. Eur. Phys. J. B **9**, 309 (1999)

70. D. Semkat, M. Bonitz, D. Kremp, Relaxation of a quantum many-body system from a correlated initial state. A general and consistent approach. Contrib. Plasma Phys. **43**, 321 (2003)
71. D. Kremp, D. Semkat, M. Bonitz, Short-time kinetics and initial correlations in quantum kinetic theory. J. Phys. Conf. Ser. **11**, 1 (2005)
72. D.F. DuBois, *Lectures in Theoretical Physics* (Gordon and Breach, New York, 1967) [edited by W.E. Brittin]
73. D.C. Langreth, *NATO Adv. Study Inst. Series B: Physics* (Plenum, New York, 1967) [edited by J.T. Devreese and V.E. Van Doren]
74. J. Rammer, H. Smith, Quantum field-theoretical methods in transport theory of metals. Rev. Mod. Phys. **58**, 323 (1986)
75. A. Griffin, Conserving and gapless approximations for an inhomogeneous Bose gas at finite temperatures. Phys. Rev. B **53**, 9341 (1996)
76. G. Stefanucci, E. Perfetto, M. Cini, Time-dependent quantum transport with superconducting leads. J. Phys. Conf. Ser. **220**, 012012 (2010)
77. G. Stefanucci, E. Perfetto, M. Cini, Time-dependent quantum transport with superconducting leads: a discrete-basis Kohn-Sham formulation and propagation scheme. Phys. Rev. B **81**, 115446 (2010)
78. M. Wagner, Expansions of nonequilibrium Green's functions. Phys. Rev. B **44**, 6104 (1991)
79. V.G. Morozov, G. Röpke, The "mixed" Green's function approach to quantum kinetics with initial correlations. Ann. Phys. **278**, 127 (1999)
80. A. Stan, N.E. Dahlen, R. van Leeuwen, Time propagation of the Kadanoff-Baym equations for inhomogeneous systems. J. Chem. Phys. **130**, 224101 (2009)
81. R. Kubo, Statistical-mechanical theory of irreversible processes. I. General theory and simple applications to magnetic and conduction problems. J. Phys. Soc. Jpn. **12**, 570 (1957)
82. Th. Bornath, D. Kremp, M. Schlanges, Two-particle problem in a nonequilibrium many-particle system. Phys. Rev. E **60**, 6382 (1999)
83. D. Kremp, M. Schlanges, W.D. Kraeft, *Quantum Statistics of Nonideal Plasmas* (Springer, Berlin, 2005)
84. N.J.M. Horing, Quantum theory of solid state plasma dielectric response. Contrib. Plasma Phys. **51**, 589 (2010)
85. M. Puig von Friesen, C. Verdozzi, C.-O. Almbladh, Kadanoff-Baym dynamics of Hubbard clusters: performance of many-body schemes, correlation-induced damping and multiple steady and quasi-steady states. Phys. Rev. B **82**, 155108 (2010)
86. R. van Leeuwen, N.E. Dahlen, A. Stan, Total energies from variational functionals of the Green function and the renormalized four-point vertex. Phys. Rev. B **74**, 195105 (2006)
87. G. Baym, Self-consistent approximations in many-body systems. Phys. Rev. **127**, 1391 (1962)
88. R. van Leeuwen, N.E. Dahlen, G. Stefanucci, C.-O. Almbladh, U. von Barth, Introduction to the Keldysh formalism, in *Time-Dependent Density Functional Theory*, ed. by M.A.L. Marques, C.A. Ullrich, F. Nogueira, A. Rubio, K. Burke, E.K.U. Gross. Lecture Notes in Physics, vol. 706 (2006)
89. R. van Leeuwen, N.E. Dahlen, An Introduction to Nonequilibrium Green Functions. Lecture notes, unpublished (2005). http://theochem.chem.rug.nl/research/vanleeuwen/literature/NGF.pdf
90. J.M. Luttinger, J.C. Ward, Ground-state energy of a many-fermion system II. Phys. Rev. **118**, 1417 (1960)
91. T. Kita, Introduction to nonequilibrium statistical mechanics with quantum field theory. Prog. Theor. Phys. **123**, 581 (2010)
92. N.E. Dahlen, A. Stan, R. van Leeuwen, Nonequilibrium Green function theory for excitation and transport in atoms and molecules. J. Phys. Conf. Ser. **35**, 324 (2006)
93. M. Zwolakz, Numerical ansatz for solving integro-differential equations with increasingly smooth memory kernels: spin-boson model and beyond. Comput. Sci. Discov. **1**, 015002 (2008)
94. E.M. Lifshitz, L.P. Pitaevskii, *Physical Kinetics* (Elsevier Science Ltd, Saint Louis, 1981)

95. M. Bonitz, D. Kremp, Kinetic energy relaxation and correlation time of nonequilibrium many-particle systems. Phys. Lett. A **212**, 83 (1996)
96. D. Kremp, M. Bonitz, W.D. Kraeft, M. Schlanges, Non-Markovian Boltzmann equation. Ann. Phys. **258**, 320 (1997)
97. M. Bonitz, D. Kremp, D.C. Scott, R. Binder, W.D. Kraeft, H.S. Köhler, Numerical analysis of non-Markovian effects in charge-carrier scattering: one-time versus two-time kinetic equations. J. Phys. Condens. Matter **8**, 6057 (1996)
98. D. Kremp, Th. Bornath, M. Bonitz, M. Schlanges, Quantum kinetic theory of plasmas in strong laser fields. Phys. Rev. E **60**, 4725 (1999)
99. V. Špička, A. Kalvová, B. Velický, Dynamics of mesoscopic systems: non-equilibrium Green's functions approach. Physica E, Low-Dimens. Syst. Nanostruct. **42**, 525 (2010)
100. P. Kleinert, Two-time quantum transport and quantum diffusion. Phys. Rev. E **79**, 051107 (2009)
101. B. Velický, A. Kalvová, V. Špička, Between Green's functions and transport equations: reconstruction theorems and the role of initial conditions. J. Phys. Conf. Ser. **35**, 1 (2006)
102. H.S. Köhler, Memory and correlation effects in the quantum theory of thermalization. Phys. Rev. E **53**, 3145 (1996)
103. N.H. Kwong, M. Bonitz, R. Binder, H.S. Köhler, Semiconductor Kadanoff-Baym equation results for optically excited electron-hole plasmas in quantum wells. Phys. Status Solidi (b) **206**, 197 (1998)
104. P. Gartner, L. Bányai, H. Haug, Two-time electron-LO-phonon quantum kinetics and the generalized Kadanoff-Baym approximation. Phys. Rev. B **60**, 14234 (1999)
105. P. Gartner, J. Seebeck, F. Jahnke, Relaxation properties of the quantum kinetics of carrier-LO-phonon interaction in quantum wells and quantum dots. Phys. Rev. B **73**, 115307 (2006)
106. Q.T. Vu, H. Haug, Time-dependent screening of the carrier-phonon and carrier-carrier interactions in nonequilibrium systems. Phys. Rev. B **62**, 7179 (2000)
107. S.V. Faleev, M.I. Stockman, Self-consistent random-phase approximation for interacting electrons in quantum wells and intersubband absorption. Phys. Rev. B **66**, 085318 (2002)
108. M. Lorke, T.R. Nielsen, J. Seebeck, P. Gartner, F. Jahnke, Influence of carrier-carrier and carrier-phonon correlations on optical absorption and gain in quantum-dot systems. Phys. Rev. B **73**, 085324 (2006)
109. M. Lorke, T.R. Nielsen, J. Seebeck, P. Gartner, F. Jahnke, Quantum kinetic effects in the optical absorption of semiconductor quantum-dot systems. J. Phys. Conf. Ser. **35**, 182 (2006)
110. K. Balzer, S. Hermanns, M. Bonitz, Electronic double-excitations in quantum wells: solving the two-time Kadanoff-Baym equations. Europhys. Lett. **98**, 67002 (2012)
111. M. Bonitz, Th. Bornath, D. Kremp, M. Schlanges, W.D. Kraeft, Quantum kinetic theory for laser plasmas. Dynamical screening in strong fields. Contrib. Plasma Phys. **39**, 329 (1999)
112. H. Haberland, M. Bonitz, D. Kremp, Harmonics generation in electron-ion collisions in a short laser pulse. Phys. Rev. E **64**, 026405 (2001)
113. S. Hermanns, K. Balzer, M. Bonitz, Non-equilibrium Green's function approach to inhomogeneous quantum many-body systems using the generalized Kadanoff Baym ansatz. Phys. Scr. **T151**, 014036 (2012)
114. H.S. Köhler, N.H. Kwong, H.A. Yousif, A Fortran code for solving the Kadanoff-Baym equations for a homogeneous fermion system. Comput. Phys. Commun. **123**, 123 (1999)
115. M. Hartmann, W. Schäfer, Real time approach to relaxation and dephasing processes in semiconductors. Phys. Status Solidi (c) **173**, 165 (1992)
116. W. Schäfer, Influence of electron-electron scattering on femtosecond four-wave mixing in semiconductors. J. Opt. Soc. Am. B **13**, 1291 (1996)
117. H.S. Köhler, Memory and correlation effects in nuclear collisions. Phys. Rev. C **51**, 3232 (1995)
118. K. Balzer, S. Hermanns, M. Bonitz, The generalized Kadanoff-Baym ansatz. Computing nonlinear response properties of finite systems, arXiv:1211.3036 (2012)

119. R. Binder, H.S. Köhler, M. Bonitz, N. Kwong, Green's function description of momentum-orientation relaxation of photoexcited electron plasmas in semiconductors. Phys. Rev. B **55**, 5110 (1997)
120. D. Semkat, Kurzzeitkinetik und Anfangskorrelationen in nichtidealen Vielteilchensystemen. Dissertation, Universität Rostock, Germany, 2001
121. D. Semkat, D. Kremp, M. Bonitz, Kadanoff-Baym equations with initial correlations. Phys. Rev. E **59**, 1557 (1999)
122. N.-H. Kwong, M. Bonitz, Real-time Kadanoff-Baym approach to plasma oscillations in a correlated electron gas. Phys. Rev. Lett. **84**, 1768 (2000)
123. M. Bonitz, Correlation time approximation in kinetic theory. Phys. Lett. A **221**, 85 (1996)
124. M. Bonitz, N.H. Kwong, D. Semkat, D. Kremp, Generalized Kadanoff-Baym theory for non-equilibrium many-body systems in external fields. An effective multi-band approach. Contrib. Plasma Phys. **39**, 37 (1999)
125. D.O. Gericke, S. Kosse, M. Schlanges, M. Bonitz, T-matrix approach to equilibium and nonequilibrium carrier-carrier scattering in semiconductors. Phys. Rev. B **59**, 10639 (1999)
126. E.K.U. Gross, J.F. Dobson, M. Petersilka, Density functional theory of time-dependent phenomena. Top. Curr. Chem. **181**, 81 (1996)
127. G. Onida, L. Reining, A. Rubio, Electronic excitations: density-functional versus many-body Green's-function approaches. Rev. Mod. Phys. **74**, 601 (2002)
128. C.A. Ullrich, *High Performance Computing in Science and Engineering, Garching/Munich 2009* (Oxford University Press, New York, 2012)
129. K. Balzer, M. Bonitz, R. van Leeuwen, A. Stan, N.E. Dahlen, Nonequilibrium Green's function approach to strongly correlated few-electron quantum dots. Phys. Rev. B **79**, 245306 (2009)
130. N.E. Dahlen, R. van Leeuwen, A. Stan, Propagating the Kadanoff-Baym equations for atoms and molecules. J. Phys. Conf. Ser. **35**, 340 (2006)
131. A. Stan, N.E. Dahlen, R. van Leeuwen, Fully self-consistent GW calculations for atoms and molecules. Europhys. Lett. **76**, 298 (2006)
132. N.E. Dahlen, R. van Leeuwen, Solving the Kadanoff-Baym equations for inhomogeneous systems: application to atoms and molecules. Phys. Rev. Lett. **98**, 153004 (2007)
133. M.S. Lee, M. Head-Gordon, Polarized atomic orbitals for self-consistent field electronic structure calculations. J. Chem. Phys. **107**, 9085 (1997)
134. N. Marzari, D. Vanderbilt, Maximally localized generalized Wannier functions for composite energy bands. Phys. Rev. B **56**, 12847 (1997)
135. P.L. Silvestrelli, N. Marzari, D. Vanderbilt, M. Parrinello, Maximally-localized Wanner functions for disordered systems: application to amorphous silicon. Solid State Commun. **107**, 7 (1998)
136. I. Schnell, G. Czycholl, R.C. Albers, Hubbard-U calculations for Cu from first-principle Wannier functions. Phys. Rev. B **65**, 075103 (2002)
137. F. Aryasetiawan, K. Karlsson, O. Jepsen, U. Schönberger, Calculations of Hubbard U from first-principles. Phys. Rev. B **74**, 125106 (2006)
138. A. Georges, G. Kotliar, W. Krauth, M.J. Rozenberg, Dynamical mean-field theory of strongly correlated fermion systems and the limit of infinite dimensions. Rev. Mod. Phys. **68**, 13 (1996)
139. T.N. Rescigno, C.W. McCurdy, Numerical grid methods for quantum-mechanical scattering problems. Phys. Rev. A **62**, 032706 (2000)
140. L.A. Collins, S. Mazevet, J.D. Kress, B.I. Schneider, D.L. Feder, Time-dependent simulations of large-scale quantum dynamics. Phys. Scr. **T110**, 408 (2004)
141. J.C. Light, I.P. Hamilton, J.V. Lill, Generalized discrete variable approximation in quantum mechanics. J. Chem. Phys. **82**, 1400 (1985)
142. J.C. Light, T. Carrington, Discrete-variable representations and their utilization. Adv. Chem. Phys. **114**, 263 (2007)
143. B.I. Schneider, L.A. Collins, S.X. Hu, Parallel solver for the time-dependent linear and nonlinear Schrödinger equation. Phys. Rev. E **73**, 036708 (2006)

144. S.X. Hu, Quantum study of slow electron collisions with Rydberg atoms. Phys. Rev. A **74**, 062716 (2006)
145. L. Tao, C.W. McCurdy, T.N. Rescigno, Grid-based methods for diatomic quantum scattering problems: a finite-element discrete-variable representation in prolate spheroidal coordinates. Phys. Rev. A **79**, 012719 (2009)
146. L. Tao, C.W. McCurdy, T.N. Rescigno, Grid-based methods for diatomic quantum scattering problems. II. Time-dependent treatment of single- and two-photon ionization of H_2^+. Phys. Rev. A **80**, 013402 (2009)
147. L. Tao, C.W. McCurdy, T.N. Rescigno, Grid-based methods for diatomic quantum scattering problems. III. Double photoionization of molecular hydrogen in prolate spheroidal coordinates. Phys. Rev. A **82**, 023423 (2010)
148. S.X. Hu, L.A. Collins, Strong-field ionization of molecules in circularly polarized few-cycle pulses. Phys. Rev. A **73**, 023405 (2006)
149. D.J. Haxton, K.V. Lawler, C.W. McCurdy, Multiconfiguration time-dependent Hartree-Fock treatment of electronic and nuclear dynamics in diatomic molecules. Phys. Rev. A **83**, 063416 (2011)
150. B.I. Schneider, L.A. Collins, The discrete variable method for the solution of the time-dependent Schrödinger equation. J. Non-Cryst. Solids **351**, 1551 (2005)
151. K. Balzer, Solving the two-time Kadanoff-Baym equations. Application to model atoms and molecules. Dissertation, Universität Kiel, Germany, 2012
152. D.E. Manolopoulos, R.E. Wyatt, Quantum scattering via the log derivative version of the Kohn variational principle. Chem. Phys. Lett. **152**, 23 (1988)
153. K. Balzer, S. Bauch, M. Bonitz, Time-dependent second-order Born calculations for model atoms and molecules in strong laser fields. Phys. Rev. A **82**, 033427 (2010)
154. A. Rios, B. Barker, M. Buchler, P. Danielewicz, Towards a nonequilibrium Green's function description of nuclear reactions: one-dimensional mean-field dynamics. Ann. Phys. **326**, 1274 (2011)
155. D. van Neck, K. Peirs, M. Waroquier, Self-consistent solution of Dyson's equation up to second order for atomic systems. J. Chem. Phys. **115**, 15 (2001)
156. K. Peirs, D. van Neck, M. Waroquier, Self-consistent solution of Dyson's equation up to second order for closed- and open-shell atomic systems. Int. J. Quantum Chem. **91**, 113 (2003)
157. G. Baym, N.D. Mermin, Determination of thermodynamic Green's functions. J. Math. Phys. **2**, 232 (1961)
158. W. Ku, A.G. Eguiluz, Band-gap problem in semiconductors revisited: effects of core states and many-body self-consistency. Phys. Rev. Lett. **89**, 126401 (2002)
159. P. Zhao, N.J.M. Horing, D.L. Woolard, H.L. Cui, Nonequilibrium Green's function formulation of quantum transport theory for multi-band semiconductors. Phys. Lett. A **310**, 258 (2003)
160. W. Gropp, E. Lusk, A. Skjellum, *Portable Parallel Programming with the Message-Passing Interface* (MIT Press, Cambridge, 1999)
161. M. Garny, M.M. Müller, Quantum Boltzmann equations in the early universe, in *High Performance Computing in Science and Engineering*, Garching/Munich, 2009 (Springer, Berlin, 2010), p. 463
162. M.D. Hill, N.P. Jouppi, G.S. Sohi, *Readings in Computer Architecture* (Academic Press, San Diego, 2000)
163. V.I. Anisimov, F. Aryasetiawan, A.I. Lichtenstein, First-principles calculations of the electronic structure and spectra of strongly correlated systems: the LDA+U method. J. Phys. Condens. Matter **9**, 767 (1997)
164. D. Vollhardt, Dynamical mean-field theory for correlated electrons. Ann. Phys. **524**, 1 (2012)
165. K.S. Thygesen, A. Rubio, Nonequilibrium GW approach to quantum transport in nano-scale contacts. J. Chem. Phys. **126**, 91101 (2007)
166. K.S. Thygesen, Impact of exchange-correlation effects on the IV characteristics of a molecular junction. Phys. Rev. Lett. **100**, 166804 (2010)

167. P. Myöhänen, A. Stan, G. Stefanucci, R. van Leeuwen, A many-body approach to quantum transport dynamics: initial correlations and memory effects. Europhys. Lett. **84**, 67001 (2008)
168. P. Myöhänen, A. Stan, G. Stefanucci, R. van Leeuwen, Kadanoff-Baym approach to quantum transport through interacting nanoscale systems: from the transient to the steady-state regime. Phys. Rev. B **80**, 115107 (2009)
169. P. Myöhänen, A. Stan, G. Stefanucci, R. van Leeuwen, Kadanoff-Baym approach to time-dependent quantum transport in AC and DC fields. J. Phys. Conf. Ser. **220**, 012017 (2010)
170. M. Puig von Friesen, C. Verdozzi, C.-O. Almbladh, Successes and failures of Kadanoff-Baym dynamics in Hubbard nanoclusters. Phys. Rev. Lett. **103**, 176404 (2009)
171. C. Verdozzi, D. Karlsson, M. Puig von Friesen, C.-O. Almbladh, U. von Barth, Some open questions in TDDFT: clues from lattice models and Kadanoff-Baym dynamics. Chem. Phys. **391**, 37 (2011)
172. A.-M. Uimonen, E. Khosravi, A. Stan, G. Stefanucci, S. Kurth, R. van Leeuwen, E.K.U. Gross, Comparative study of many-body perturbation theory and time-dependent density functional theory in the out-of-equilibrium Anderson model. Phys. Rev. B **84**, 115103 (2011)
173. N. Säkkinen, M. Manninen, R. van Leeuwen, The Kadanoff–Baym approach to double excitations in finite systems. New J. Phys. **14**, 013032 (2012)
174. P. Myöhänen, R. Tuovinen, T. Korhonen, G. Stefanucci, R. van Leeuwen, Image charge dynamics in time-dependent quantum transport. Phys. Rev. B **85**, 075105 (2012)
175. E. Khosravi, A.-M. Uimonen, A. Stan, G. Stefanucci, S. Kurth, R. van Leeuwen, E.K.U. Gross, Correlation effects in bistability at the nanoscale: steady state and beyond. Phys. Rev. B **85**, 075103 (2012)
176. M. Puig von Friesen, C. Verdozzi, C.-O. Almbladh, Kadanoff-Baym equations and approximate double occupancy in a Hubbard dimer, arXiv:1009.2917 (2010)
177. S.A. Jafari, Introduction to Hubbard model and exact diagonalization. Iran. J. Phys. Res. **8**, 113 (2008)
178. S. Hermanns, K. Balzer, M. Bonitz, in preparation (2012)
179. G.W.F. Drake (ed.), *Handbook of Atomic, Molecular and Optical Physics* (Springer, New York, 2006)
180. S.L. Haan, R. Grobe, J.H. Eberly, Numerical study of autoionizing states in completely correlated two-electron systems. Phys. Rev. A **50**, 378 (1994)
181. J. Javanainen, J.H. Eberly, Q. Su, Numerical simulations of multiphoton ionization and above-threshold electron spectra. Phys. Rev. A **38**, 3430 (1988)
182. V.C. Reed, P.L. Knight, K. Burnett, Suppression of ionization in superintense fields without dichotomy. Phys. Rev. Lett. **67**, 1415 (1991)
183. U. Schwengelbeck, F.H.M. Faisal, Ionization of the one-dimensional Coulomb atom in an intense laser field. Phys. Rev. A **50**, 632 (1994)
184. M.S. Pindzola, D.C. Griffin, C. Bottcher, Validity of time-dependent Hartree-Fock theory for the multiphoton ionization of atoms. Phys. Rev. Lett. **66**, 2305 (1991)
185. R. Grobe, J.H. Eberly, Photoelectron spectra for a two-electron system in a strong laser field. Phys. Rev. Lett. **68**, 2905 (1992)
186. R. Grobe, J.H. Eberly, Single and double ionization and strong-field stabilization of a two-electron system. Phys. Rev. A **47**, R1605 (1993)
187. K. Richter, G. Tanner, D. Wintgen, Classical mechanics of two-electron atoms. Phys. Rev. A **48**, 4182 (1993)
188. D. Bauer, Two-dimensional, two-electron model atom in a laser pulse: exact treatment, single-active-electron analysis, time-dependent density-functional theory, classical calculations, and nonsequential ionization. Phys. Rev. A **56**, 3028 (1997)
189. M. Lein, E.K.U. Gross, V. Engel, Intense-field double ionization of helium: identifying the mechanism. Phys. Rev. Lett. **85**, 4707 (2000)
190. A. López-Castillo, M.A.M. de Aguiar, A.M. Ozorio de Almeida, On the one-dimensional helium atom. J. Phys. B, At. Mol. Opt. Phys. **29**, 197 (1996)

191. N.E. Dahlen, R. van Leeuwen, Double ionization of a two-electron system in the time-dependent extended Hartree-Fock approximation. Phys. Rev. A **64**, 023405 (2001)
192. M. Ruggenthaler, D. Bauer, Rabi oscillations and few-level approximations in time-dependent density functional theory. Phys. Rev. Lett. **102**, 233001 (2009)
193. M. Ruggenthaler, D. Bauer, Local Hartree-exchange and correlation potential defined by local force equations. Phys. Rev. A **80**, 052502 (2009)
194. D. Hochstuhl, S. Bauch, M. Bonitz, Multiconfigurational time-dependent Hartree-Fock calculations for photoionization of one-dimensional helium. J. Phys. Conf. Ser. **220**, 012019 (2010)
195. H. Yu, T. Zuo, A.D. Bandrauk, Molecules in intense laser fields: enhanced ionization in a one-dimensional model of H_2. Phys. Rev. A **54**, 3290 (1996)
196. I. Kawata, H. Kono, A.D. Bandrauk, Mechanism of enhanced ionization of linear H_3^+ in intense laser fields. Phys. Rev. A **64**, 043411 (2001)
197. N. Suzuki, I. Kawata, K. Yamashita, Comparison of the mechanisms of enhanced ionization of H_2 and in intense laser fields. Chem. Phys. **338**, 348 (2007)
198. M.C. Gutzwiller, *Chaos in Classical and Quantum Mechanics* (Springer, Heidelberg, 1990)
199. A. López-Castillo, Semiclassical study of the one-dimensional hydrogen molecule. Chaos **18**, 033130 (2008)
200. N. Takemoto, A. Becker, Visualization and interpretation of attosecond electron dynamics in laser-driven hydrogen molecular ion using Bohmian trajectories. J. Chem. Phys. **134**, 074309 (2011)
201. M. Nakano, K. Yamaguchi, Electron-correlation dynamics of a one-dimensional H_2 model in a quantized photon field. Chem. Phys. Lett. **317**, 103 (2000)
202. J. Zanghellini, M. Kitzler, C. Fabian, Th. Brabec, A. Scrinzi, An MCTDHF approach to multielectron dynamics in laser fields. Laser Phys. **13**, 1064 (2003)
203. J. Zanghellini, M. Kitzler, Th. Brabec, A. Scrinzi, Testing the multi-configuration time-dependent Hartree-Fock method. J. Phys. B, At. Mol. Opt. Phys. **37**, 763 (2004)
204. D.G. Tempel, T.J. Martínez, N.T. Maitra, Revisiting molecular dissociation in density functional theory: a simple model. J. Chem. Theory Comput. **5**, 770 (2009)
205. P. Schlagheck, A. Buchleitner, Nondispersive two-electron wave packets in driven helium. Eur. Phys. J. D **22**, 401 (2003)
206. C. Ruiz, L. Plaja, L. Roso, A. Becker, Ab initio calculation of the double ionization of helium in a few-cycle laser pulse beyond the one-dimensional approximation. Phys. Rev. Lett. **96**, 053001 (2006)
207. K. Balzer, S. Bauch, M. Bonitz, Efficient grid-based method in nonequilibrium Green's function calculations: application to model atoms and molecules. Phys. Rev. A **81**, 022510 (2010)
208. D. Hochstuhl, K. Balzer, S. Bauch, M. Bonitz, Nonequilibrium Green function approach to photoionization processes in atoms. Physica E, Low-Dimens. Syst. Nanostruct. **42**, 513 (2010)
209. S. Bauch, K. Balzer, P. Ludwig, A. Filinov, M. Bonitz, Introduction to quantum plasma simulations, in *Introduction to Complex Plasmas*, ed. by M. Bonitz, N. Horing, P. Ludwig. Springer Series Atomic, Optical and Plasma Physics, vol. 59 (Springer, Berlin, 2010)
210. K. Balzer, S. Bauch, M. Bonitz, Finite elements and the discrete variable representation in nonequilibrium Green's function calculations. Atomic and molecular models. J. Phys. Conf. Ser. **220**, 012020 (2010)
211. P.-O. Löwdin, Exchange, correlation, and spin effects in molecular and solid-state theory. Rev. Mod. Phys. **34**, 80 (1962)
212. A. Stan, N.E. Dahlen, R. van Leeuwen, Levels of self-consistency in the GW approximation. J. Chem. Phys. **130**, 114105 (2009)
213. R.C. Ashoori, Electrons in artificial atoms. Nature **379**, 413 (1996)
214. S.M. Reimann, M. Manninen, Electronic structure of quantum dots. Rev. Mod. Phys. **74**, 1283 (2002)
215. L. Bányai, S.W. Koch, *Semiconductor Quantum Dots* (World Scientific, Singapore, 1993)

216. W.G. van der Wiel, S. De Franceschi, J.M. Elzerman, T. Fujisawa, S. Tarucha, L.P. Kouwenhoven, Electron transport through double quantum dots. Rev. Mod. Phys. **75**, 1 (2002)
217. M.A. Kastner, The single-electron transistor. Rev. Mod. Phys. **64**, 849 (1992)
218. D. Loss, D.P. DiVincenzo, Quantum computation with quantum dots. Phys. Rev. A **57**, 120 (1998)
219. P. Harrison, *Quantum Wells, Wires and Dots—Theoretical and Computational Physics of Semiconductor Nanostructures* (Wiley, Chichester, 2005)
220. G.W. Hanson, *Fundamentals of Nanoelectronics* (Pearson/Prentice Hall, Upper Saddle River, 2008)
221. A.V. Filinov, M. Bonitz, Yu.E. Lozovik, Wigner crystallization in mesoscopic 2D electron systems. Phys. Rev. Lett. **86**, 3851 (2001)
222. K. Balzer, M. Bonitz, Nonequilibrium properties of strongly correlated artificial atoms—a Green's functions approach. J. Phys. A, Math. Theor. **42**, 214020 (2009)
223. P. Ludwig, K. Balzer, A. Filinov, H. Stolz, M. Bonitz, On the Coulomb-dipole transition in mesoscopic classical and quantum electron-hole bilayers. New J. Phys. **10**, 083031 (2008)
224. S. Bednarek, B. Szafran, T. Chwiej, J. Adamowski, Effective interaction for charge carriers confined in quasi-one-dimensional nanostructures. Phys. Rev. B **68**, 045328 (2003)
225. H. Haug, S.W. Koch, *Quantum Theory of the Optical and Electronic Properties of Semiconductors* (World Scientific, Singapore, 1994)
226. J.F. Stanton, R.J. Bartlett, The equation of motion coupled-cluster method. A systematic biorthogonal approach to molecular excitation energies, transition probabilities, and excited state properties. J. Chem. Phys. **98**, 7029 (1993)
227. J. Schwinger, On the Green's functions of quantized fields. I. Proc. Natl. Acad. Sci. **37**, 452 (1951)
228. J. Schwinger, On the Green's functions of quantized fields. II. Proc. Natl. Acad. Sci. **37**, 455 (1951)
229. V. Fock, Konfigurationsraum und zweite Quantelung. Z. Phys. A., Hadrons Nucl. **75**, 622 (1932)
230. D. Hochstuhl, M. Bonitz, Time-dependent restricted active space configuration interaction for the photoionization of many-electron atoms. Phys. Rev. A **86**, 053424 (2012)

Index

K. Balzer, M. Bonitz, *Nonequilibrium Green's Functions Approach to Inhomogeneous Systems*, Lecture Notes in Physics 867,
DOI 10.1007/978-3-642-35082-5, © Springer-Verlag Berlin Heidelberg 2013